PART I

CONVECTIVE THERMAL TRANSFER IN A STEADY, NEARLY UNIFORM FLOW OF AIR BETWEEN PARALLEL PLATES

PART II

A STUDY OF ORGAN-PIPE COMBUSTION OSCILLATIONS OF PREMIXED GASES IN A COMBUSTOR WITH VARIABLE LENGTH AT ATMOSPHERIC PRESSURE

Thesis by

Wu-sun Chia

In Partial Fulfillment of the Requirements

For the Degree of

Doctor of Philosophy

California Institute of Technology

Pasadena, California

1969

(Submitted May 6, 1969)

ACKNOWLEDGMENTS

The author wishes to express his sincere gratitude to Professor B. H. Sage for his inspiring guidance and most helpful advice during the course of this investigation.

The author also wishes to express his appreciation for the assistance given him by others in his research, and in the preparation of this manuscript. H. Hollis Reamer contributed materially to the experimental program and Henry E. Smith assisted with most of the experimental measurements. Malcolm C. Morrison aided in the evaluation of the physicochemical equilibrium data and Harry C. Wiese assisted in collecting the experimental data leading to Part II of this thesis. Joan Jacobs assisted in the reduction of the data and generously took the time to review the manuscript. Virginia Berry assisted with many of the computations of the data and June Gray with the illustrations.

Financial support for the research projects made available by the Peter E. Fluor Foundation and the United States Public Health Service is gratefully acknowledged. The author also acknowledges the financial support in the form of Scholarships and Graduate Assistantships from the California Institute of Technology.

ABSTRACT

PART I

Measurements of the total viscosity and total conductivity were made as a function of position and Reynolds number for the flow of air between two parallel plates with a separation of approximately 0.75 in. The temperature of the upper plate was 130.0°F and that of the lower plate 70.0°F. The investigations were carried out at Reynolds numbers from 40,000 to 100,000 and were in good agreement with earlier data obtained at Reynolds numbers up to 40,000. The results obtained indicate little change in the total Prandtl number with increasing Reynolds number from the value of the molecular Prandtl number.

PART II

The effect of varying the length of the combustor upon the frequency and the amplitude of the organ-pipe oscillations has been investigated in a cylindrical combustor 3.836 in. in diameter and approximately 162 in. in length. Measurements of the perturbations in pressure were made in a premixed flame of air and natural gas at a mixture ratio of about 90 per cent stoichiometric. Results indicate some discontinuous variations in frequency, along with the presence of some quiet regions, as the length of the combustor is systematically changed. A

driving mechanism of the combustion oscillation is proposed and is examined in the light of Rayleigh's criterion. The calculated results based upon this driving mechanism turn out to be in good agreement with the experimental data.

TABLE OF CONTENTS

PART	TITLE	PAGE
	ACKNOWLEDGMENTS	ii
	ABSTRACT	iii
	TABLE OF CONTENTS	v
	LIST OF FIGURES	vii
	LIST OF TABLES	x
	PART I. CONVECTIVE THERMAL TRANSFER IN A STEADY, NEARLY UNIFORM FLOW OF AIR BETWEEN PARALLEL PLATES	1
I	INTRODUCTION	2
II	ANALYTICAL RELATIONS	4
III	EXPERIMENTAL METHODS	8
IV	EXPERIMENTAL RESULTS	16
V	REFERENCES	30
VI	NOMENCLATURE	32
VII	TABLES	34
	PART II. A STUDY OF ORGAN-PIPE COMBUSTION OSCILLATIONS OF PREMIXED GASES IN A COMBUSTOR WITH VARIABLE LENGTH AT ATMOSPHERIC PRESSURE	42
I	INTRODUCTION	43
II	THEORETICAL APPROACHES AND LITERATURE REVIEW	49

PART	TITLE	PAGE
	A. THEORETICAL APPROACHES	49
	B. RAYLEIGH'S CRITERION OF DRIVING	54
	C. COMPARISON BETWEEN BOTH APPROACHES	58
III	EQUIPMENT	61
IV	EXPERIMENTAL METHODS	75
V	EXPERIMENTAL RESULTS	79
VI	ANALYSIS AND DISCUSSION OF RESULTS	100
	A. PRELIMINARY CONSIDERATIONS OF SOUND WAVES	100
	B. THE DISTRIBUTION OF LOCAL AVERAGE GAS TEMPERATURE	105
	C. THE CALCULATION OF THE FREQUENCIES OF COMBUSTOR	110
	D. AN ANALYSIS OF OSCILLATION MECHANISM	116
	E. COMPARISON OF PREDICTED RESULTS WITH EXPERIMENTAL DATA AND DISCUSSION OF RESULTS	123
VII	CONCLUSIONS	129
VIII	REFERENCES	132
IX	NOMENCLATURE	136
X	TABLES	140
XI	APPENDICES	153
	PROPOSITIONS	159
	PROPOSITION I	159
	PROPOSITION II	174
	PROPOSITION III	182

LIST OF FIGURES

FIGURE	TITLE	PAGE
	PART I	
1	Temperature Distribution near Upper Wall	14
2	Effect of Reynolds Number and Position upon Viscous Dissipation	18
3	Experimental Values of Total Viscosity	20
4	Experimental Values of Total Conductivity	22
5	Comparison of Total Viscosity and Total Conductivity for a Reynolds Number of 80,000	24
6	Comparison of Reynolds Analogy with Experimental Measurements near the Upper Wall	25
7	Effect of Viscous Dissipation upon Total Conductivity for a Reynolds Number of 100,000	26
8	Experimental Values of Total Prandtl Number as a Function of Reciprocal Reynolds Number	28
	PART II	
1	General Assembly of the Combustion Tube	62
2	Lower End Details of the Combustor	64
3	Details of the Flameholder "Grid 7C"	66
4	General Arrangements of the Ports	67
5	A Photographic View of the Pressure Transducer	69
6	General Arrangement of Reflecting Disk within Combustor	71

FIGURE	TITLE	PAGE
7	Details of the Reflecting Disk and the Supporting Rod	72
8	Three Typical Records of Perturbations in Pressure	80
9	Sound Wave With a Strong Octave Overtone	81
10	Typical Perturbations in Pressure with a Large Irregularity	83
11	Typical Phase-relationship Records	84
12	Perturbations in Pressure in a "Quiet Region"	86
13	Frequencies as a Function of Length of Combustor at Three Ports	88
14	Amplitudes as a Function of Effective Length of Combustor at Three Ports along Combustor	90
15	Perturbations of Total Optical Intensity and Pressure	92
16	Perturbations of Monochromatic Intensity for Carbon Dioxide	93
17	Perturbation of Monochromatic Intensity for Water	94
18	Effect of Mixture Ratio upon Frequency	97
19	Effect of Mixture Ratio upon Magnitude of Perturbations	98
20	Thermal Losses as a Function of Equilibrium Temperature	108
21	Temperature as a Function of Distance from Flameholder	111
22	Calculated Frequencies as a Function of Effective Length of Combustor	115

FIGURE	TITLE	PAGE
23	A Schematic Diagram of the Combustion Chamber along with the Plenum Chamber	117
24	Graphical Presentation of Rayleigh's Criterion of Driving	119
25	Superposition of the Calculated Frequencies upon the Shaded "Quiet Region"	122
26	Predicted Intervals of Frequencies as a Function of the Effective Length of Combustor	124
27	Comparison of Predicted Frequencies with Experimental Data	125

LIST OF TABLES

TABLE	TITLE	PAGE
	PART I	
1	Experimental Conditions	35
2	Properties of Dry Air at Atmospheric Pressure	38
3	Local Values of Total Viscosity	39
4	Local Values of Total Conductivity	40
5	Local Values of Total Prandtl Number	41
	PART II	
1	Typical Mass Spectrographic Analyses of Natural Gas	140
2	Summary of Experimental Conditions	141
3	Experimental Analysis of Perturbations in Pressure	143
4	Average Apparent Temperature of the Gas	152

PART I

CONVECTIVE THERMAL TRANSFER IN A STEADY, NEARLY UNIFORM FLOW OF AIR BETWEEN PARALLEL PLATES*

*Chia, Wu-sun, and Sage, B. H., "Temperature Gradients in Turbulent Gas Streams: Investigation of the Limiting Value of Total Prandtl Number."

This article has been accepted by the A.I.Ch.E. Journal for publication in June, 1968 and is presented here as Part I of the author's Ph.D. thesis.

I. INTRODUCTION

An understanding of the interrelation of momentum and energy transport in turbulent flow is a matter of engineering interest. A great deal of effort has been directed to the measurement of momentum transfer from knowledge of local values of velocity and shear. More limited investigations have been carried out in the field of thermal transfer. The experimental techniques in the field of thermal transfer are often simpler and may permit a more accurate evaluation of such transport phenomena than can be obtained readily from the measurements of momentum transfer. The solution of the equations representing the energy balance in a turbulent stream can be readily determined for a variety of conditions[15,27], provided local values of thermal transport are available.

Reynolds[26] was one of the first scientists to recognize the existence of a relationship between momentum and thermal transfer. He did considerable theoretical work on the subject and obtained a simple relationship between the two processes. According to his postulates, the basic characteristics of convective thermal transfer was indicated when treated as directly analogous to momentum transfer. Prandtl[25] did further theoretical work on the relationship and refined Reynolds formula. The

work of von Karman[17] outlined the principal relationships associated with the concepts of eddy viscosity and eddy conductivity which afford a useful, although empirical, tool in the evaluation of the effect of turbulence upon the transfer of momentum and energy. Boelter[3] and coworkers extended the Reynolds analogy[26] and the concepts of von Karman[17], and utilized such approaches to predict the thermal transfer to fluids flowing in conduits. More recent studies[8,13,22,24,27] have determined more fully the effect of Reynolds number and position in the flow channel upon the values of the eddy viscosity and the eddy conductivity for a steady, nearly uniform flow of air between parallel plates.

It is evident that a thorough understanding of the quantitative relationships between momentum and thermal transfer should improve the prediction of one type of transfer if the other is known since information obtained for one type of transfer could then be applied to the evaluation of the other without further work. Such methods appear to be of particular utility in case information as to the local behavior is desired. Furthermore, there has been increasing interest in the course of chemical reactions in turbulent flow, which has made desirable more detailed understanding of the temperature distribution and thermal transfer in flowing streams.

II. ANALYTICAL RELATIONS

Von Karman[17] defined eddy viscosity for steady, uniform flow between parallel plates as:

$$\epsilon_m = \frac{\tau g}{\sigma \frac{du}{dy}} - \nu \qquad (1)$$

The total viscosity was defined as the sum of the kinematic viscosity and eddy viscosity:

$$\underline{\epsilon}_m = \epsilon_m + \nu = \frac{\tau g}{\sigma \frac{du}{dy}} \qquad (2)$$

For uniform flow between parallel plates, the shear in Equations (1) and (2) is defined by the following expression:

$$\tau = \frac{y_o}{2}\left(-\frac{dP}{dx}\right)\left(1 - 2\frac{y}{y_o}\right) \qquad (3)$$

It should be noted that Equations (1) and (2) cannot be used directly to evaluate values of eddy and total viscosity at the axis of the flow since the shear and the velocity gradient are zero at this point. However, by application of L'Hospital's rule to Equation (3), the following expression was obtained, which permits a direct evaluation of eddy and total viscosity at the center of the channel:

$$\epsilon_m = \underline{\epsilon}_m - \nu = \frac{g\,(dP/dx)}{\sigma\,(d^2u/dy^2)} - \nu \qquad (4)$$

The values of eddy and total viscosity can also be estimated analytically[4,27] from available generalizations[1,16] of the velocity profile for flow between parallel plates. It should be pointed out that this approach yields zero values of total viscosity at the center of the conduit. However, experimental evidence[22, 24,27] indicates that this situation is by no means true. For this reason it does not appear desirable to utilize these analytical expressions to establish the total viscosity near the center of the channel.

The eddy and total conductivities have been defined in the following way:

$$\epsilon_c = \frac{\mathring{q}}{c_p \sigma} \frac{dy}{dt} - \kappa \qquad (5)$$

$$\underline{\epsilon}_c = \epsilon_c + \kappa = \frac{\mathring{q}}{c_p \sigma} \frac{dy}{dt} \qquad (6)$$

All the variables involved in Equations (5) and (6) may be measured directly under steady, uniform conditions. However, the thermal flux obtained by conventional calorimetric techniques only provides information concerning the

flux at the upper boundary. To obtain the local fluxes, the effect of viscous dissipation must be taken into account. The contribution of the thermal flux due to viscous dissipation may be approximated by[29]:

$$\mathring{q}_j = \int_{y_o}^{y} \eta \Phi \, dy = \int_{y_o}^{y} \tau \frac{\partial u}{\partial y} dy$$

$$= \frac{1}{2}\left(-\frac{dP}{dx}\right) \int_{y_o}^{y} \left(y_o - 2y \right) \frac{du}{dy} dy \qquad (7)$$

Hence, the corrected local overall thermal flux becomes:

$$\mathring{q} = \mathring{q}_a + \mathring{q}_j \qquad (8)$$

where $\mathring{q}_a$ is the thermal flux at the upper wall obtained directly from calorimetric measurements[28,29].

In the treatment of the relationship between momentum and thermal transfers, the Prandtl number is often useful. The molecular Prandtl number is defined as the ratio of the kinematic viscosity to the thermometric conductivity. The ratio of the total viscosity to the total conductivity has been defined[9] as the total Prandtl number:

$$\underline{Pr} = \frac{\underline{\epsilon}_m}{\underline{\epsilon}_c} = \frac{c_p \tau g}{\mathring{q}} \frac{dt}{du} \qquad (9)$$

Correspondingly, the eddy Prandtl number may be defined as:

$$Pr_e = \frac{\epsilon_m}{\epsilon_c} = \underline{Pr}\left(1 + \frac{\kappa}{\epsilon_c}\right) - \frac{\nu}{\epsilon_c} \qquad (10)$$

On the basis of earlier experimental information [9,13,24], it appears that for a fluid with a molecular Prandtl number corresponding to that of air, the ratio of total viscosity to total conductivity, hereafter called the total Prandtl number, does not approach unity at Reynolds numbers up to 40,000. However, no experimental information was available concerning the values of total viscosity and total conductivity at higher Reynolds numbers. It was of interest to establish the trend of the total Prandtl number as the Reynolds number was still further increased above 40,000. The purpose of the present investigation was to establish values of eddy and total viscosity and conductivity at Reynolds numbers between 40,000 and 100,000 for a steady, nearly uniform air stream flowing between parallel plates.

III. EXPERIMENTAL METHODS

The equipment employed in these investigations has been described in some detail[7,8]. It consisted of two parallel copper plates between which air was circulated under steady, nearly uniform conditions. The channel was approximately 13 ft. in length, 12 in. in width, and 0.75 in. in height. The temperatures of the upper and lower surfaces of the duct were maintained at constant but different values by circulating oil above and below the parallel plates. Under such conditions a temperature gradient normal to the direction of flow was imposed upon the air stream. The local velocity was established by means of a 0.008 in. pitot tube and a hot-wire anemometer mounted on traversing equipment, whereas the gross flow rate was measured by the use of a Venturi meter in the supply duct. The actual vertical position of the traversing pitot tube and hot-wire anemometer was determined by means of a small cathetometer mounted upon the traversing equipment.

The hot-wire anemometer consisted of a 1-mil platinum wire 0.4 in. in length. The constant resistance method was applied in the local velocity measurements with the anemometer. The anemometer was calibrated against

pitot tube measurements near the center of the channel. In applying the constant resistance method, the platinum wire was held at an optimum operating temperature of about 50°F. above that of the air stream. Such an approach decreased changes in the resistance characteristics of the wire due to aging. Corresponding values of velocity were obtained with both the hot-wire anemometer and the pitot tube. These data were used to establish the calibration of the hot-wire anemometer. The hot-wire anemometer was also used as a resistance thermometer. After making a velocity measurement the resistance of the wire at the stream temperature was established. Measurements with the traversing equipment indicated that the hot wire could be located within 0.003 in. relative to the copper plates. The behavior of the hot-wire anemometer near the wall has been described[8].

The pressure gradients in the flowing stream were ascertained from piezometer bars used in conjunction with kerosene-in-glass manometers observed with a cathetometer [7]. In addition, the pressure was measured at the position of the traversing equipment which was 88.6 in. downstream of the approach section. Thermocouples were provided in the upper and lower copper plates to establish the temperature at the boundary of the air stream. The

thermal flux normal to the air stream was determined by the use of two calorimeters located in the upper plate, one near the downstream end and the other near the middle of the flow channel[7]. The copper plates were parallel within 0.005 in. throughout the working section. The width of the channel did not vary by more than 0.010 in. throughout the length.

A knowledge of the relationship between the pressure and the distance along the channel was used to determine the uniformity of the flow. Under uniform velocity for a fluid at constant specific volume and viscosity, a linear relationship should exist between the pressure and the position along the channel. As would be expected for a compressible fluid, the pressure gradient at the downstream end of the channel was slightly larger than at the entrance. However, the weight rate of flow of air was uniform as long as there were no leaks of air to or from the channel through the side blocks. Consequently, the Reynolds number of the flow was uniform throughout the channel. In any event, the deviation from uniform flow was sufficiently small as not to impair the analysis of the thermal transfer measurements.

In the present investigation, most of the measurements were made with the upper and lower plate maintained

at 130°F. and 70°F., respectively, whereas the entering bulk air temperature was maintained at 100°F. Effort was directed to the refinement of the apparatus in order to permit the experimental measurements to be of as high an accuracy as was feasible. The temperatures were measured with resistance thermometers, which were compared with a similar instrument calibrated by the National Bureau of Standards, with an error of not more than 0.05 °F., and the thermal flux at the upper wall was established with a standard error of estimate of not more than 1%. The probable error associated with the velocity and shear measurements was estimated to be less than 1%. The details of velocity, temperature, energy, and pressure measurements followed closely the methods described earlier[8] and it does not appear necessary to describe further the details of the experimental techniques.

Table I records a summary of the experimental conditions covered in this investigation. Table II shows the properties of air which were employed in the analysis of this work. Most of these data were based upon those selected by Keenan and Kaye[18]. The primary uncertainty associated with the application of these values resulted from the presence of a small amount of moisture in the air used. The influence of composition upon specific volume

of the air-water system in the gas phase at atmospheric pressure was established on the assumption that the phase was an ideal solution. The values of specific volume so obtained compared well with available measured values for gaseous mixtures of air and water. The viscosity of the air-water mixture was established from the theoretical considerations suggested by Chapman and Cowling[5]. The details of these calculations are available elsewhere[23].

Near the wall the error in establishing the position of the wire exceeded the uncertainty in the measurements of the velocity and temperature of the air. It was found helpful to establish the behavior near the boundary from the knowledge of the limiting velocity and temperature gradient at the wall. The velocity gradient at the wall was established from:

$$\left(\frac{du}{dy}\right)_w = \frac{g\,\tau_o}{\sigma\,\nu_w} \qquad (11)$$

Equation (11) can also be written in terms of the pressure gradient as:

$$\left(\frac{du}{dy}\right)_w = \frac{g\,y_o}{2\,\sigma\,\nu_w}\left(-\frac{dP}{dx}\right) \qquad (12)$$

Correspondingly, the temperature gradient at the wall was given by:

$$\left(\frac{dt}{dy}\right)_w = -\frac{\dot{q}_w}{k} \qquad (13)$$

From these limiting gradients and a few experimental data in the vicinity of the walls, the velocity and temperature profiles near the boundaries were established more accurately than would otherwise be possible. Figure 1 illustrates the variation of temperature with position near the wall for two Reynolds numbers. The significant effect of Reynolds number upon the temperature distribution near the wall is evident.

In the measurement of the temperature of a moving stream by means of a stationary wire, it is necessary to take into account the rise in temperature of the fluid immediately surrounding the wire as a result of the viscous dissipation and pressure distribution in the vicinity of the wire. For this purpose, it was found convenient to utilize the recovery factor concept to determine the actual temperature of the flowing air. This factor[21,28] is defined as:

$$\xi = \frac{T_o - T}{T_s - T} = \frac{T_o - T}{u^2/(2 g c_p)} \qquad (14)$$

Earlier studies with air[9,10,22] yielded recovery factors varying from 0.62 to approximately 0.69. In the present

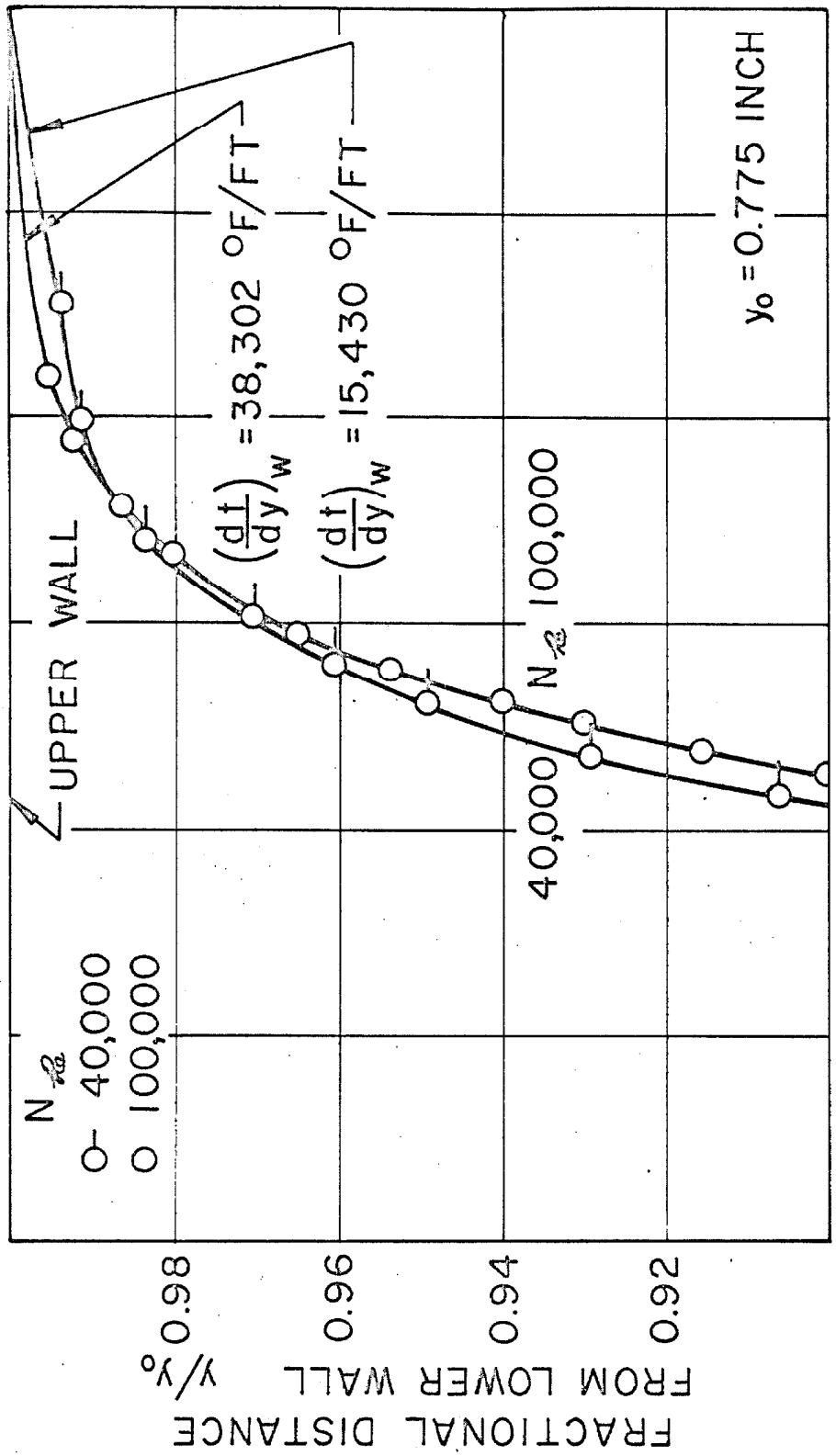

Fig. 1. Temperature distribution near upper wall

investigation a recovery factor of 0.66 was employed[21]. This corresponds to a maximum temperature deviation of 0.22°F. at a Reynolds number of 40,000 and a maximum temperature deviation of 1.30°F. at a Reynolds number of 100,000 at the center of the channel. The temperature measurements have been corrected for such effects.

IV. EXPERIMENTAL RESULTS

A series of experimental measurements of the velocity and temperature distribution in steady, nearly uniform flow was made at Reynolds numbers between 40,000 and 100,000. The Reynolds number was evaluated in the following fashion:

$$\mathrm{Re} = \frac{2\, y_o\, U}{(\nu)_{y/y_o\,=\,0.5}} = \frac{2}{(\nu)_{y/y_o\,=\,0.5}} \int_0^{y_o} u\, dy$$

$$= \frac{2\, y_o\, \dot{\underline{m}}}{\eta\, g\, A} \qquad (15)$$

It is noted from Table II that the variation of kinematic viscosity with temperature in the range of conditions encountered in the present investigation is virtually linear. For this reason the value of viscosity at the center plane of the channel was employed in Equation (15) instead of using a space-averaged value. The last equality involving the weight rate of flow was used in the actual calculation of the Reynolds number.

Because the qualitative aspects of these measurements are similar to those found earlier[13,22], there does not appear to be any justification for graphical presentation of the velocity and temperature distributions.

Measurements were made in a regular sequence in order to establish the general trend of the velocity and temperature with position. Also for each test, several measurements were made in which the position was chosen at random in order to determine the reproducibility of the measurements. These random measurements did not yield greater standard errors of estimate from the velocity and temperature profiles than the data obtained in a regular sequence of positions.

Utilizing the measurements of velocity and shear as a function of position across the channel, the measured values of thermal flux were corrected for the effect of viscous dissipation. This "correction factor" has been defined[29] as the ratio of the corrected value of heat flux to the uncorrected value. In carrying out these calculations, the values of thermal flux $\mathring{q}_a$ determined from calorimetric measurements[8,28] were employed for the evaluation of the term $\mathring{q}$, as indicated by Equation (8). The quantity $\mathring{q}_j$ was established by application of Equation (7) to the measured values of pressure gradient and velocity gradient.

The extent of the correction for viscous dissipation is illustrated in Figure 2 as a function of position

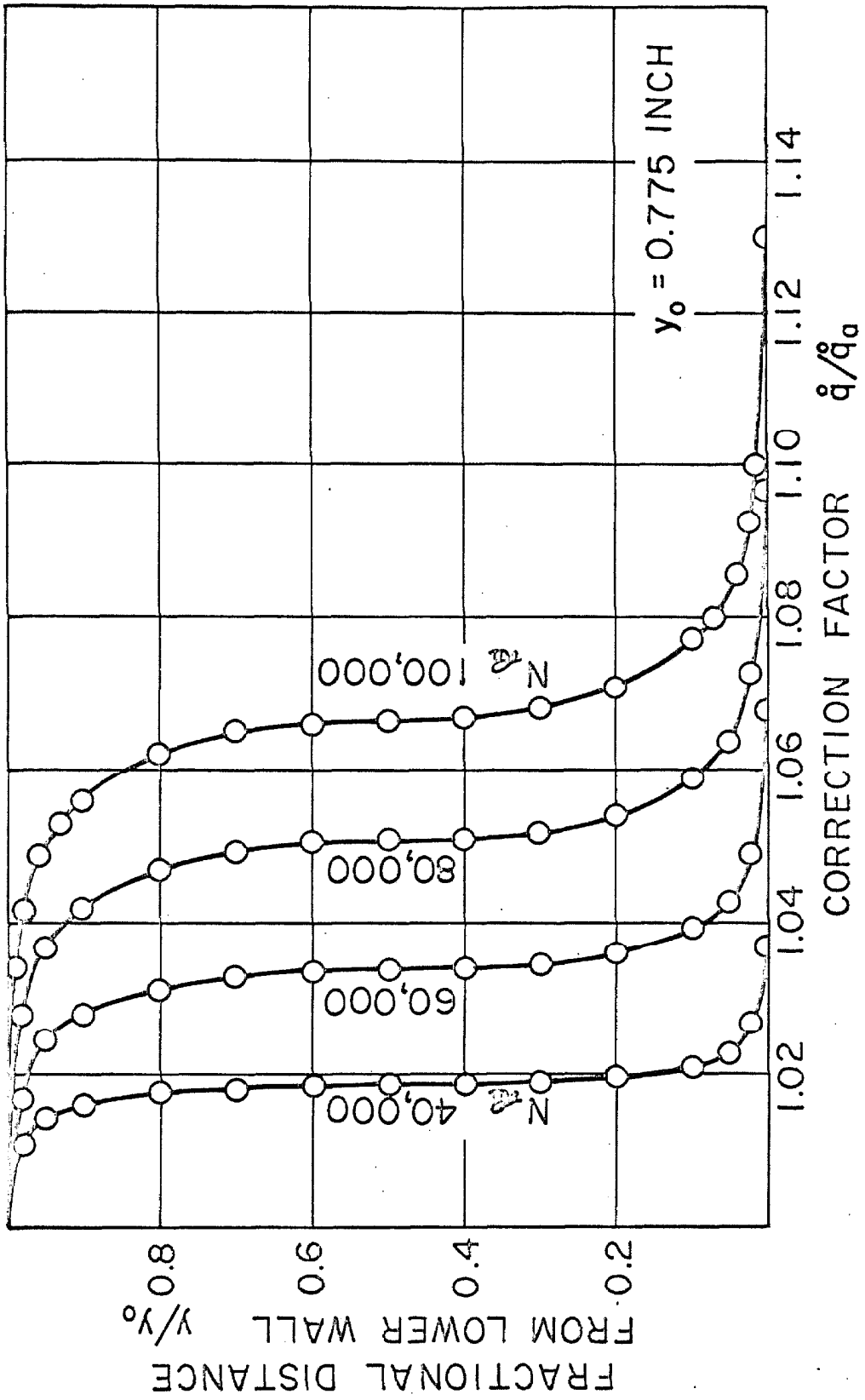

Fig. 2. Effect of Reynolds number and position upon viscous dissipation

in the channel for several Reynolds numbers. It is evident that the correction is zero at the top of the channel and attains a maximum at the bottom. The contribution due to viscous dissipation is much greater in the boundary flows than in the central part of the stream. Furthermore, the correction factor increases rapidly with increase in Reynolds number.

From the information concerning the flow conditions and the available velocity distribution and pressure difference, values of the total and eddy viscosity were calculated by application of Equations (1) and (2). Such calculations established, from the current data, the total and eddy viscosity as a function of position for Reynolds numbers between 40,000 and 100,000. Comparison was made with the earlier data[24] and good agreement was obtained between the two sets of point values of total viscosity for air flowing between parallel plates at Reynolds numbers of approximately 40,000. The current and older data[24] established the total viscosity as a function of position in the stream. Experimental values of the total viscosity for several different Reynolds numbers are depicted in Figure 3. The data shown in Figure 3 were similar in form to those obtained earlier[13,24]. The minima at the center of the channel become more pronounced at the higher

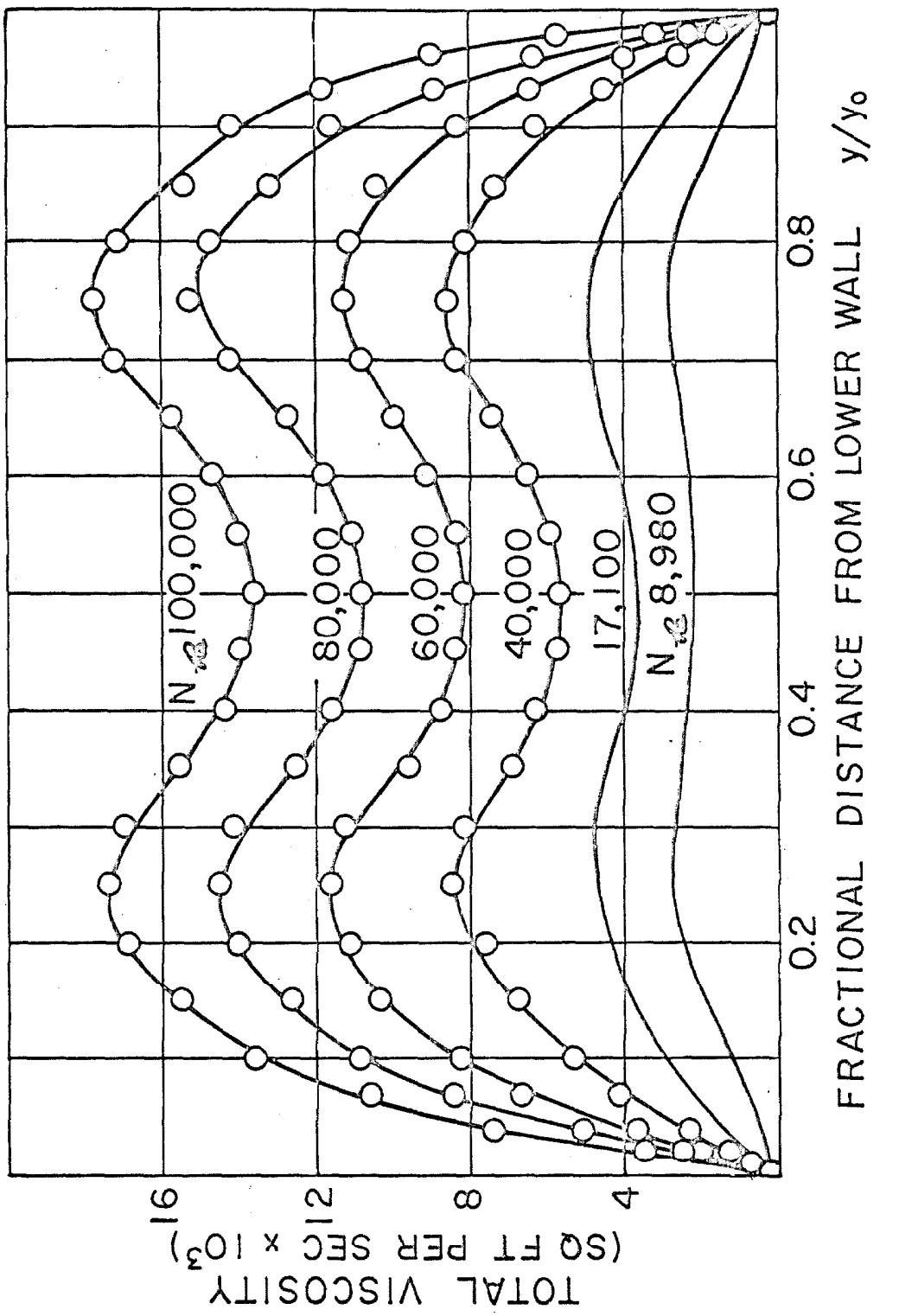

Fig. 3. Experimental values of total viscosity

Reynolds numbers. Table III sets forth values of the total viscosity as a function of position in the channel for several Reynolds numbers.

Correspondingly, point values of the total and eddy conductivity were calculated from the experimental temperature distribution and thermal flux by application of Equations (5) and (6). The results of such calculations for several Reynolds numbers are indicated in Figure 4 as a function of position in the channel. These data were corrected for viscous dissipation effect, as set forth in Equations (7) and (8). The behavior of the total conductivity appears to be analogous to that for total viscosity. The dotted curve shown in Figure 4 was recorded from earlier measurements[24] corresponding to the Reynolds number of 37,300. The deviation between the two sets of data was estimated to be within 3%. Smoothed values of total conductivity as a function of position in the channel are recorded in Table IV for several Reynolds numbers. The details of the experimental data for total viscosity and total conductivity are available[6].

It should be pointed out that the values of total viscosity and total conductivity are sensitive to the velocity and temperature distribution in the channel. As is shown in Figures 3 and 4, a small lack of symmetry

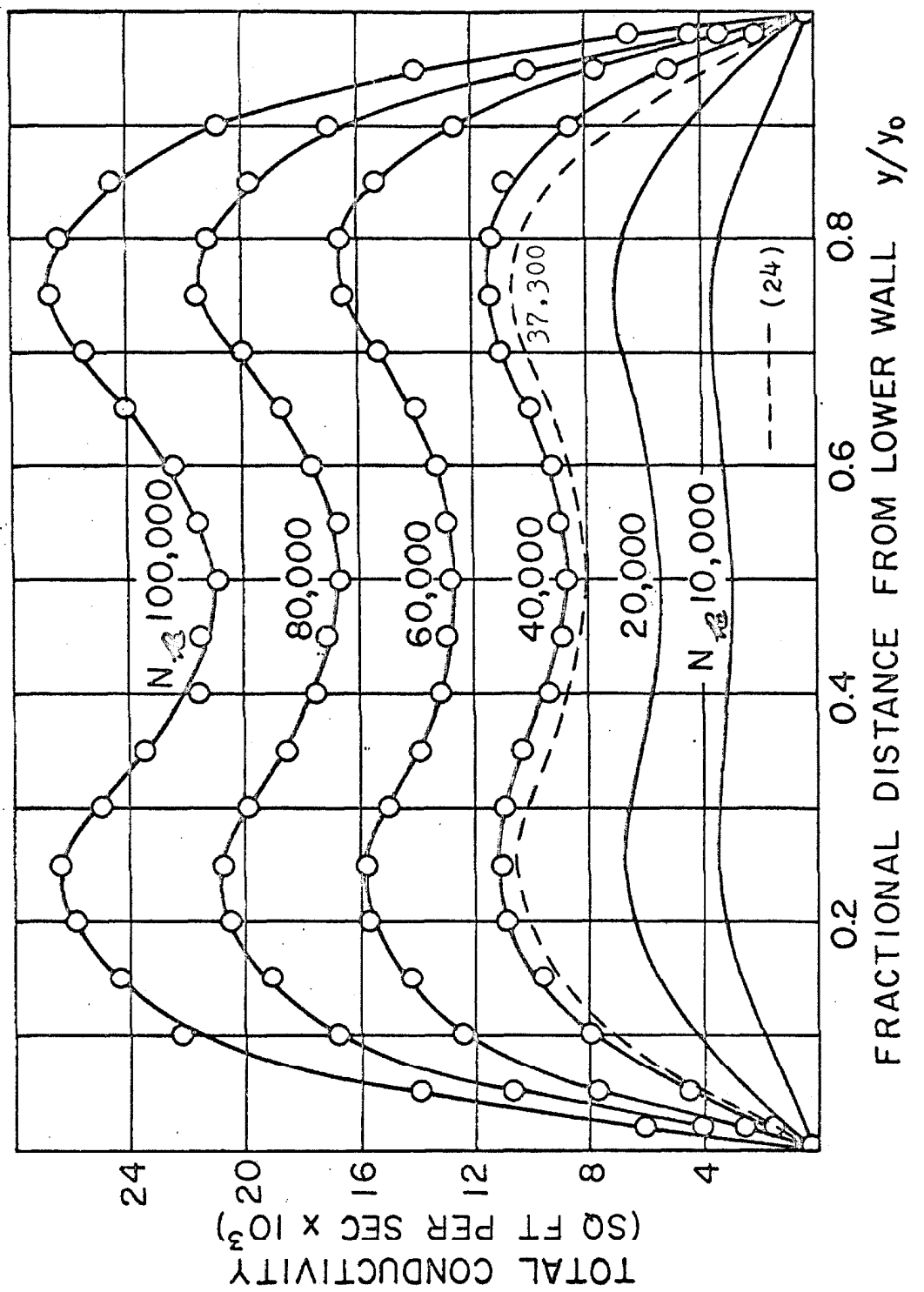

Fig. 4. Experimental values of total conductivity

about the horizontal axis of the channel persisted in the experimental values of total viscosity and total conductivity. It is not believed that the asymmetry of these data resulted from changes in conditions during measurements but rather as a result of a lack of symmetry of the molecular properties in the flowing stream as a result of the transverse temperature gradient. Figure 5 shows a comparison between the values of total viscosity and total conductivity at a Reynolds number of 80,000.

The influence of Reynolds number upon the relative conductivity in the boundary flow near the upper wall is indicated in Figure 6. Similar behavior was found near the lower wall. As indicated earlier, the flow is nearly uniform in all respects throughout the flow channel at distances greater than 40 in. from the entrance. The behavior predicted from the Reynolds analogy is shown as a dotted curve. The deviation from the analogy is many times the experimental uncertainty.

The effect of viscous dissipation upon the value of total conductivity is demonstrated in Figure 7 for a Reynolds number of 100,000. The dotted curve represents the values of total conductivity uncorrected for viscous dissipation. The symmetry of the data involving the corrected

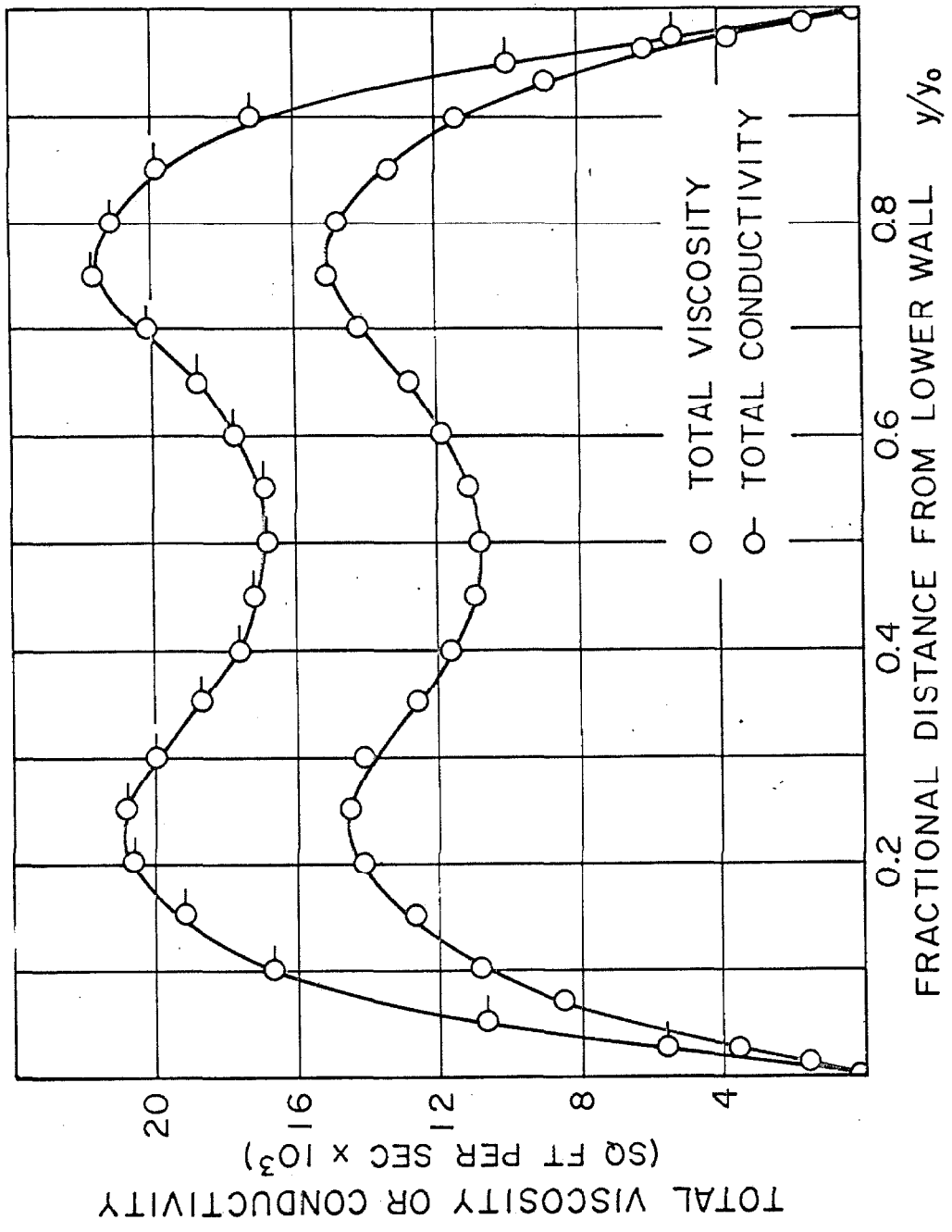

Fig. 5. Comparison of total viscosity and total conductivity for a Reynolds number of 80,000

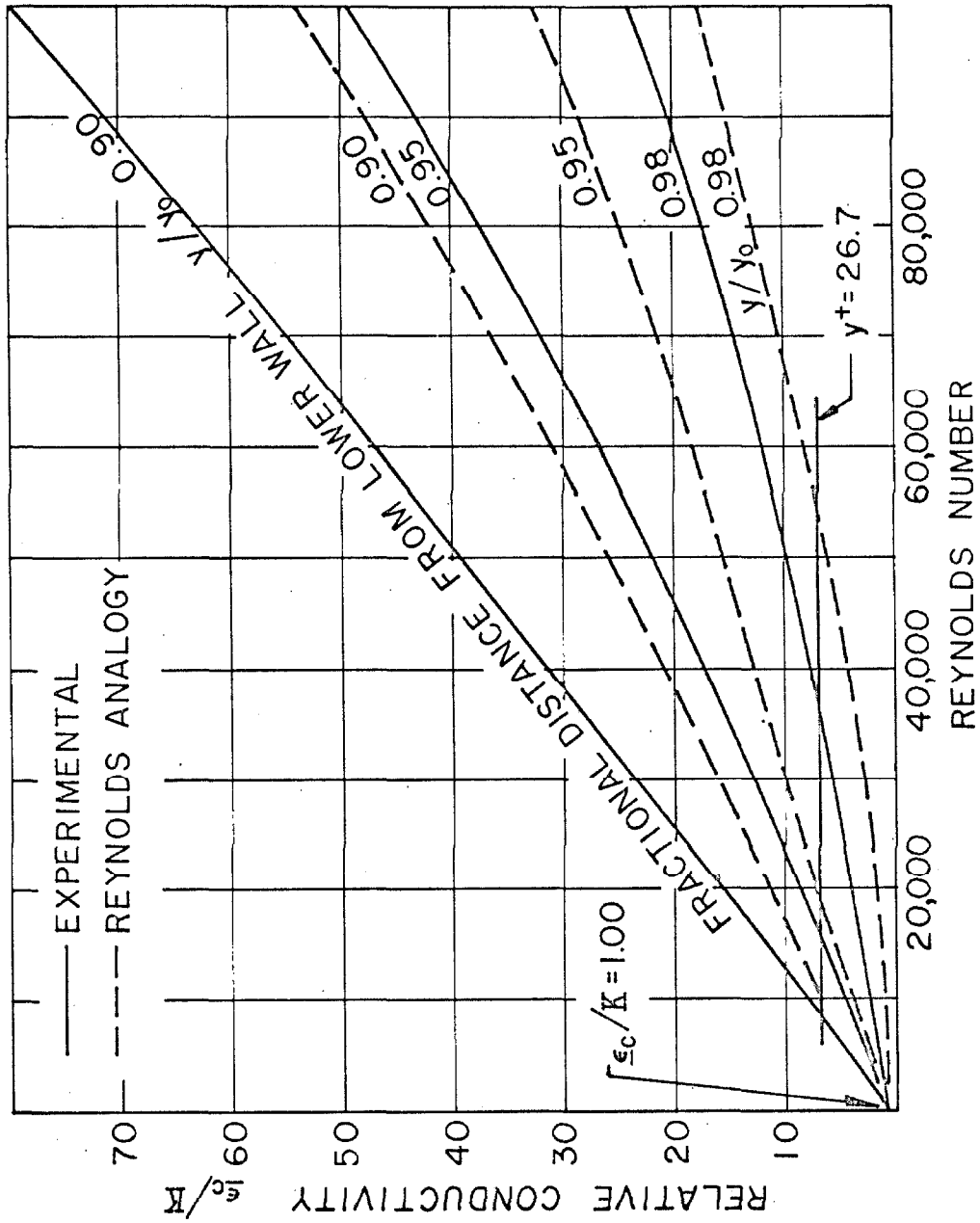

Fig. 6. Comparison of Reynolds analogy with experimental measurements near the upper wall

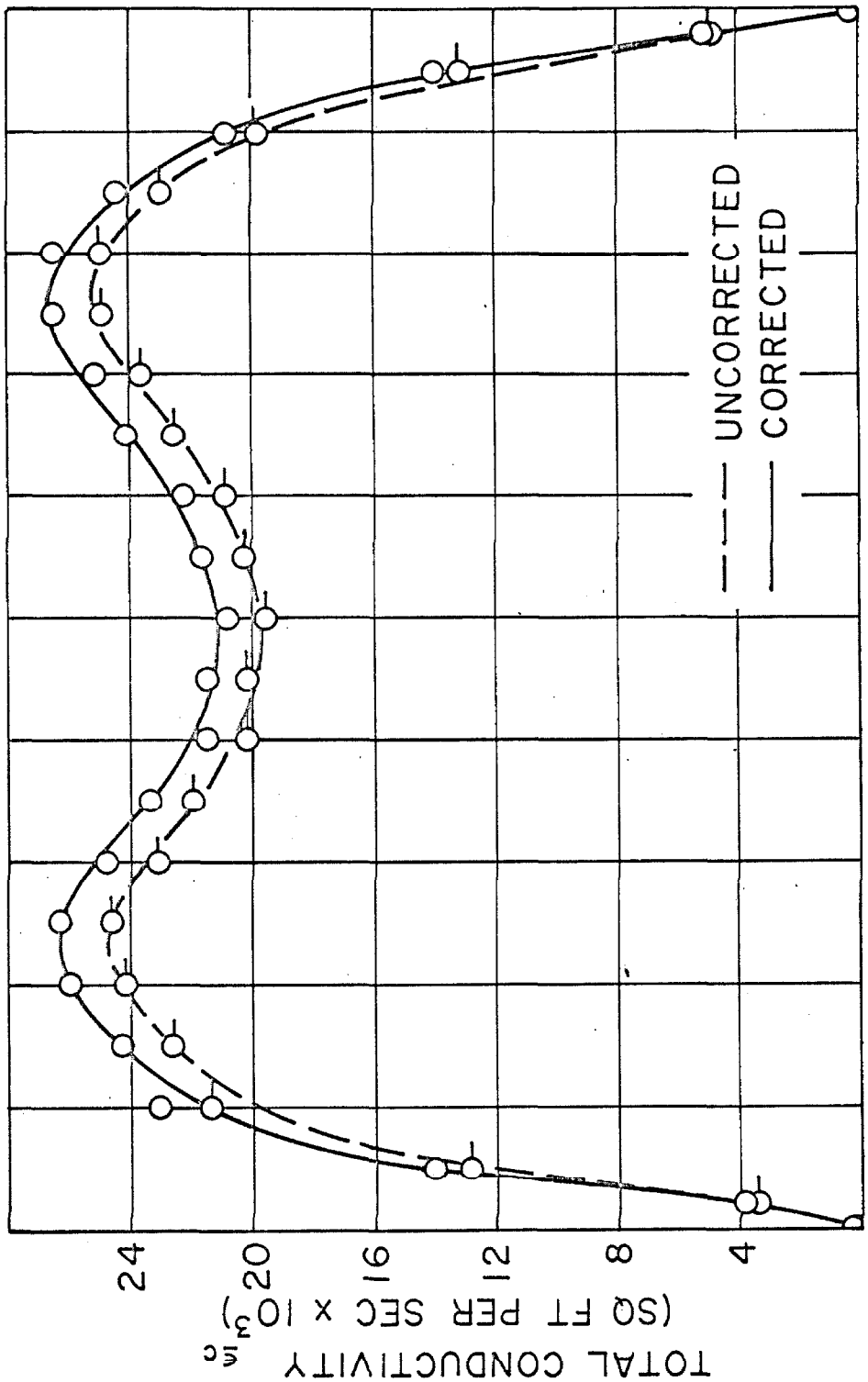

Fig. 7. Effect of viscous dissipation upon total conductivity for a Reynolds number of 100,000

values of total conductivity is markedly better than for the uncorrected data.

The values of total Prandtl number were calculated from the information concerning total viscosity and total conductivity. The results are presented in Table V as a function of position and Reynolds number. The space-average values of the total Prandtl number were also evaluated as a function of Reynolds number. The full curve of Figure 8 depicts the variation in the space-average value of total Prandtl number with the reciprocal Reynolds number. Total Prandtl numbers at several positions in the channel are also included as experimental points in Figure 8. The results indicate that the total Prandtl number is relatively insensitive to the Reynolds number of the flow and shows no trend toward a value of unity as the Reynolds number is increased. The values of the total Prandtl number are nearly equal to the molecular Prandtl number even at high Reynolds numbers.

Until further investigations are carried out involving fluids with molecular Prandtl numbers which differ markedly from unity, it remains to be ascertained if the trend indicated in this investigation for air persists for fluids which possess Prandtl numbers markedly greater

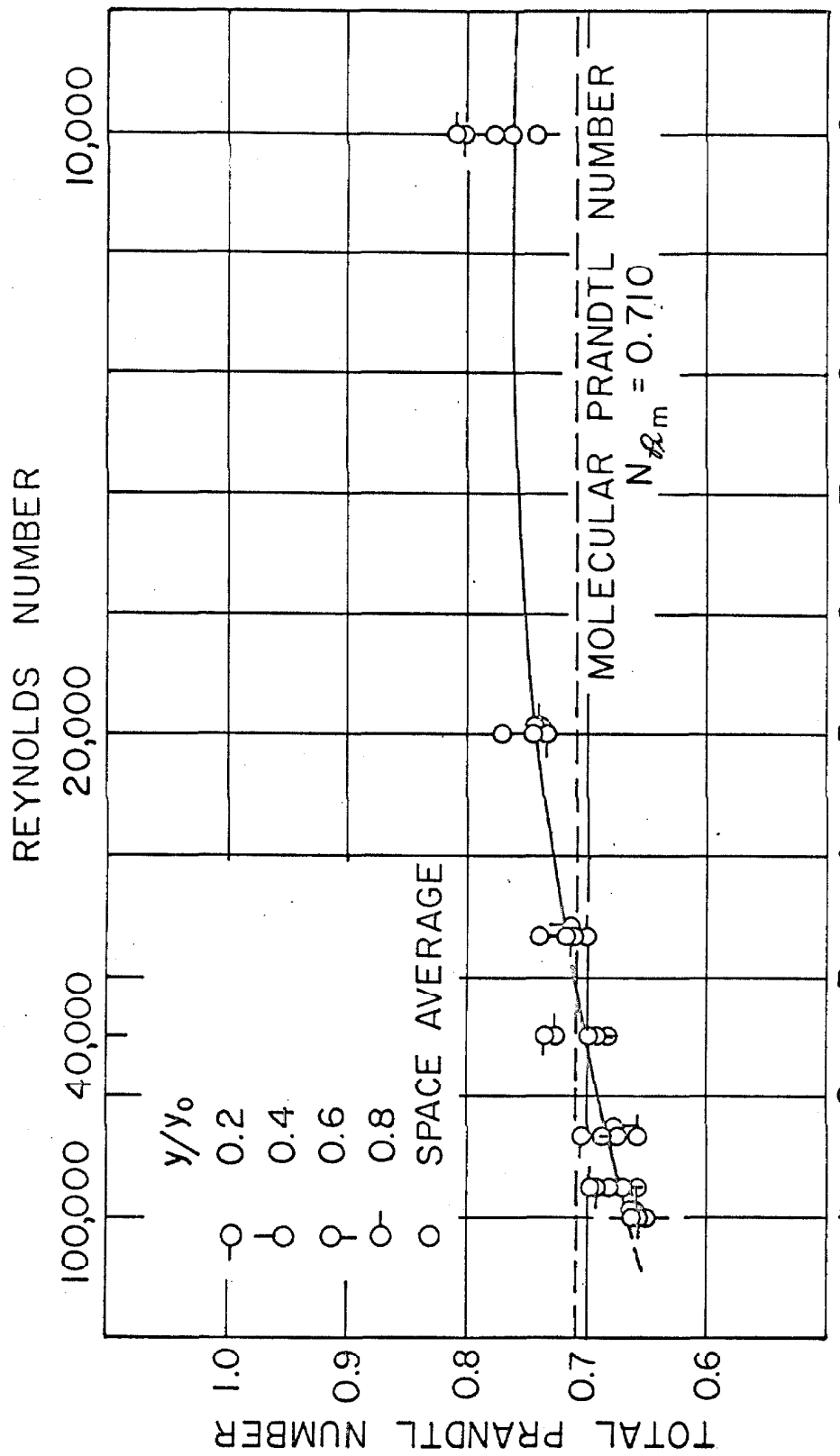

Fig. 8. Experimental values of total Prandtl number as a function of reciprocal Reynolds number

or smaller than unity. If such trends are encountered for other fluids, it becomes a relatively simple matter to predict local thermal transfer in turbulent flow for situations where the local momentum transport is known. The trends indicated by the current investigation show that the molecular properties of the fluid exert a controlling influence upon the transport even under rather highly turbulent conditions.

V. REFERENCES

1. Bakhmeteff, B. A., "The Mechanics of Turbulent Flow," Princeton University Press (1951).

2. Berry, V. J., D. M. Mason, and B. H. Sage, Ind. Eng. Chem., 45, 1596 (1953).

3. Boelter, L. M. K., R. C. Martinelli, and F. Jonassen, Trans. Am. Soc. Mech. Engrs., 63, 447 (1947).

4. Cavers, S. D., N. T. Hsu, W. G. Schlinger, and B. H. Sage, Ind. Eng. Chem., 45, 2139 (1953).

5. Chapman, S., and T. G. Cowling, "The Mathematical Theory of Nonuniform Gases," Cambridge University Press (1939).

6. Chia, W. S., and B. H. Sage, Am. Doc. Inst., Washington, D. C. (1969).

7. Corcoran, W. H., Ph.D. Thesis, Calif. Inst. Tech. (1948).

8. Corcoran, W. H., F. Page, Jr., W. G. Schlinger, and B. H. Sage, Ind. Eng. Chem., 44, 410 (1952).

9. Corcoran, W. H., and B. H. Sage, A.I.Ch.E. Journal, 2, No. 2, 251 (1956).

10. Eckert, E., Natl. Advisory Comm. Aeronaut. Tech. Mem., 983, (1941).

11. Gerhart, R. V., F. C. Brunner, H. S. Mickley, B. H. Sage, and W. N. Lacey, Mech. Eng., 64, 270 (1942).

12. Hottel, H. C., and A. J. Kalitinsky, Appl. Mech., 12, A25 (1945).

13. Hsu, N. T., K. Sato, and B. H. Sage, Ind. Eng. Chem., 48, 2218 (1956).

14. "International Critical Tables" Vol. 3, p.3, National Research Council, McGraw-Hill Book Co., N. Y. (1928).

15. Jenkins, R., H. W. Brough, and B. H. Sage, Ind. Eng. Chem., 43, 2483 (1951).

16. Karman, Th. von, J. Aeronaut. Sci., 1, No. 1 (1934).

17. Karman, Th. von, Trans. Am. Soc. Mech. Engrs., 61, 705 (1939).

18. Keenan, J. H., and J. Kaye, "Thermodynamic Properties of Air," John Wiley & Sons, N. Y. (1936).

19. Kellstrom, G., Phil. Mag., 23, 7th Series, 313 (1937).

20. Millikan, R. A., Phil. Mag., 19, 6th Series, 209 (1910).

21. Opfell, J. B., K. Sato, and B. H. Sage, Ind. Eng. Chem., 47, 1243 (1955).

22. Page, F., Jr., W. H. Corcoran, W. G. Schlinger, and B. H. Sage, ibid., 44, 419 (1952).

23. Page, F., Jr., W. H. Corcoran, W. G. Schlinger, and B. H. Sage, Am. Doc. Inst., Doc. No. 3293, Washington, D. C. (1950).

24. Page, F., Jr., W. G. Schlinger, D. K. Breaux, and B. H. Sage, Ind. Eng. Chem., 44, 424 (1952).

25. Prandtl, L., Phys. Z., 29, 487 (1928).

26. Reynolds, O., Mem. Proc. Manchester Lit. & Phil. Soc., 14, 7 (1874); also "Papers on Mechanical and Physical Subjects," Vol. I, 81, Cambridge (1890).

27. Schlinger, W. G., N. T. Hsu, S. D. Cavers, and B. H. Sage, Ind. Eng. Chem., 45, 662 (1953).

28. Schlinger, W. G., V. J. Berry, J. L. Mason, and B. H. Sage, ibid., 45, 864 (1953).

29. Venezian, E., and B. H. Sage, A.I.Ch.E. Journal, 7, No. 4, 688 (1961).

VI. NOMENCLATURE

A. Roman Type Symbols

A	Area, sq.ft.
c_p	Isobaric heat capacity, B.t.u./(lb.)($^{\circ}$F.).
g	Acceleration due to gravity, ft./sec.^{2}
k	Thermal conductivity, B.t.u./(sec.)(ft.)($^{\circ}$F.).
$\mathring{\underline{m}}$	Weight rate of air flow, lb./sec.
P	Pressure, lb./sq.ft.
$\underline{Pr}$	Total Prandtl number.
Pr_e	Eddy Prandtl number.
$\mathring{q}$	Thermal flux, B.t.u./(sec.)(sq.ft.).
$\mathring{q}_a$	Thermal flux at upper plate, B.t.u./(sec.)(sq.ft.).
$\mathring{q}_j$	Thermal flux due to viscous dissipation, B.t.u./(sec.)(sq.ft.).
Re	Reynolds number.
t	Temperature, $^{\circ}$F.
T	Absolute temperature, $^{\circ}$R.
T_o	Temperature at surface of the wire, $^{\circ}$R.
T_s	Temperature at the stagnation point, $^{\circ}$R.
u	Local time-average velocity, ft./sec.
U	Gross velocity, ft./sec. $= \frac{1}{y_o}\int_0^{y_o} u\,dy$.
x	Downstream distance along axis of stream, ft.
y	Distance normal to axis of stream measured from lower plate, ft.
y^+	Distance parameter $= \frac{y_d}{\nu}(\frac{\tau}{\sigma})^{\frac{1}{2}}$.

y_d Distance from nearer wall, ft.

B. Greek Type Symbols

ϵ_c Eddy conductivity, sq.ft./sec.

$\underline{\epsilon}_c$ Total conductivity, sq.ft./sec.

ϵ_m Eddy viscosity, sq.ft./sec.

$\underline{\epsilon}_m$ Total viscosity, sq.ft./sec.

η Absolute viscosity, (lb.)(sec.)/sq.ft.

κ Thermometric conductivity, sq.ft./sec., $k/\sigma c_p$.

ν Kinematic viscosity, sq.ft./sec.

ξ Recovery factor.

σ Specific weight, lb./sq.ft.

τ Shear, lb./sq.ft.

Φ Dissipation function, $sec.^{-2}$.

C. Subscripts

a At upper plate.

w Wall.

x in the x - direction.

y in the y - direction.

VII. TABLES

Table 1. Experimental Conditions

Quantity	Test Number 380	382	383	384
Distance between plates, ft.	0.0648	0.0639	0.0639	0.0639
Traverse location *, ft.	7.39	7.39	7.38	7.38
Incoming air temperature, ft.	100.023	100.010	100.018	100.043
Upper plate temperature, $^{o}F.$	129.95	129.31	130.01	130.04
Lower plate temperature, $^{o}F.$	70.29	69.34	69.73	69.70
Gross air velocity, ft./sec.	59.24	89.28	89.52	89.06
Reynolds number	41,124	61,322	61,536	60,918
Thermal flux, B.t.u./(sec.)(ft.^{2})	0.07005	0.10206	0.10265	0.10300
Weight rate of flow, lb./sec.	0.27281	0.40447	0.40588	0.40365
Weight fraction water	0.0102	0.0116	0.0119	0.0095
Pressure at traverse location, psi.	14.3771	14.3689	14.3530	
Barometric pressure, lb./in.^{2}	14.3720	14.3588	14.3427	
Pressure gradient, lb./cu.ft.	-0.6480	-1.4861	-1.4861	

Table 1. (Cont.)

Quantity	Test Number 386	387	388	389
Distance between plates, ft.	0.0640	0.0643	0.0642	0.0646
Traverse location *, ft.	7.38	7.38	7.38	7.38
Incoming air temperature, $^{o}F.$	100.018	100.000	99.995	99.984
Upper plate temperature, $^{o}F.$	129.95	129.74	129.64	129.97
Lower plate temperature, $^{o}F.$	70.32	70.30	70.24	70.30
Gross air velocity, ft./sec.	119.08	118.26	118.17	118.15
Reynolds number	81,294	81,771	81,432	82,012
Thermal flux, B.t.u./(sec.)(ft.^{2})	0.12733			0.13285
Weight rate of flow, lb./sec.	0.53630	0.53934	0.53711	0.54093
Weight fraction water	0.0114	0.0113	0.0114	0.0099
Pressure at traverse location, psi.	14.2550	14.3839	14.3538	
Barometric pressure, lb./sq.ft.	14.2455	14.3748	14.3435	
Pressure gradient, lb./cu.ft.	-2.2032	-2.2032	-2.2032	

Table 1. (Cont.)

Quantity	Test Number 391	392	393	394
Distance between plates, ft.	0.0642	0.0643	0.0643	0.0642
Traverse location *, ft.	7.38	7.38	7.38	7.38
Incoming air temperature, $^{o}F.$	100.019	100.031	100.013	99.983
Upper plate temperature, $^{o}F.$	129.90	129.72	129.97	129.82
Lower plate temperature, $^{o}F.$	70.08	70.22	70.22	69.53
Gross air velocity, ft./sec.	147.20	146.86	146.98	147.37
Reynolds number	101,239	101,494	101,293	101,295
Thermal flux, B.t.u./(sec.)(ft.^{2})	0.15745	0.15906	0.15774	0.17389
Weight rate of flow, lb./sec.	0.66775	0.66943	0.66807	0.66912
Weight fraction water	0.0098	0.0137	0.0125	0.0122
Pressure at traverse location, lb./in.^{2}	14.3133	14.3615	14.3101	14.2872
Barometric pressure, lb./sq.in.	14.2968	14.3448	14.2938	14.2717
Pressure gradient, lb./cu.ft.	-2.8656	-2.8656	-2.8656	-2.8656

* Traverse location measured from the end of the converging section.

Table 2. Properties of Dry Air at Atmospheric Pressure

Property	Reference	Temperature 70°F	100°F	130°F
Isobaric heat capacity B.t.u./(lb.)(°F.)	(11,18,19)	0.2403	0.2406	0.2409
Kinematic viscosity x 10^4 sq.ft./sec.	(18,19,21,24)	1.64	1.81	1.98
Molecular Prandtl number		0.713	0.710	0.707
Specific volume cu.ft./lb.	(14,18,24)	13.35	14.11	14.86
Thermal conductivity x 10^6 B.t.u./(sec.)(ft.)(°F.)	(24)	4.14	4.34	4.54
Thermometric conductivity x 10^4 sq.ft./sec.	(24)	2.30	2.54	2.80
Viscosity x 10^7 (lb.)(sec.)/sq.ft.	(18,19,21,24)	3.82	3.98	4.19

Table 3. Local Values of Total Viscosity*

Fractional Distance from Lower Wall	Reynolds Number				
	17,000	40,000	60,000	80,000	100,000
0	0.164×10^{-3}	$.164 \times 10^{-3}$	$.164 \times 10^{-3}$	$.164 \times 10^{-3}$	$.164 \times 10^{-3}$
0.02	0.74	1.27	1.76	2.35	3.37
0.05	1.68	2.97	4.78	6.60	8.97
0.10	2.92	5.26	8.32	10.30	13.20
0.15	3.79	6.89	10.30	12.87	15.56
0.20	4.40	8.00	11.09	14.20	16.95
0.25	4.70	8.39	11.70	14.48	17.38
0.30	4.76	7.89	11.05	13.77	16.83
0.35	4.54	6.95	9.83	12.56	15.55
0.40	4.04	6.43	8.90	11.58	14.63
0.45	3.68	5.82	8.31	10.97	13.90
0.50	3.62	5.65	8.15	10.81	13.80
0.55	3.77	5.94	8.40	11.10	13.95
0.60	4.20	6.51	8.96	11.75	14.78
0.65	4.64	7.35	9.84	12.83	15.77
0.70	4.90	8.27	10.85	14.15	17.05
0.75	4.87	8.64	11.28	14.95	17.78
0.80	4.62	8.22	10.82	14.68	17.17
0.85	4.03	7.22	10.00	13.20	15.83
0.90	2.99	5.71	8.29	11.03	13.93
0.95	1.42	3.43	5.12	7.20	10.61
0.98	0.58	1.55	2.24	3.01	5.20
1.00	0.198	0.198	0.198	0.198	0.198

* Total viscosity expressed in sq.ft. per sec.

Table 4. Local Values of Total Conductivity*

Fractional Distance from Lower Wall	Reynolds Number 10,000	20,000	40,000	60,000	80,000	100,000
0	0.23×10^{-3}	$.23 \times 10^{-3}$	$.23 \times 10^{-3}$	$.23 \times 10^{-3}$	$.23 \times 10^{-3}$	$.23 \times 10^{-3}$
0.02	0.34	0.93	1.76	2.75	3.95	6.15
0.05	0.89	2.40	4.57	7.73	10.51	14.18
0.10	1.84	4.35	8.03	12.38	16.81	21.57
0.15	2.67	5.67	9.87	14.37	19.20	24.33
0.20	3.24	6.46	10.87	15.70	20.60	25.86
0.25	3.50	6.76	11.16	15.80	20.78	26.35
0.30	3.45	6.60	11.03	14.99	19.95	25.27
0.35	3.32	6.20	10.46	14.03	18.66	23.50
0.40	3.17	5.81	9.44	13.17	17.65	22.12
0.45	3.06	5.59	9.03	12.80	17.02	21.37
0.50	3.05	5.52	8.82	12.70	16.76	21.16
0.55	3.13	5.63	8.97	12.88	16.96	21.67
0.60	3.30	5.89	9.42	13.28	17.62	22.67
0.65	3.46	6.26	10.05	14.17	18.73	24.05
0.70	3.61	6.78	11.00	15.11	20.18	25.67
0.75	3.60	7.03	11.38	16.42	21.38	26.71
0.80	3.31	6.78	11.28	16.47	21.08	26.10
0.85	2.73	6.00	10.42	15.26	19.55	24.20
0.90	1.89	4.57	8.72	12.73	16.58	20.83
0.95	0.97	2.55	5.01	7.85	9.70	13.40
0.98	0.41	1.12	2.00	3.51	4.25	6.43
1.00	0.28	0.28	0.28	0.28	0.28	0.28

* Total conductivity expressed in sq.ft. per sec.

Table 5. Local Values of Total Prandtl Number

Fractional Distance from Lower Wall	Reynolds Number 10,000	20,000	30,000	40,000	60,000	80,000	100,000
0	0.713	0.713	0.713	0.713	0.713	0.713	0.713
0.10	0.759	0.762	0.736	0.655	0.672	0.638	0.612
0.20	0.808	0.733	0.710	0.736	0.706	0.689	0.656
0.30	0.803	0.787	0.740	0.715	0.737	0.690	0.666
0.40	0.776	0.745	0.711	0.681	0.676	0.656	0.661
0.50	0.749	0.707	0.682	0.641	0.642	0.645	0.652
0.60	0.742	0.778	0.740	0.691	0.675	0.667	0.652
0.70	0.784	0.802	0.757	0.752	0.718	0.701	0.664
0.80	0.817	0.741	0.698	0.729	0.657	0.696	0.658
0.90	0.789	0.744	0.727	0.655	0.651	0.665	0.669
1.00	0.707	0.707	0.707	0.707	0.707	0.707	0.707
Space Average*	0.768	0.747	0.720	0.698	0.687	0.679	0.665
Flow Average**				0.696	0.682	0.672	0.655

* Space average defined by $\frac{1}{y_o}\int_0^{y_o} \underline{Pr}\, dy$

** Flow average defined by $\frac{1}{y_o U}\int_0^{y_o} \underline{Pr}\, u\, dy$

PART II

A STUDY OF ORGAN-PIPE COMBUSTION OSCILLATIONS OF PREMIXED GASES IN A COMBUSTOR WITH VARIABLE LENGTH AT ATMOSPHERIC PRESSURE

I. INTRODUCTION

It has been known for some time that combustion systems in which the flame is partially or totally confined frequently generate acoustic oscillations. This combustion oscillation or combustion instability usually results from the interaction between the flame and the gas flow. When an energy source is present in a flow system, the gas flow through it may be disturbed by oscillations which are coupled with a periodic energy release of the energy source. Consequently, sound is produced if the release of energy is nearly in phase with the variation in pressure of the gas flow. This kind of phenomenon is known also as oscillatory combustion, unstable combustion, chugging, screaming, or flame-driven oscillation[1].

Combustion oscillations may at times occur in industrial combustion systems and in jet engines. As a matter of fact, every combustion system clearly may be a potential oscillatory system in which oscillations may occur under certain circumstances. These oscillations are for the most part undesirable. Aside from their nuisance and noisiness, they may interfere with the normal progress of the combustion process, thus causing the flame to blow out. In some cases, the oscillations may become so violent that

they cause physical damage to the equipment or to its surroundings. Sometimes, however, the oscillations in themselves are not so violent, but they may trigger other high-amplitude modes of oscillations which may be destructive. On the other hand, oscillatory combustion represents a much more intense process than stable combustion. The presence of oscillations may improve mixing, heat transfer rate, and flame holding, and lead to increased efficiency of combustion. Therefore, investigation of the behavior of the combustion oscillation should provide important information for the optimum design and development of rockets and industrial burners, as to whether it should be suppressed or utilized.

There has been increasing interest in the mechanism of the formation of oxides of nitrogen and other reaction products of industrial fuels during combustion. The oxides of nitrogen have been reported to be capable of accelerating the formation of eye irritants and other undesirable compounds associated with air pollution[2-7]. Earlier reconnaissance studies[8,9] of the combustion of natural gas and air at atmospheric pressure indicate that perturbations of pressure add materially to the formation of oxides of nitrogen. More recent experimental investigations[10-12] have shown that during oscillatory combustion the

residual quantities of the oxides of nitrogen may be as much as 50 times that encountered during steady combustion. It was also found that[10] the frequency of the perturbations is of greater importance than their magnitude in the formation of oxides of nitrogen. Thus, as an effort to eliminate the formation of oxides of nitrogen for the sake of the increasing air pollution problem, a more detailed understanding of the nature and the driving mechanism of heat-driven oscillations during combustion appears to be desirable.

During oscillatory combustion, the excitation of spontaneous oscillations may depend on various mechanisms. But in the presence of energy source, the most important mechanism may well be the response of the energy source to the perturbations in the gas flow. The energy released by the energy source may not be inherently periodic, but the reaction of the energy source to the disturbances in the gas flow induces a periodicity in the release of energy. The result is that oscillations will be promoted if the energy thus added is sufficient to overcome the damping losses of the disturbances.

Heat-driven oscillations have been reported to be observed in almost every type of flow combustor[1,13]. The most common of all the types of combustion oscillations

is the "organ-pipe". In the organ-pipe acoustic oscillation, the wavelength of the oscillation is related to the long dimension of the combustion chamber. The gases usually travel along this dimension through the combustion chamber so that the oscillations are also recognized as in a longitudinal mode. The oscillating component of the flow may be considered as a movement of the gases back and forth along the axis of the combustor. The well-known phenomena of singing flame[14,15] and gauze tones[16,17] are all included in this category. There are also combustion oscillations of the transverse type for which the wavelength is related to a transverse dimension of the combustor. In most cases the combustion chamber is of a cylindrical shape, the transverse mode of oscillation should then be replaced by both radial and tangential modes. However, the organ-pipe acoustic oscillation is considered far more important than the transverse type, although the latter has become increasingly important in recent years[18-21].

In the longitudinal mode, the oscillations are prevailingly in standing-wave form. However, traveling waves have also been encountered in some combustion systems[22-24]. It appears that there is no inherent reason why both standing waves and traveling waves can not exist

simultaneously. Consequently, there can be oscillations of both these wave forms. In fact, a standing wave may be considered as a superposition of two traveling waves of the same amplitude that travel in opposite directions [25]. Records of the combined modes of both wave forms have been reported[26] although the standing-wave mode normally predominates in a cylindrical combustor.

A complete understanding of the nature of oscillatory combustion has not yet been resolved. Quite divergent points of view are held by various investigators as to the proper method to apply in an attempt to analyze a problem of combustion oscillation. The purpose of the present work is directed to a more detailed understanding of the combustion oscillations that were encountered in a long, cylindrical combustor. Measurements of the perturbations in pressure were conducted in a premixed flame of air and natural gas at a mixture ratio of about 90 per cent stoichiometric. It should be pointed out here that the measured perturbations are not exactly the same in all directions owing to the contribution of the bulk flow of the combustion gases. Such contribution amounts to approximately 3% of the total perturbation of combustion. For this reason, the maximum perturbations measured in a plane normal to the direction of the flow have been called

the perturbations of normal stress[11,12]. However, it is preferable to designate them as the perturbations of pressure hereafter in order to be in agreement with the literature[1,22,23].

In portions of the experimental work, measurements of the perturbations of the total optical intensity and of the monochromatic intensities were made, along with the measurements of the perturbations of pressure. The effect of mixture ratio upon the frequency and the amplitude of the combustion oscillations has also been investigated for a full-length open combustor of 168 in. Emphasis was placed upon the investigation of the longitudinal resonant phenomena that were observed as the length of the combustor was varied. A driving mechanism of the combustion oscillation is proposed and is examined in the light of Rayleigh's criterion[27]. The observed results are to be compared with those predicted based upon this proposed driving mechanism.

II. THEORETICAL APPROACHES AND LITERATURE REVIEW

There are essentially two ways whereby the problems concerning combustion oscillations are analyzed and solved. One approach emphasizes a formal analytical solution or an approximate solution to the one-dimensional flow equations governing the combustion process. These differential equations have to be linearized, some simplifying assumptions have to be made, and the perturbation theory has to be employed in most cases before the differential equations can be finally solved. The other approach prefers a semi-quantitative solution by means of the description of a physical model[1]. This technique usually involves the application of the important features of a driving mechanism so that certain ranges in which oscillations can occur may be determined. The well-known Rayleigh's criterion of driving[27] is considered to be the most important tool in this category. For the convenience of comparing this work with the theoretical and the experimental studies made by the other investigators, those previous works directly related to this investigation are reviewed as the situation arises.

A. THEORETICAL APPROACHES

Consider a simple model of a flow system consisting

of a straight section of a tube with constant cross-section. For simplicity, the heat source is assumed to be concentrated in a plane perpendicular to the axis of the tube so that we have a disk-shaped heat source with negligible thickness. Now the following equations can be written for this flow system[28]:

Equation of Continuity:

$$\frac{\partial \rho}{\partial t} + \nabla \cdot (\rho \vec{v}) = 0 \qquad (1)$$

Equation of Momentum:

$$\rho \left\{ \frac{\partial \vec{v}}{\partial t} + (\vec{v} \cdot \nabla)\vec{v} \right\} = -\nabla P + \mu \left\{ \nabla^2 \vec{v} + \frac{1}{3} \nabla (\nabla \cdot \vec{v}) \right\} \qquad (2)$$

Equation of Energy:

$$\rho c_p \frac{DT}{Dt} = k \nabla^2 T + \left(\frac{\partial \ln V}{\partial \ln T} \right)_p \frac{DP}{Dt} \qquad (3)$$

For an ideal gas, $\left(\partial \ln V / \partial \ln T \right)_p = 1$. Equation (3) becomes

$$\rho c_p \left\{ \frac{\partial T}{\partial t} + (\vec{v} \cdot \nabla) T \right\} = k \nabla^2 T + \frac{\partial P}{\partial t} + (\vec{v} \cdot \nabla) P \qquad (4)$$

These three conservation equations, along with the equation of state for an ideal gas, furnish an adequate basis for analytical solutions.

A formal procedure for solving this set of differential equations is the application of the principle of dynamic stability[29] which means that small fluctuations are superimposed upon the steady-state flow of the gas. Thus, all the variables may be split into steady-state and oscillating components. A very important feature of this method is that the fluctuating component of each variable may be assumed to be proportional to a time factor $\exp(-\beta t)$, where β is a complex parameter. Then the stability of this flow system depends solely upon the value of β ; the flow becomes dynamically unstable and is capable of producing spontaneous oscillations if the real part of β is negative, the reverse is also true. From the foregoing differential equations and their relevant boundary conditions, a characteristic equation in terms of β can be derived. Therefore, the main problem is the derivation and solution of this characteristic equation, which involves linearized treatment, as well as the application of perturbation methods.

In a series of papers, Merk[29-33] has provided a very detailed systematic analysis for this problem. In his analysis, Merk regarded the oscillation as consisting of three components: an acoustic mode, an entropy mode, and a vorticity mode. He eliminated the vorticity mode

from consideration by limiting the wave propagation to one-dimensional model. He noted that upstream of the heat source the oscillations are mainly acoustic, but downstream of the heat source there exist both the acoustic and entropy modes of the oscillations. The three conservation relations are then established across the flame front to match the acoustic fluctuations. Through a series of linearized treatment, Merk finally expressed his transfer function in terms of acoustic admittances at the two sides of the flame; the real part of this equation provides the instability criterion, while the imaginary part can be used to determine the frequency of the oscillations.

Blackshear[34] provided a one-dimensional analysis for the explanation of the mechanism whereby a flame drives or damps a standing wave. He based his analysis on the following mechanism: Waves pass through the flame front with their velocity amplitude unaltered. When the net velocity causes a change in the flame front area, waves are propagated simultaneously into the hot and cold gases. These flame-generated waves will drive the standing wave when they are phased with the existing components of the standing waves. The strength of the wave was found to depend largely upon the relative magnitude of

the disturbance of the flame area and its phase relation with the perturbation velocity.

Bailey[35] studied the combustion oscillations produced by a flame burning above a grid from both the experimental and theoretical standpoint. He assumed that no time lag was involved in this oscillating system and that the important damping forces were the radiation losses occurring at the ends of the tube. Then, a linear, one-dimensional theory was presented, taking into account both the driving and damping effects in the system. The resultant instability criterion was found to be in accordance with Rayleigh's criterion.

In their theoretical investigation of combustion oscillations in rocket systems, Crocco and Cheng[22,36] emphasized the aspect of time lag by neglecting the feedback effect which was employed by most of the other investigators. They then developed an instability criterion in terms of the delay time. They found that the time lag for excitation of organ-pipe oscillations must be within certain intervals and that there exists a specific steady-state relation between time lag and pressure.

It should be pointed out that Crocco and Cheng used conservation relations for momentum and mass across the

flame front to set up their equations, whereas Merk used conservation relations for momentum and energy. In this connection Merk[29] explained that to match the acoustic fluctuations the laws of conservation of momentum and energy must be used since these laws contain only acoustic quantities, while the law of conservation of mass determines the non-isentropic fluctuations in the vicinity of the heat source.

Putnam and Dennis[1,13], and Roginskii[37] have presented an excellent survey of the literature on flame-driven oscillations of the organ-pipe type.

B. RAYLEIGH'S CRITERION OF DRIVING

Rayleigh[27] was the first to give a satisfactory explanation of the singing-flame phenomenon which is associated with the noise emanating from a tube with a flame in it[38]. He later generalized his explanation to a fundamental postulate applicable to all gas-column oscillations sustained by heat. Rayleigh's hypothesis is summarized in the following manner: In any problem involving the driving of oscillations by heat, the basic issue is the relation between the heat transfer and oscillation phases. If heat is imparted to the gas at

the instant of maximum compression, or is abstracted from it at the instant of maximum rarefaction, the oscillation is encouraged, the converse is also true. When the transfer of heat takes place at the moment of either highest or lowest pressure,the oscillation frequency is not affected. If, however, the gas has a density equal to that under quiescent condition at the instant of heat transfer, the frequency will be altered, but not its amplitude. It should be noted that Rayleigh's postulates presuppose the presence of standing pressure waves in the combustion system. Rayleigh also pointed out that the amplitude of the sound depends primarily on the length of the combustion column, while the flame merely serves to restore the damping losses associated with the combustion system[1].

Thus it is easy to visualize from the above statement that, except at the pressure nodes and antinodes, alteration of both the amplitude and frequency is produced by a periodic transfer of heat from the heat source to the gases. The oscillation is augmented if the addition of heat takes place within the interval when the pressure is greater than its average value. To iterate, heat must be added to the gas at a time less than a quarter period either before or after the time corresponding to maximum

pressure, and vice versa. Similarly, the frequency is raised if heat is added to the gas within a half period before the occurrence of the highest pressure, and is lowered if heat is added to the gas within a half period after the occurrence of the highest pressure. Obviously the increase in frequency attains a maximum when heat is added to the gas exactly at the instant of a quarter period before the phase of highest pressure.

It should be emphasized that the aforementioned addition or transfer of heat is in fact the addition or transfer of energy across the boundary of a system. The need for this distinction results solely from the necessity of dealing with friction which is very complicated in nature. Thus, the gain in internal energy of the system will be equal to the net transfers of energy from the surroundings, without regard to whether these transfers are accomplished by thermal means or mechanical means or by both combined[39].

Wood[40] has devised an ingenious graphical presentation for the physical interpretation of Rayleigh's criterion. He considered the increment of energy as being proportional to a corresponding increment of pressure. Thus a picture indicating the relation between the sus-

taining of oscillations and the phase shifts can be clearly seen.

Putnam[1] gave a more detailed explanation of Wood's graphical presentation. To explain flame-driven oscillations, Putnam and Dennis[41] proposed a mathematical formulation of Rayleigh's criterion in the form:

$$\int_{\text{cycle}} Hp' \, dt > 0 \qquad (5)$$

where H is the rate of heat release and p' is the oscillating component of the pressure. Driving is considered to occur when the above inequality is satisfied. In separate papers, Putnam and Dennis investigated experimentally the acoustic oscillations occurred in multiple-port rocket-shape burners[42] and in a burner with deep ports[43]. The observed results were all examined by means of Rayleigh's criterion. Furthermore, in order to justify the expression given by Equation (5), Putnam and Dennis[42] presented a thermodynamic analysis of phase requirement for heat-driven oscillations.

Some refinements and revisions have then been made upon Rayleigh's criterion. Raushenbakh[44] showed that Rayleigh's treatment involved an error in considering heat source of energy as the only energy source available for

the excitation of oscillations. In fact, acoustic energy evolves not only from a source which includes both heat and internal energy, but also from any source of kinetic energy. Therefore, in cases the kinetic energy becomes important, the excitation of oscillations is sometimes possible even if the heat liberation is out of phase with pressure. Chu[45,46] studied Rayleigh's postulates in detail and found that they are valid only if the amplitude of the oscillations is low and the ratio of isobaric to isochoric specific heats remains constant across the flame front. However, these assumptions are considered to be fulfilled for most combustion systems.

C. COMPARISON BETWEEN BOTH APPROACHES

It is generally believed that a formal analytical solution to the differential equations governing a combustion process furnishes the clearest and most detailed information for the oscillating system. Such an approach should lead to a thorough explanation of all observed results subject to the given boundary conditions. Nevertheless, in practice, this situation is very seldom attainable because of the mathematical complexity. Up to the present, linearized treatments still have to be employed

in most cases even for the simplest, one-dimensional model of a combustion system. The use of linearized treatment and of other simplifying assumptions tends to oversimplify the problem. Some modes of oscillation may be eliminated from consideration, and the predicted results may depart appreciably from the real physical situations. Moreover, a clear picture of the physical aspects of the problem is apt to be lost in the process of detailed mathematical treatments. The final form of the analytical solution is usually so complicated that a suitable physical interpretation is often found to be very difficult to obtain. Furthermore, there may be a wider variety of driving mechanisms predicted than actually exist due to the large number of variables involved, and the non-linear characteristics of an oscillating system are not in general identified in a linearized solution[1].

The application of Rayleigh's driving criterion usually does not provide complete information for an oscillating system. The ranges of frequency in which oscillations are possible may be determined by the instability criterion, but not its amplitude. However, the most important feature of nonlinearities for a combustion system is preserved in this treatment. In addition, the mathematical manipulations for this approach are far

simpler than those for analytical solutions. This method has been shown to be successful for the explanation and correlation of some observed oscillation results[42,43]. For this reason, it will be employed as the principal theoretical basis for the analysis of the current experimental work.

III. EQUIPMENT

The equipment employed in this investigation consisted of a water-cooled combustion tube mounted in a vertical position. The tube was used earlier for studies of combustion in a turbulent diffusion flame[8,47]. The combustor was constructed of a heavy-walled copper tube 3.826 in. in inside diameter and 162 in. long. An appropriate mixture of air and natural gas was introduced into the lower part of the combustor and passed through a perforated copper-plate flameholder. The combustible mixture was then ignited by means of an electric spark located just above the flameholder. A cooling jacket surrounded the tube, and ports were provided along the wall of the combustor to permit measurements of pressure perturbations and the time-averaged apparent temperature as a function of the distance along the combustion zone. A silencer was installed at the exit of the combustor in an effort to minimize acoustic discomfort in the surrounding area. In many occasions an afterburner was inserted into the upper part of the combustor to ensure more complete combustion of the exhaust gases. The arrangement of the combustion tube is shown schematically in Figure 1.

Air and Gas Supply Systems

Air was supplied by a pair of centrifugal blowers

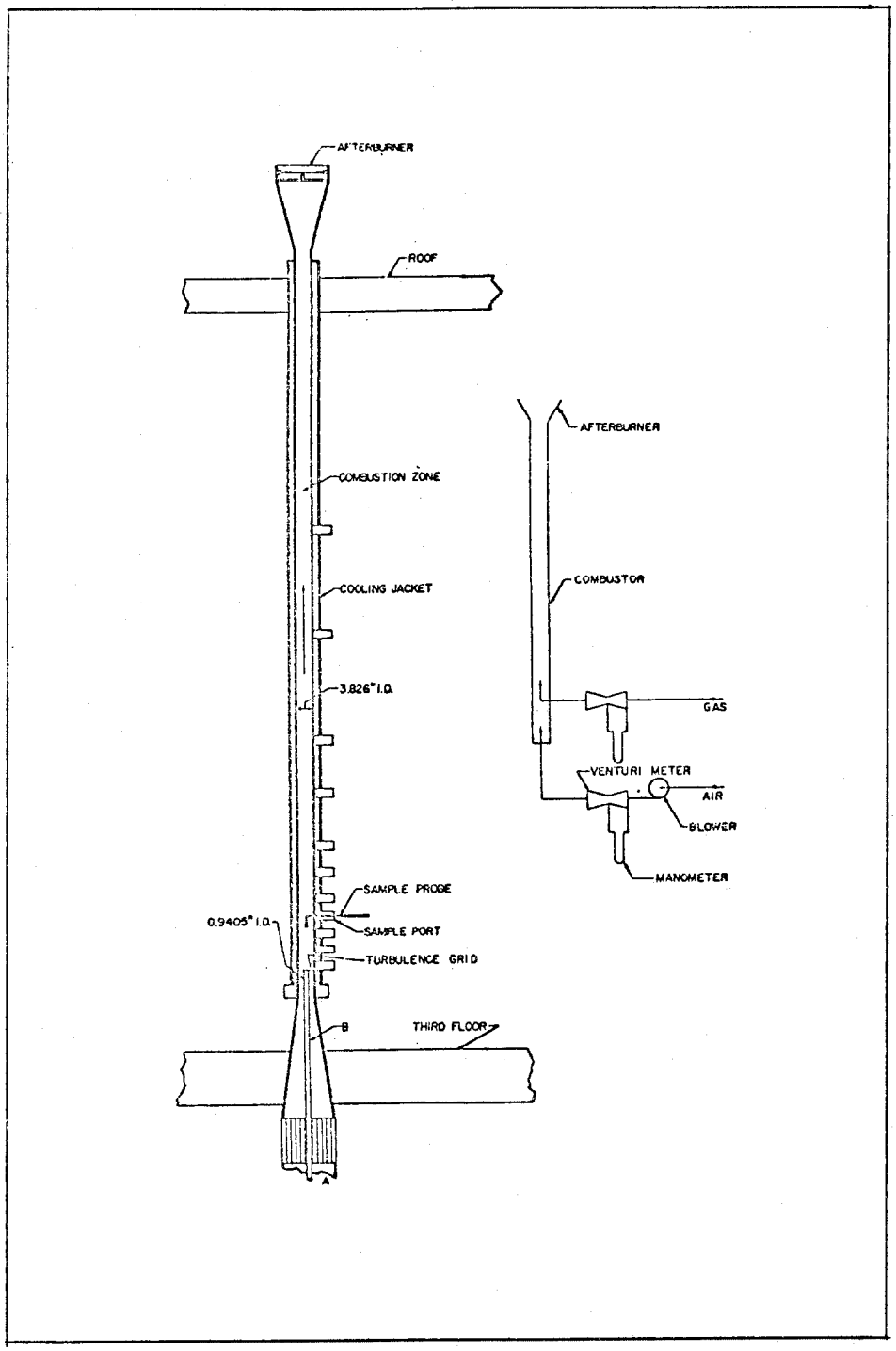

Figure 1. General Assembly of the Combustion Tube.

driven by a D.C. motor, the speed of which was controlled by a quartz oscillator and a preset counter[48]. The flow rate of air was established through the use of a Venturi meter which was calibrated in accordance with existing standards[49]. Kerosene-in-glass manometers were employed in conjunction with a cathetometer for the measurement of pressure differences. The natural gas was supplied at a pressure of approximately 18 psia. and its flow rate was determined by means of a small calibrated Venturi meter. The flow rates of both the air and the natural gas were known within approximately 0.5 per cent after suitable calibrations.

Plenum Chamber

Air and natural gas were mixed in a small plenum chamber about 1.0 sq. ft. in cross section and 1.0 ft. high. The mixing process was carried out by injecting natural gas through many small holes provided on a rank of parallel tubes in the plenum chamber. The gas mixture then passed through some straightening vanes for stablizing purposes, a flame arrestor, and a flameholder. Figure 2 shows a schematic diagram of the air and natural gas supply systems and the mixing chamber. A blow-out plate was shown on the air supply duct to ensure safety for this section.

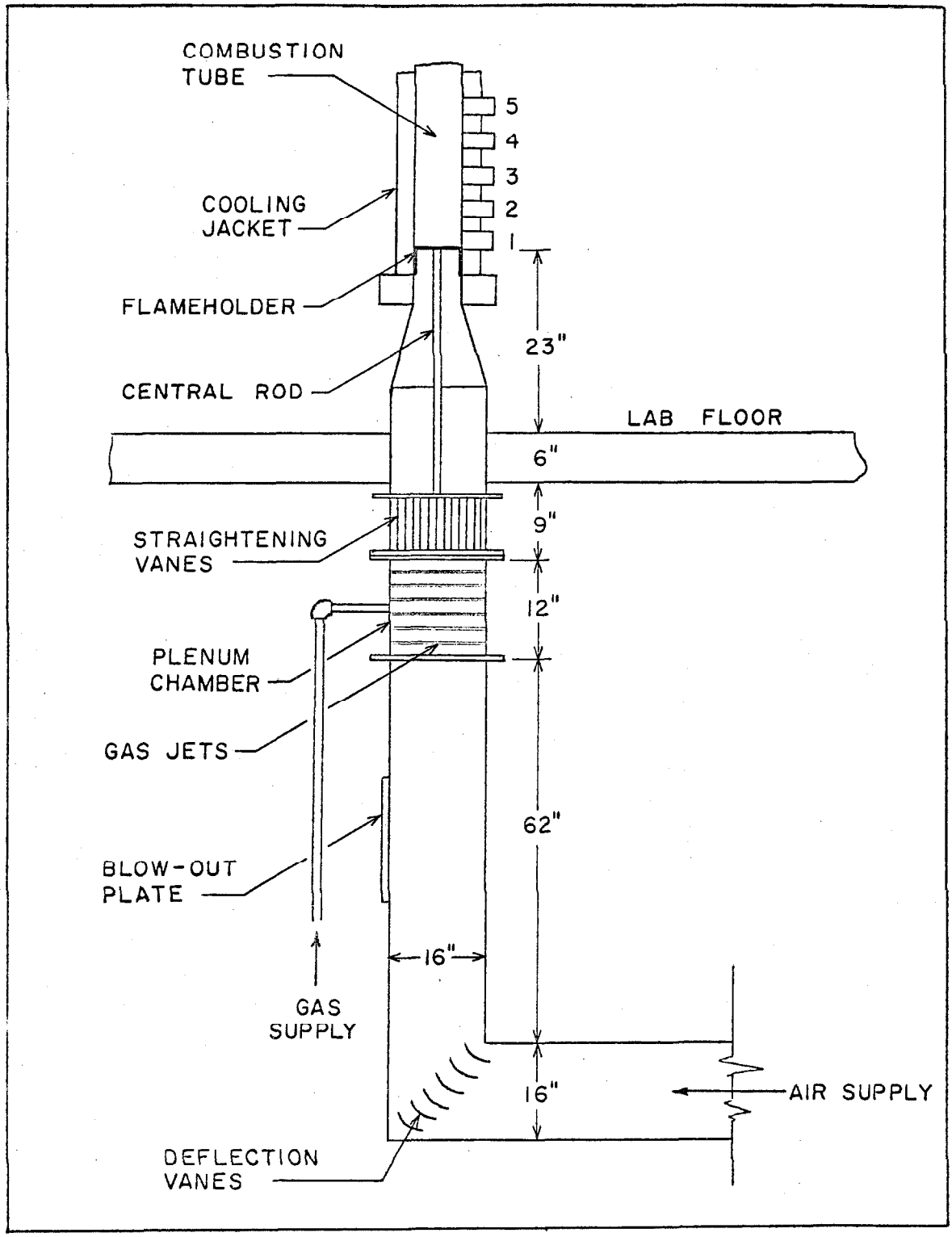

Figure 2. Lower End Details of the Combustor.

Flameholder

The flameholder was constructed of copper and was sealed to the wall by an O-ring so that the entire cross section of the combustor could be covered. The grid set employed in this investigation consisted of a flat plate 0.187 in. in thickness with 0.0625 in. diameter sharp-edged holes on 0.250 in. centers. This grid set was identified as "Grid 7 C" , as shown in Figure 3. A short, four-vane baffle was placed above the flameholder. The holes were free from burrs and other gross imperfections. An effort was made to maintain the same velocity in all the holes of the flameholder. In the course of experimental measurements the perforations in the flameholder were found to have decreased to a diameter of approximately 0.0617 in.

Ports

The arrangement for the location of eleven ports is indicated in Figure 4. The first port was used primarily for ignition and for visual observation of the combustion. The second port was employed to provide spark ignition and temperature measurements when required. The average pressure in the combustion chamber was usually measured at port 5 which was located 16.7 in. above the flameholder. The rest of the ports were used for the measurements of

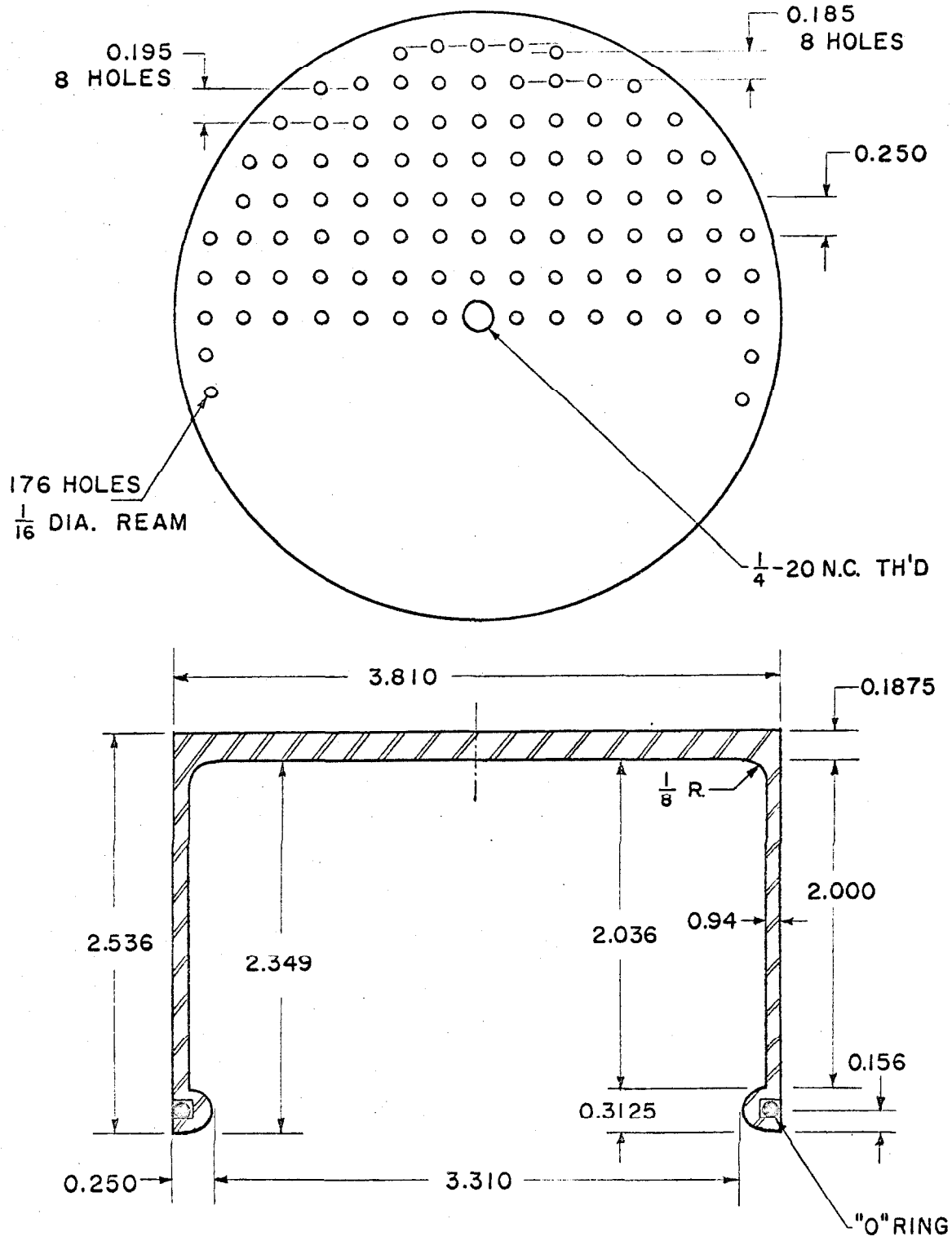

Figure 3. Details of the Flameholder "Grid 7 C".

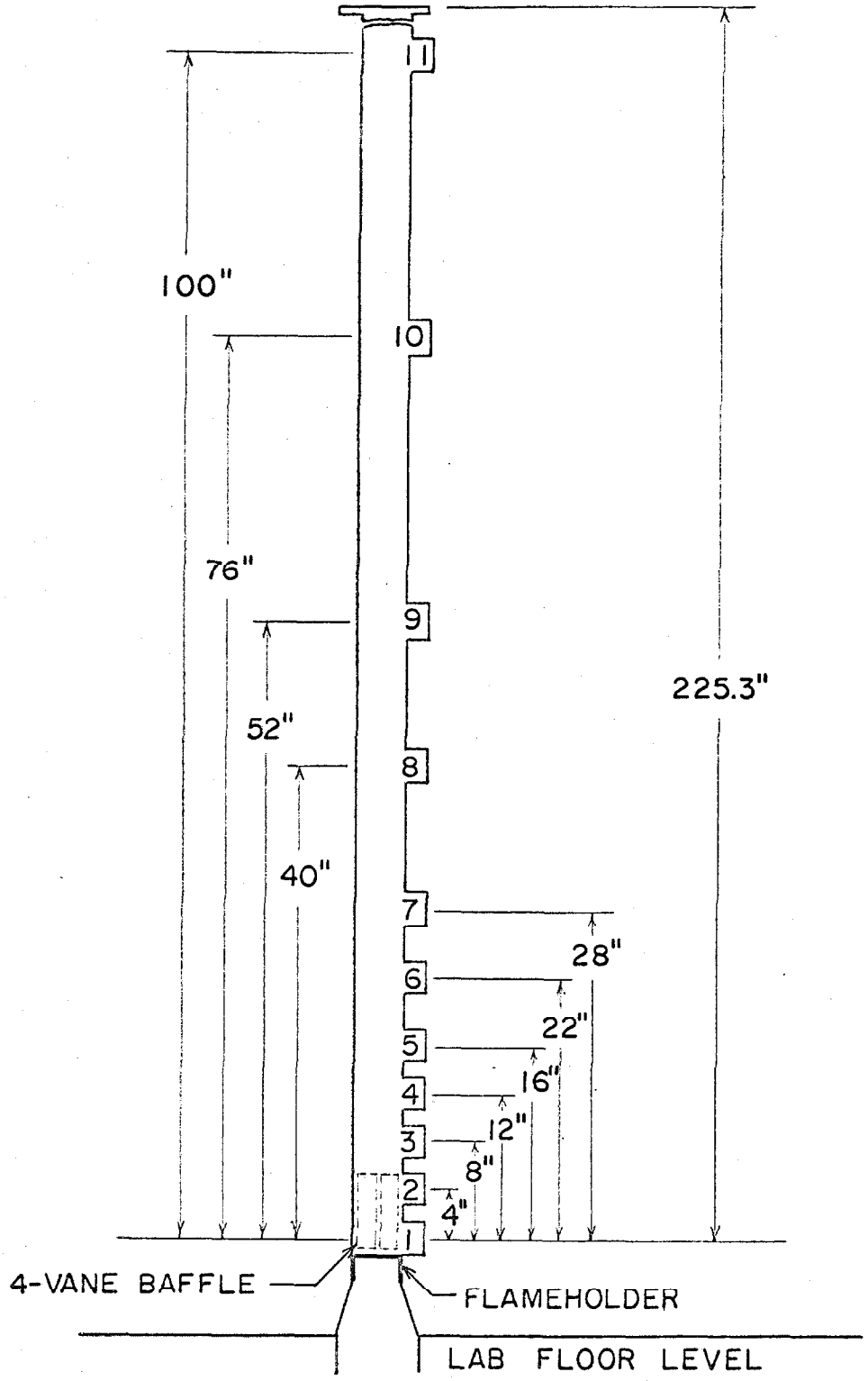

Figure 4. General Arrangement of the Ports.

pressure perturbations and of time-averaged temperature, as well as for withdrawal of samples. However, measurements of pressure perturbations in this work were only made at ports 4, 6, and 10, corresponding to 12.7, 22.7, and 76.7 inches from the flameholder.

Pressure Transducers

Water-cooled, condenser-type, pressure transducers manufactured by Photocon Research Products were used for the measurement of the perturbations in pressure, as shown in Figure 5. The transducers possessed a linear response up to frequencies of approximately 10,000 cycles per sec. and a sensitivity of 0.01 psi. In order to increase the linearity of the response, the transducers were employed without a flame shield. This technique avoids difficulties arising from the accumulation of water between the active diaphragm of the transducer and the flame shield. Conventional single- and dual-beam cathode-ray oscilloscopes were used in conjunction with the transducers to obtain a visual trace of the behavior of the system. In addition, photographs were taken of the oscillograph traces for quantitative measurements.

Reflecting Disk

In order to understand better the effect of the length of the combustor upon the oscillating conditions

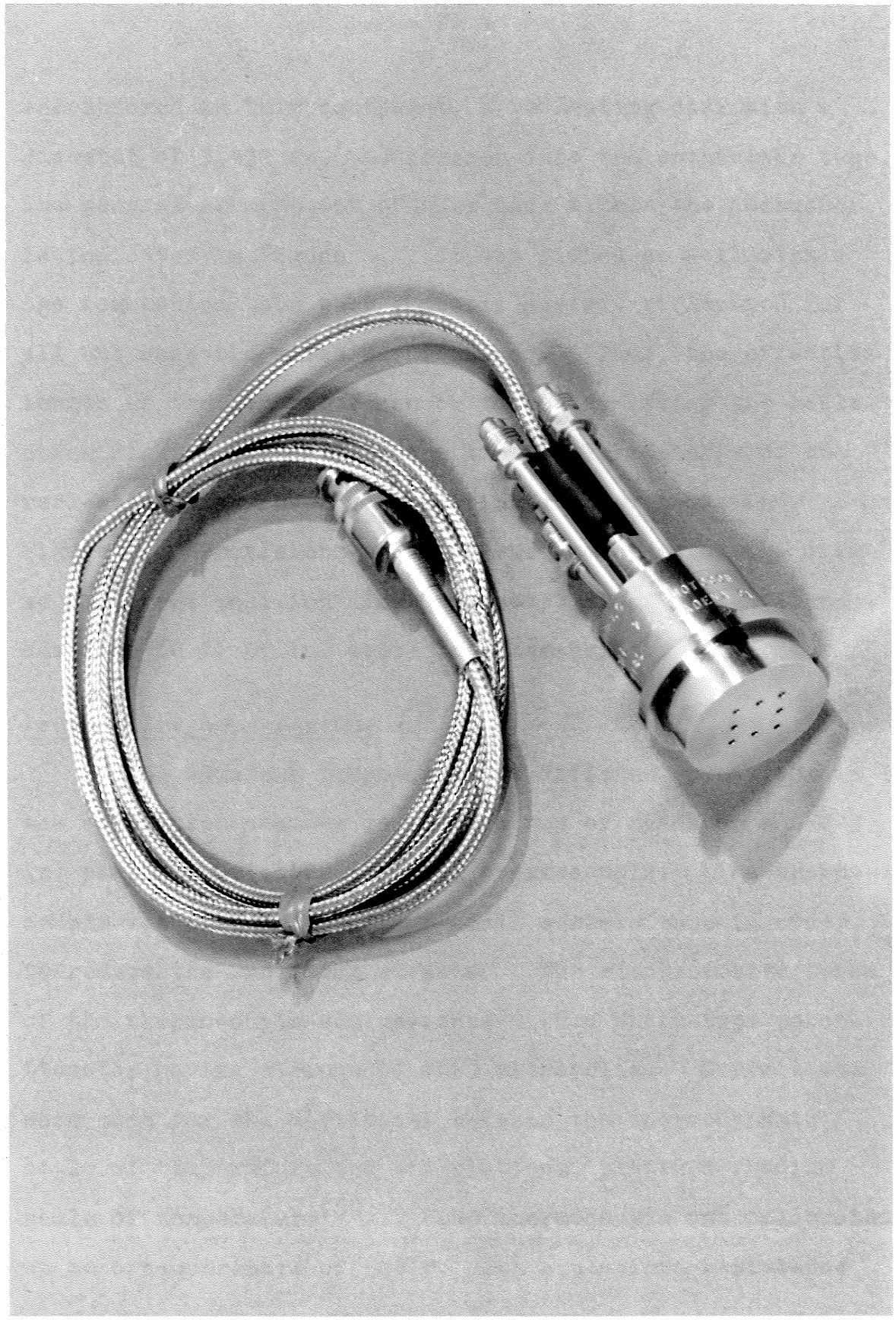

Figure 5. A Photographic View of the Pressure Transducer.

encountered in this equipment, a reflecting disk with a diameter of 3.435 in. was lowered into the combustion tube. The general arrangement of this disk within the combustor is indicated in Figure 6. It was fitted so well within the combustion tube that a nearly perfect reflection for all the acoustic waves was obtained. Thus, the effective length of the combustor can be varied by moving the reflecting disk up and down in the tube. The details of the reflecting disk and its supporting rod are shown in Figure 7. Provisions were made for movement of the disk to different position along the combustion tube at distances from 60 to 90 in. above the flameholder.

Temperature Measurements

The apparent temperature at different positions in the combustion chamber was determined by means of a 0.003 in. platinum / platinum-rhodium thermocouple. The thermocouple was shrouded within a small ceramic tube in order to reduce the radiation effects. The electromotive force of the thermocouple was measured with a White-type potentiometer having a range of 1000 microvolts. Corrections were made for the deviations between the thermodynamic scale of temperature and the platinum / platinum-rhodium scale of temperature[50]. The thermocouple was calibrated up to a temperature of 500°F. with a platinum resistance

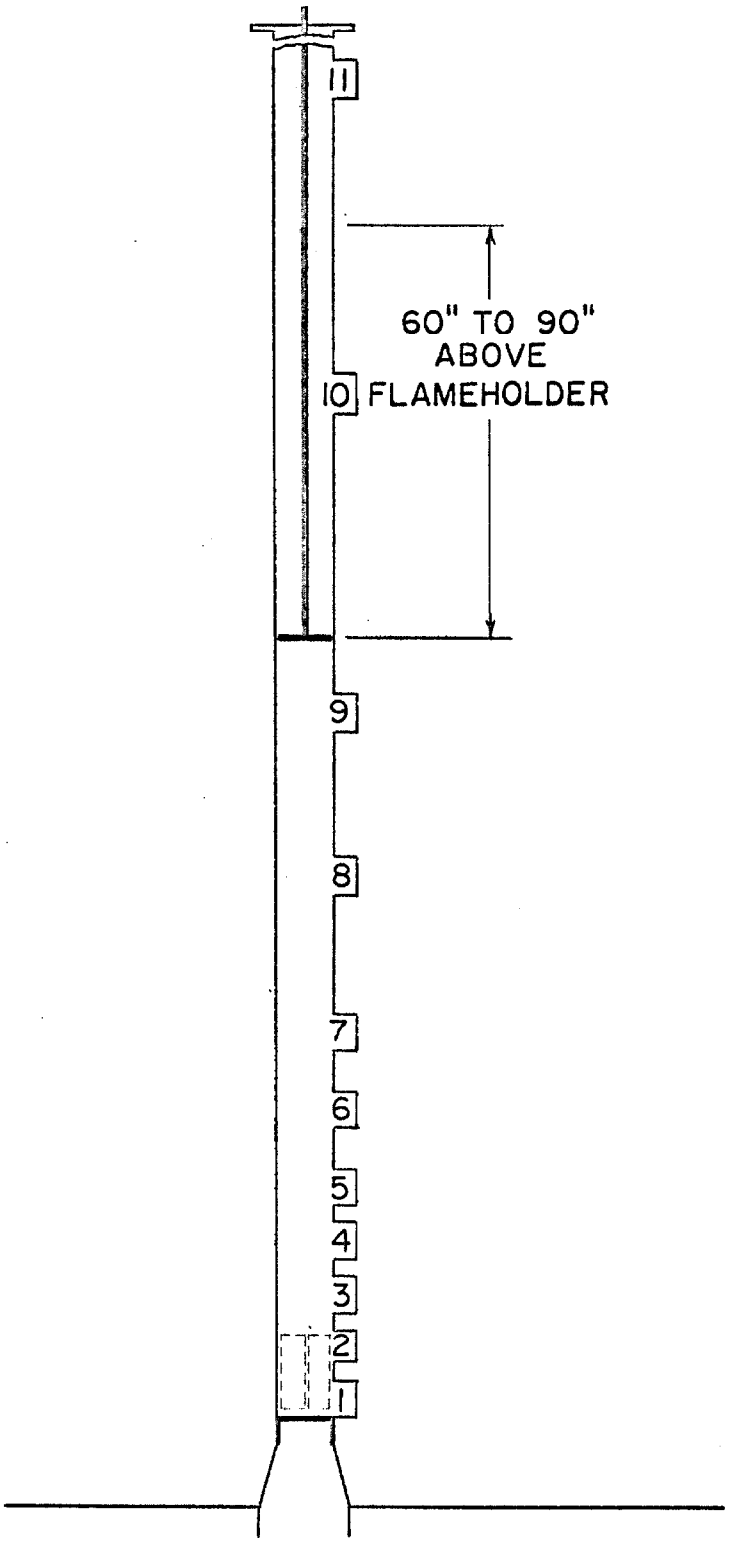

Figure 6. General Arrangement of Reflecting Disk within Combustor.

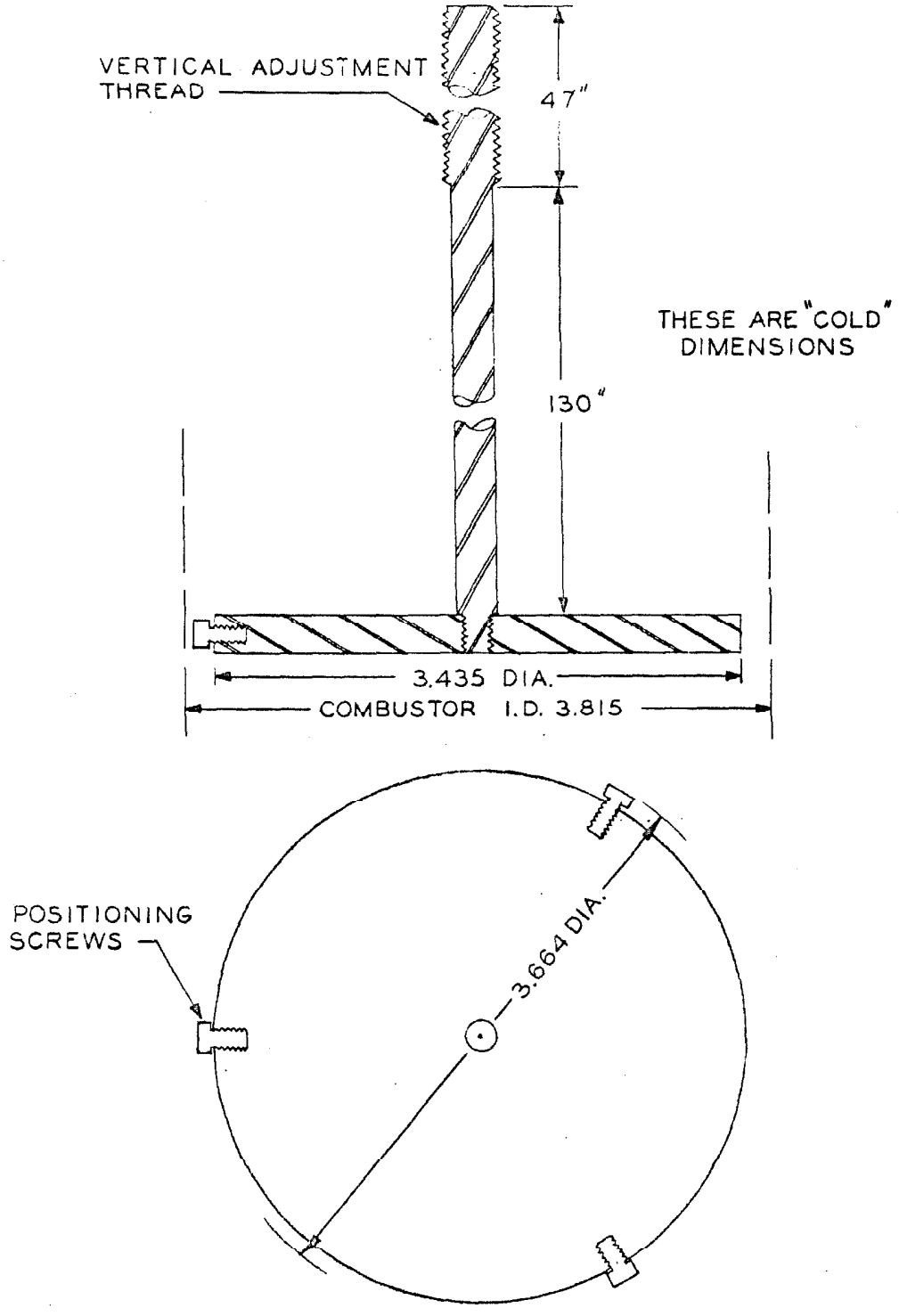

Fig. 7. Details of Reflecting Disk and Supporting Rod.

thermometer of the strain-free type which had been calibrated by the National Bureau of Standards. Above this temperature the characteristics of platinum/platinum-rhodium thermocouples from available tabulations[51] were used. The shrouded thermocouple, however, was not employed at apparent temperatures in excess of 2000°F. owing to rapid deterioration. Because of the uncertainties arising from radiation and possible catalytic effects, the indications of the thermocouple were not believed to be the actual temperature. Therefore, all temperatures have been designated as apparent temperatures. Nevertheless, the measurements of the thermocouple were at least indicative of the approximate temperature range encountered in the combustor.

Total and Monochromatic Optical Intensity

In addition to the measurement with pressure transducers as described above, the perturbations of combustion were also established in terms of total and monochromatic optical intensities in portions of the experimental work. In essence the equipment for the measurement of total optical intensity consisted of a self-reflecting collimator and a photo-sensitive element. In this study the photo-sensitive element employed for the determination of total optical intensity was a Type P-2 lead sulphide photocon-

ductive cell manufactured by Eastman Kodak Co. The total optical intensity of the hot gases was first detected by means of the collimator through a fused aluminium oxide window located approximately 10 in. above the flameholder. The output of the collimator was focused upon the photoconductive cell, the output of which was then transmitted to a Model 150 A Hewlett-Packard oscilloscope equipped with recording film[11]. The equipment for the establishment of monochromatic optical intensity was also available. A monochromator was used in lieu of the collimator. The output of the monochromator was then transmitted to a Type N-2 lead sulphide photoconductive cell.

IV. EXPERIMENTAL METHODS

To initiate the operation, air and natural gas were introduced into the combustor at the desired mixture ratio and flow rate, and combustion was initiated by an electric spark. After a period of about 10 minutes the temperature of the cooling water attained a steady value. The effect of the minor variations in the temperature of the incoming air and natural gas upon operation at this point was disregarded. After approximately 15 minutes of operation, quasi-steady state was reached and measurements of the perturbations in pressure were initiated. The combustion process was usually terminated after two to three hours of continuous operation.

Both single- and dual-beam oscilloscopes were employed in conjunction with the transducers for the establishment of perturbations in pressure. The use of the dual-beam oscilloscope permitted two sets of measurements to be recorded at the same time. Thus a direct evaluation of the phase relationships of the data from different ports was possible. In addition, the amplitudes and frequencies of the oscillations that occurred simultaneously at two different ports could also be compared.

All of the measurements with the reflecting disk

were carried out at a mixture ratio of approximately 90 per cent stoichiometric, unless otherwise specifically indicated. The effective length of the combustion tube for these measurements was varied by gradually moving the reflecting disk up and down between 60 and 90 in. above the flameholder. Also for each test, several measurements were made in which the position of the reflecting disk was chosen at random in order to determine the reproducibility of the measurements. It was found that the measurements were reproducible within the precision of measurement of the primary variable. In portions of this study, measurements of the perturbations in monochromatic intensity were taken with the reflecting disk removed, which corresponded to a full-length open combustor of 168 in. in length. Under such condition, the length of the combustion chamber will be specifically indicated in the course of the discussion.

The weight rate of air flow was maintained at the same value within the experimental uncertainty throughout these measurements, except for a limited number of special tests where a slightly higher air flow rate was employed. Time-averaged apparent temperatures were measured frequently in the course of the measurements at various longitudinal positions, as well as several radial positions. The

time-averaged pressure was determined at port 5 by means of a mercury-in-glass manometer, and it was found that the small change in this average pressure usually resulted from the variations in the barometer.

Samples of the products of combustion were withdrawn periodically from the combustor through a sampling tube introduced through one of the ports. The port selected for this purpose in this series of measurements was port 11 which was located about 100 in. above the flameholder. During the sampling process the gas were allowed to flow slowly into an evacuated glass bulb for a period of about two minutes. The sampling tube was heated outside the combustion zone in order to avoid the condensation of water and, consequently, the absorption of oxides of nitrogen. The gross quantities of carbon monoxide, carbon dioxide, and oxygen in the gas samples were determined by conventional Orsat techniques, whereas the quantities of the oxides of nitrogen were established by means of a phenol-disulphonic acid method[52]. No attempt was made to eliminate the minor changes in composition during the sampling process.

The air used in this investigation was taken from outside the laboratory and was filtered and cleaned by means of activated charcoal. The humidity of the air was

controlled at a dew point of about 35°F. corresponding to 0.0045 pounds of water per pound of dry air. The natural gas was supplied by the Southern California Gas Co. at a pressure of 18 psia. It was dried by passing through calcium chloride before being introduced into the combustor. The composition of the natural gas was established by a mass spectrograph. Table 1 shows typical mass spectrographic analyses of the natural gas being used. Because of the minor variations in the combustion of the natural gas with time, a gas density balance was employed which enabled a first-order correction to be made to account for these small variations.

The pressure transducers were calibrated under both static and dynamic conditions. The static calibration was carried out before and after each set of measurements, and apparently there was no deterioration of their behavior during the course of the experimental work[11]. The dynamic calibration was made by treating the cylindrical combustor as a closed, gas-filled chamber which was subjected to a local increase in pressure. The rather good agreement between the oscillation frequencies and those predicted by simple acoustic theory reflects well that the response of the transducer at a frequency of approximately 1000 cycles per sec. is satisfactory.

V. EXPERIMENTAL RESULTS

Typical perturbations in pressure obtained at port 10 at a mixture ratio of 0.90 fraction stoichiometric are shown in Figure 8. The corresponding macroscopic measurements of the behavior of the system are set forth at the side of each record. Each of the three examples illustrated in Figure 8 has different values of frequency and amplitude corresponding to different effective lengths of the combustor. The rather regular variations in the magnitude of these perturbations with time are typical of the measurements that have been obtained in earlier investigations with this equipment. It was noted that in most cases the acoustic waves observed consisted of not only a fundamental tone, but also a considerable number of higher partials or overtones. However, the general simplicity and smoothness of the wave forms that were usually encountered indicate that all these overtones are of much lower intensity than the fundamental.

During oscillatory combustion a ringing sound was sometimes produced in which the ear could distinguish a high-pitched tone which is believed to be a natural overtone of the fundamental. Figure 9 shows a typical photographic view of such a sound wave recorded by a high-speed camera at port 6. The "kinks" in the wave shown in

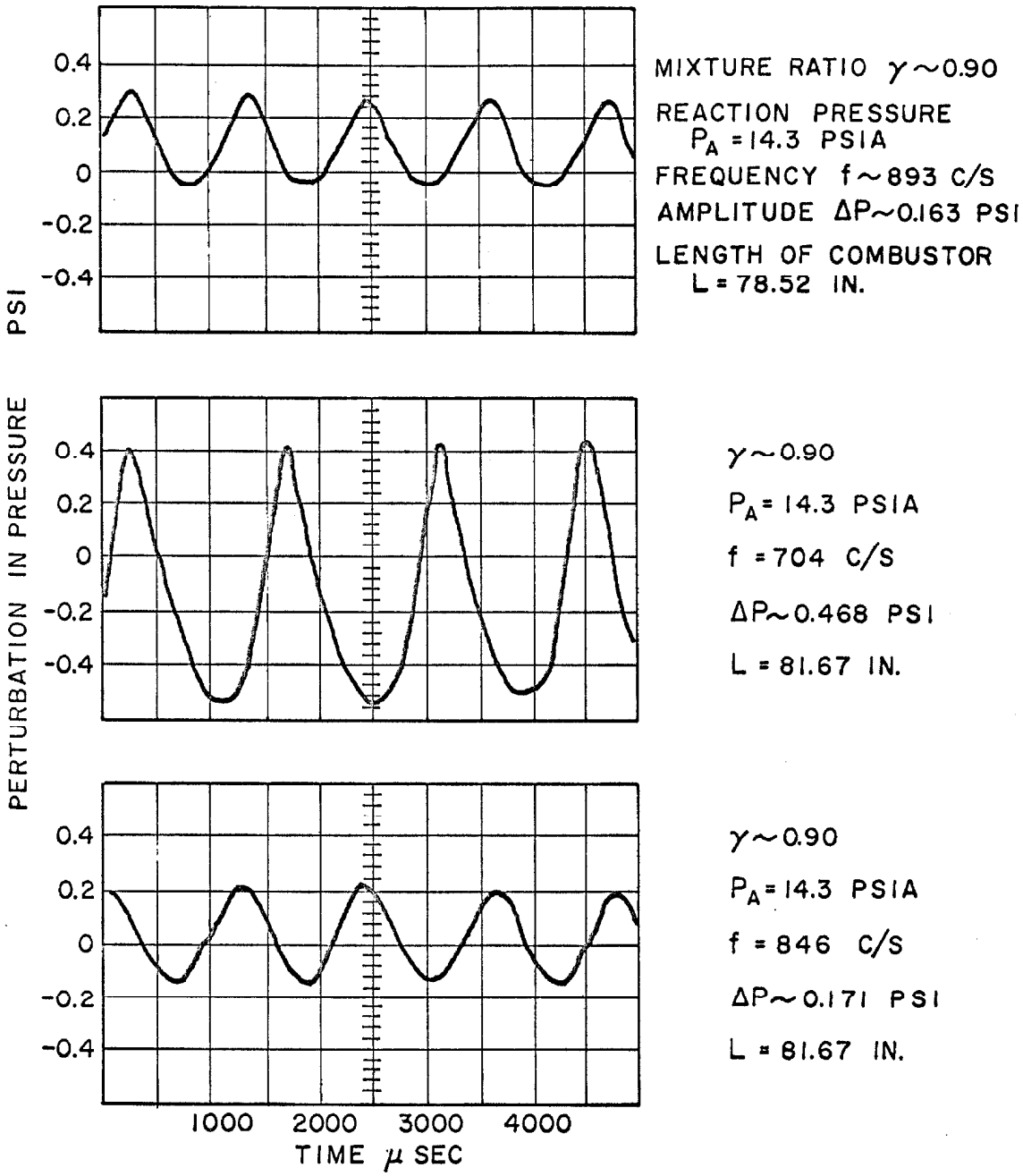

Figure 8. Three Typical Records of Perturbations in Pressure.

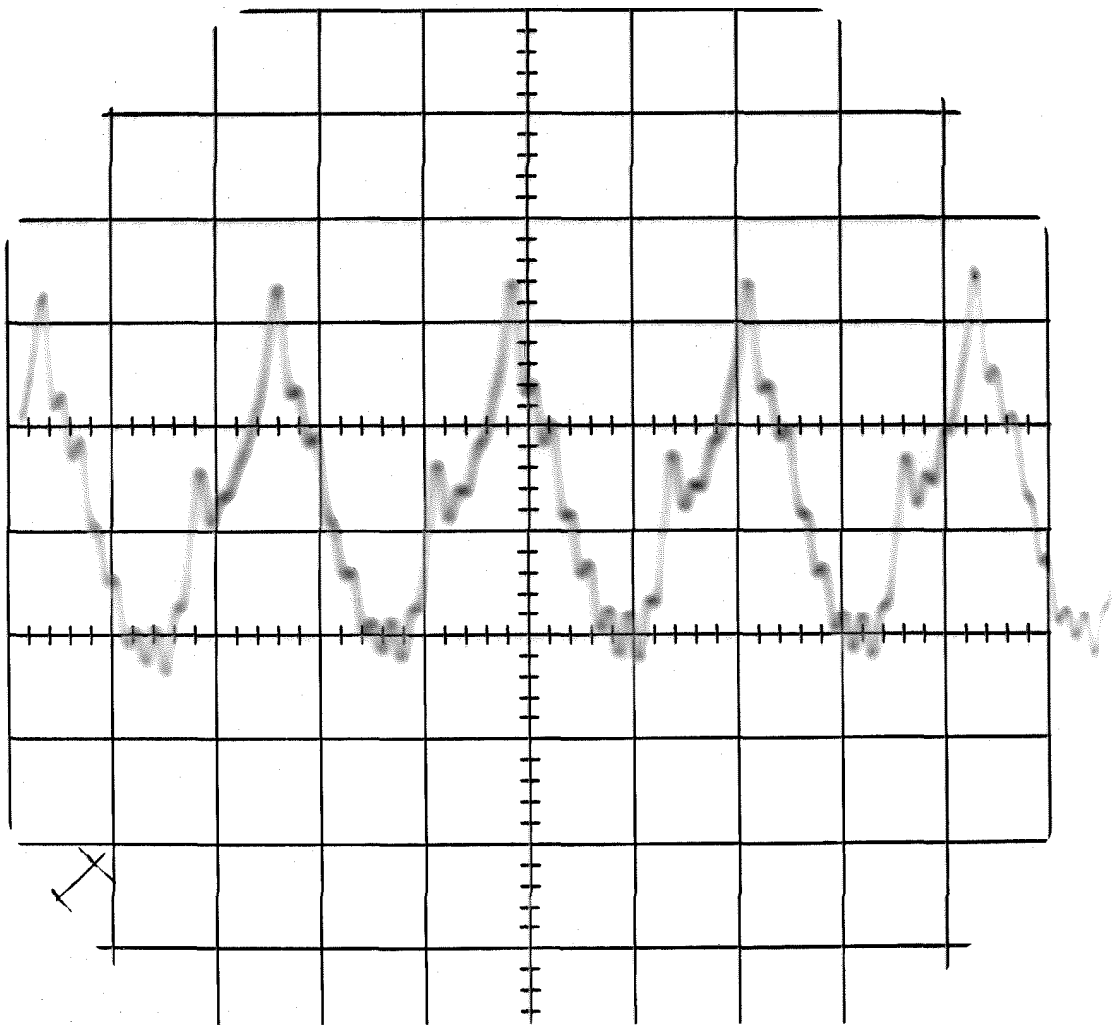

Figure 9. Sound Wave with a Strong Octave Overtone.

Figure 9 indicate the record of the overtone. Inspection shows that the frequency of the overtone is about six times that of the fundamental. In addition, the intensity of the fundamental appears to be more than ten times that of the overtone. The clanging or metallic sound was usually produced when the partials were inharmonic or out of tune with the fundamental(53).

Figure 10 shows another irregular wave form recorded at port 4. In this case the sound consisted of a fundamental tone and the octave overtone and probably some higher partials. The fundamental constitutes the greater part of the tone; the larger kink in the top of the curve corresponds to the overtone with considerable intensity, while the smaller kinks are due to the higher partials which are of much less intensity. In some instances the wavelets due to the higher partials are very pronounced in portions of the wave and almost disappear at intermediate parts which indicate that there were beats between certain partials(53).

In order to investigate the phase relationships and to compare the frequency and amplitude of the perturbations that occurred simultaneously at two ports, most of the measurements were carried out by the use of two transducers and a dual-beam oscilloscope. Figure 11 shows a typical

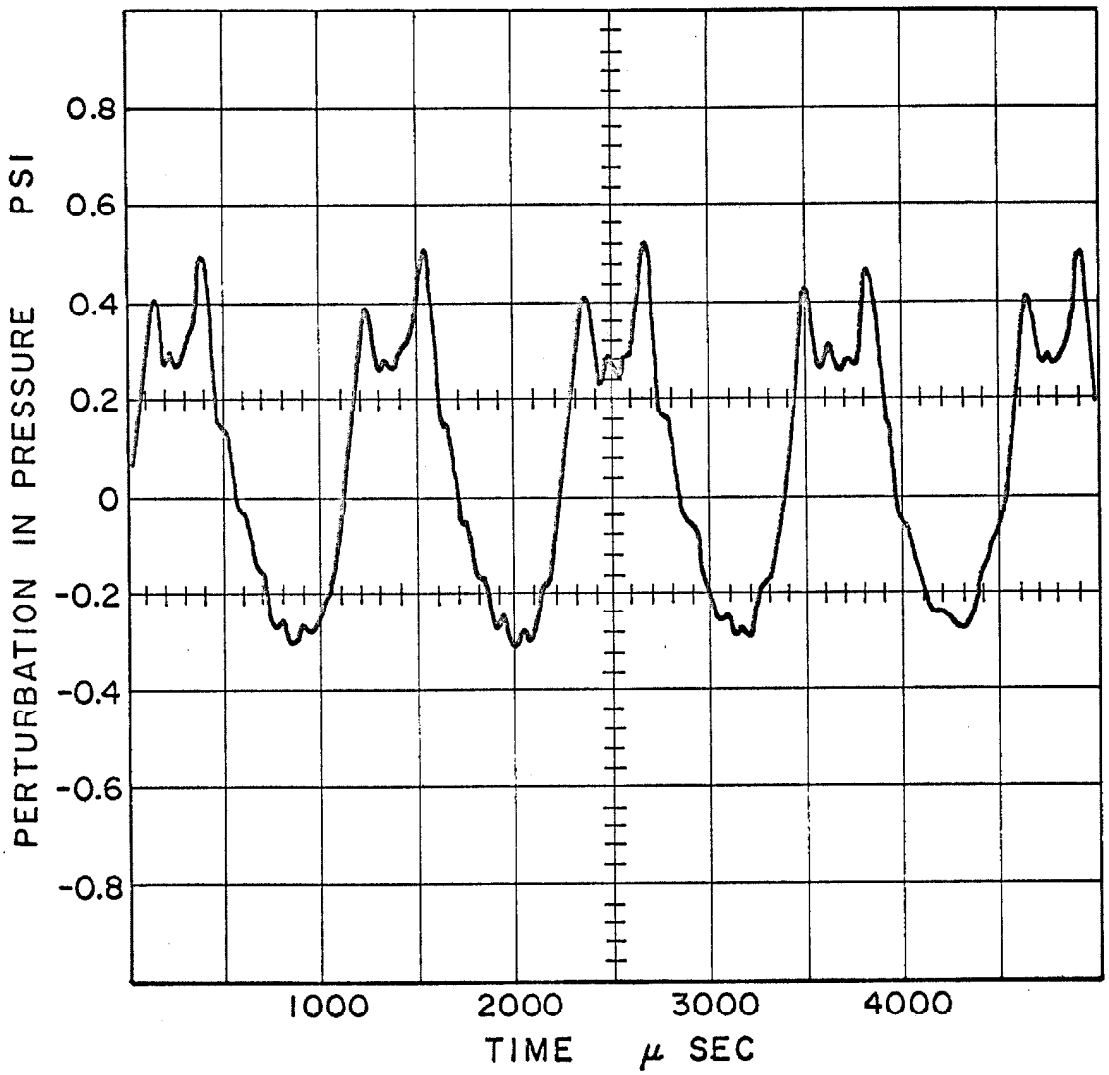

Figure 10. Typical Perturbation in Pressure with a Large Kink.

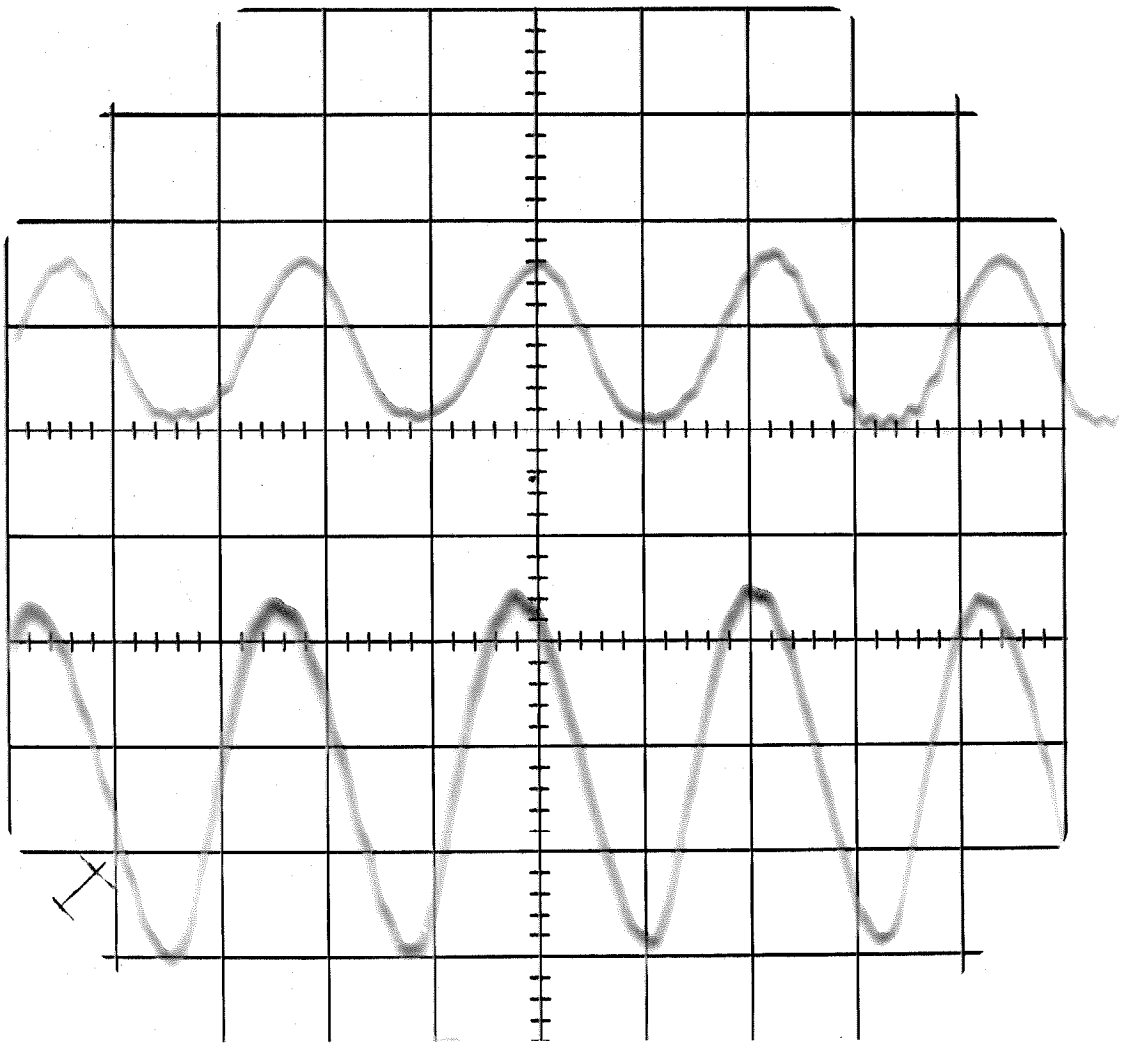

UPPER TRACE: PORT 6

LOWER TRACE: PORT 10

Figure 11. Typical Phase-relationship Records.

record of perturbations in pressure obtained at the same time from ports identified as 6 and 10, with the former corresponding to the upper trace and the latter corresponding to the lower one. We may note that the waves at the two ports are not exactly in phase with each other; this implies that some traveling acoustic waves are also present in the combustion tube along with the standing waves[1]. Furthermore, inspection of the other photographic records shows that the phase lag between two ports is a function of the length of the combustion tube. The frequencies of the two waves appear to be the same within experimental uncertainty, whereas the amplitude seems to be larger the further away from the flameholder.

At certain lengths of the combustor the combustion was quiet and the oscillations almost disappeared. Figure 12 shows the perturbations in pressure when the effective length of the combustor yielded such a "quiet region". The upper trace represents the perturbations in pressure at port 6, while the lower trace represents those at port 4. It appears that in these quiet regions the oscillations may still exist, but they were so weak in intensity that virtually no measurable perturbations could be detected. The combustion with no measurable perturbations will be called "stable combustion". It should be pointed

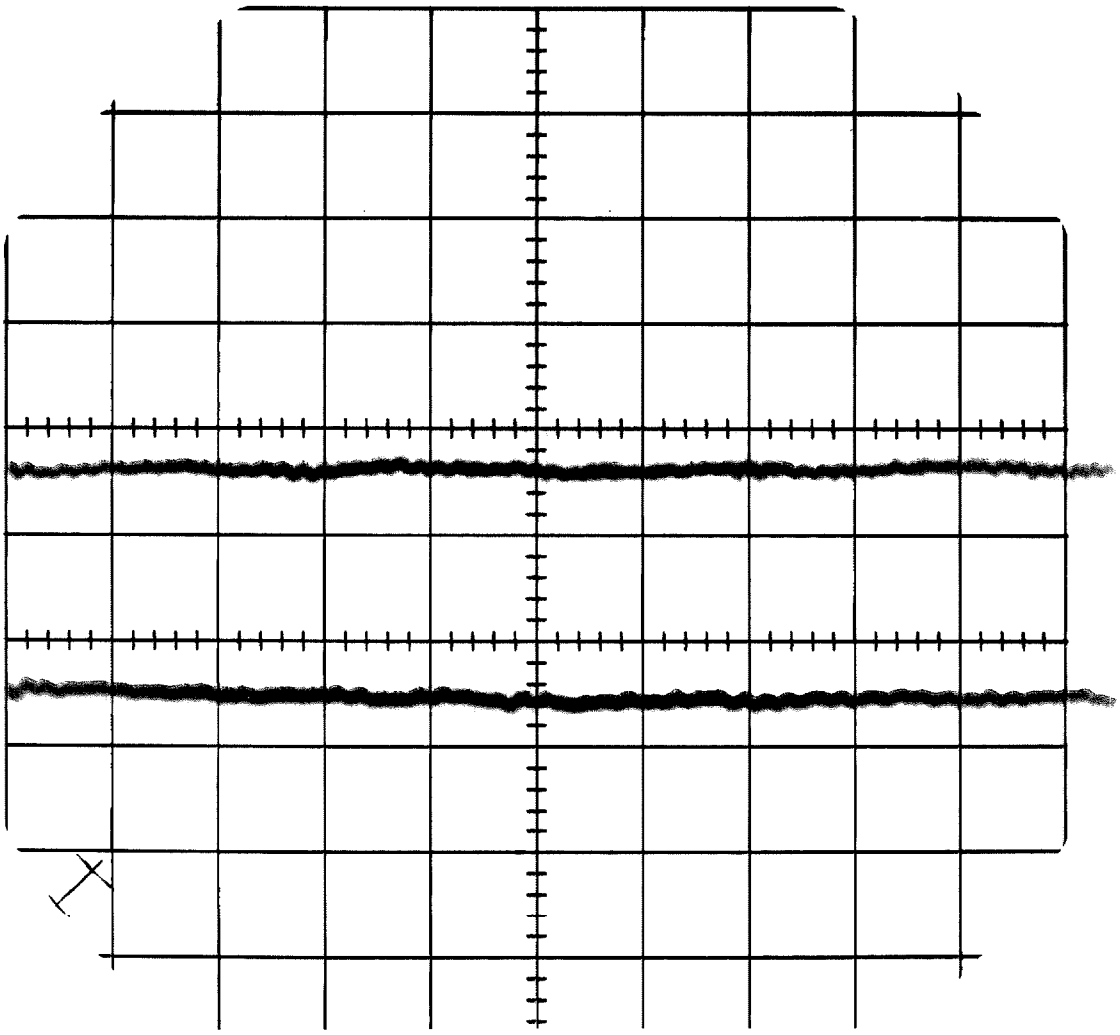

UPPER TRACE: PORT 6

LOWER TRACE: PORT 4

Figure 12. Perturbations in Pressure in a "Quiet Region".

out that when the effective length of the combustor yielded a quiet region, the combustion was quiet throughout the entire combustor. The quiet zone encountered was not related to the port at which the measurements were made.

Figure 13 depicts all frequency data obtained at ports 4, 6, and 10 as a function of the effective length of the combustor. These experimental data indicate that oscillations occurred only for certain positions of the reflecting disk corresponding to specific effective lengths of the combustion chamber. These positions were not marked by single points, but each was marked by an interval of positions in which the observed frequency was nearly constant. In most such intervals there were several different values of frequency. Between such oscillating zones were quiet regions where either no oscillations occurred, or the oscillations were of negligible intensity. It should be pointed out that only frequencies of the fundamental oscillations and their major overtones were recorded. Oscillations with an intensity less than approximately 5% of that of the fundamental were eliminated from consideration. From the information presented in Figure 13, it appears that the frequency of the combustion oscillations ranges from approximately 630 to 1080 cycles per sec.

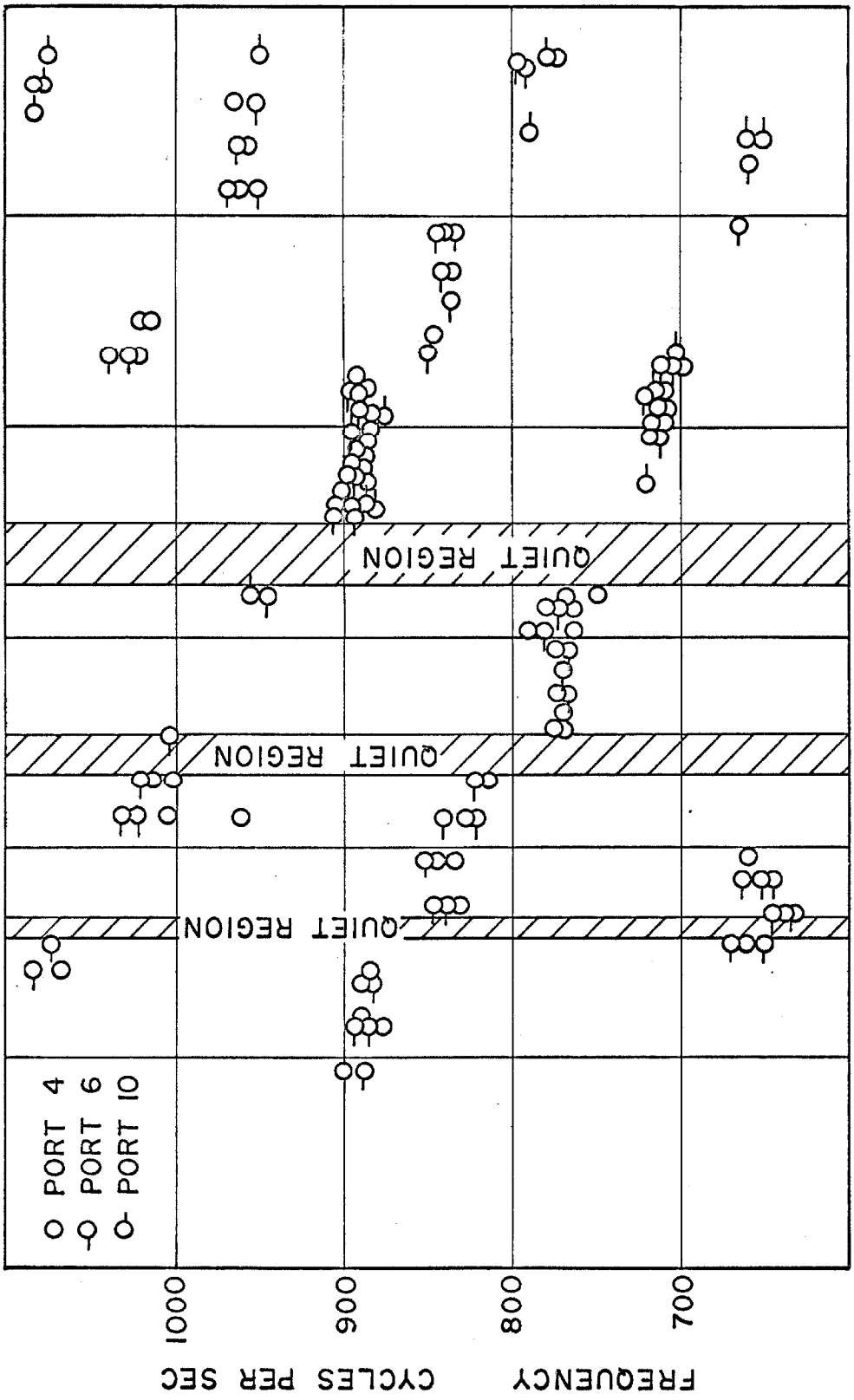

Figure 13. Frequencies as a Function of Effective Length of Combustor at Three Ports.

The experimental conditions covered in this investigation are summarized in Table 2. Figure 14 presents the amplitude of the oscillations as a function of the effective length of the combustor at ports 4, 6, and 10. The shaded regions between each two curves represent the range of the variation of amplitudes recorded. The number of experimental points has been indicated on each curve. The magnitude of the perturbations in pressure increased gradually when the effective length of the combustor was increased from a quiet region. In most cases the amplitude reached a maximum when the effective length of the combustion chamber was just below that corresponding to the next quiet zone. Further increase in length results in a remarkably rapid decrease in magnitude of the perturbations until the quiet region is reached. It is evident from Figure 14 that the amplitude of perturbations in pressure increased with the distance from the flameholder. Furthermore, the oscillations were in general intensified when the effective length of the combustor was increased. Intense oscillations were encountered when the reflecting disk was located at approximately 71, 76, and 82 in. from the flameholder.

Table 3 presents the experimental analysis of the frequency and the amplitude of the perturbations in pres-

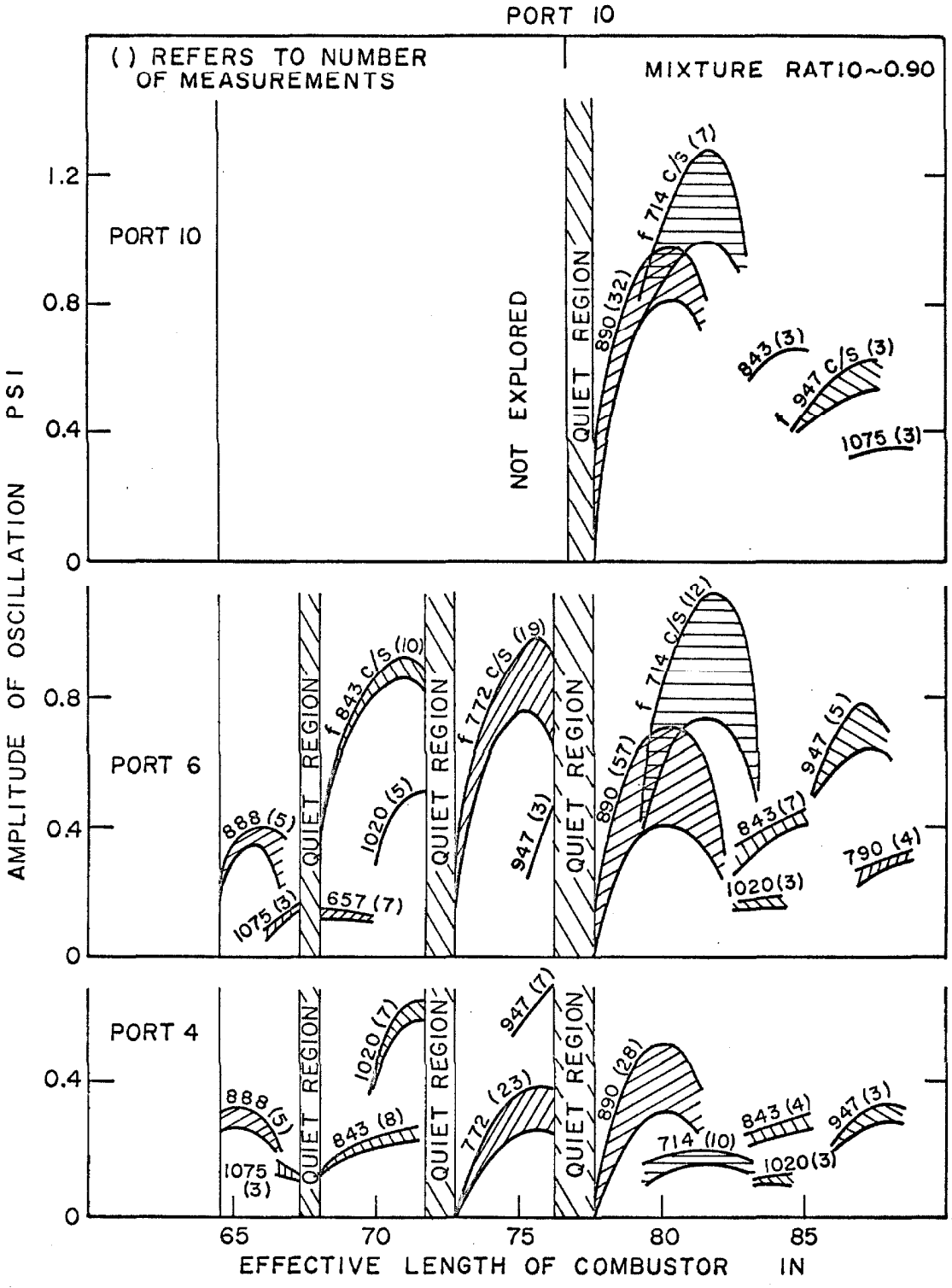

Figure 14. Amplitudes as a Function of Effective Length of Combustor at Three Positions along Combustor.

sure corresponding to the conditions recorded in Table 2. In this analysis, the perturbations in pressure were shown as a function of time for each test. The measured values of the perturbations in pressure were established within approximately 5%. However, there was a small variation with time in the magnitude of the perturbations in pressure even with the precautions that were taken to maintain as near steady state as possible. This effect was believed to be resulted from change in length of the primary combustion zone.

In portions of the experimental work, measurements of the perturbations of the total optical intensity and of the monochromatic intensities were made, along with the measurements of the perturbations in pressure. In Figures 15, 16, and 17 are shown, for a full-length open combustor of 168 in., the typical perturbations of total optical intensity and of monochromatic intensities corresponding to carbon dioxide and water, respectively. It is apparent that the perturbations in the total and monochromatic intensities are much more irregular than the perturbations in pressure. The magnitude of the perturbations in monochromatic and total optical intensities were found to be much more susceptible to minor variations in combustion conditions than the perturbations in pressure. Thus the

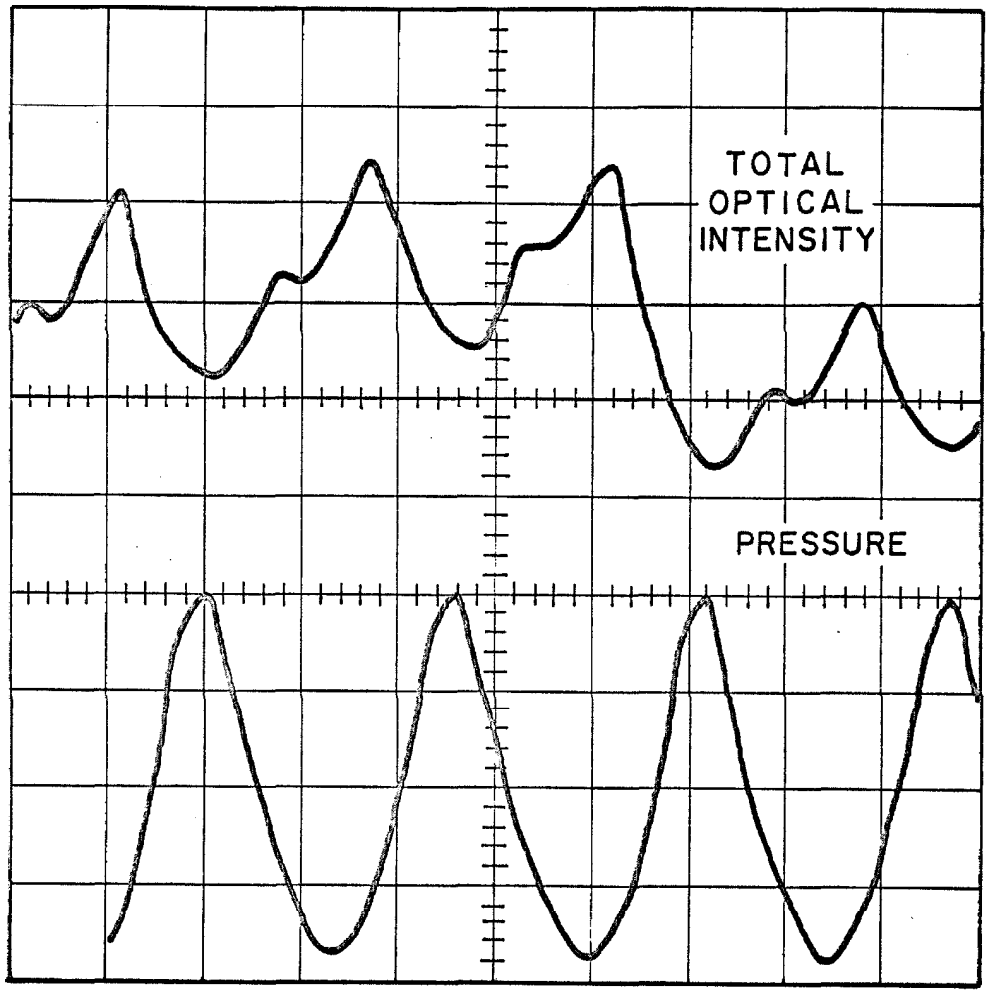

Figure 15. Perturbations of Total Optical Intensity and Pressure.

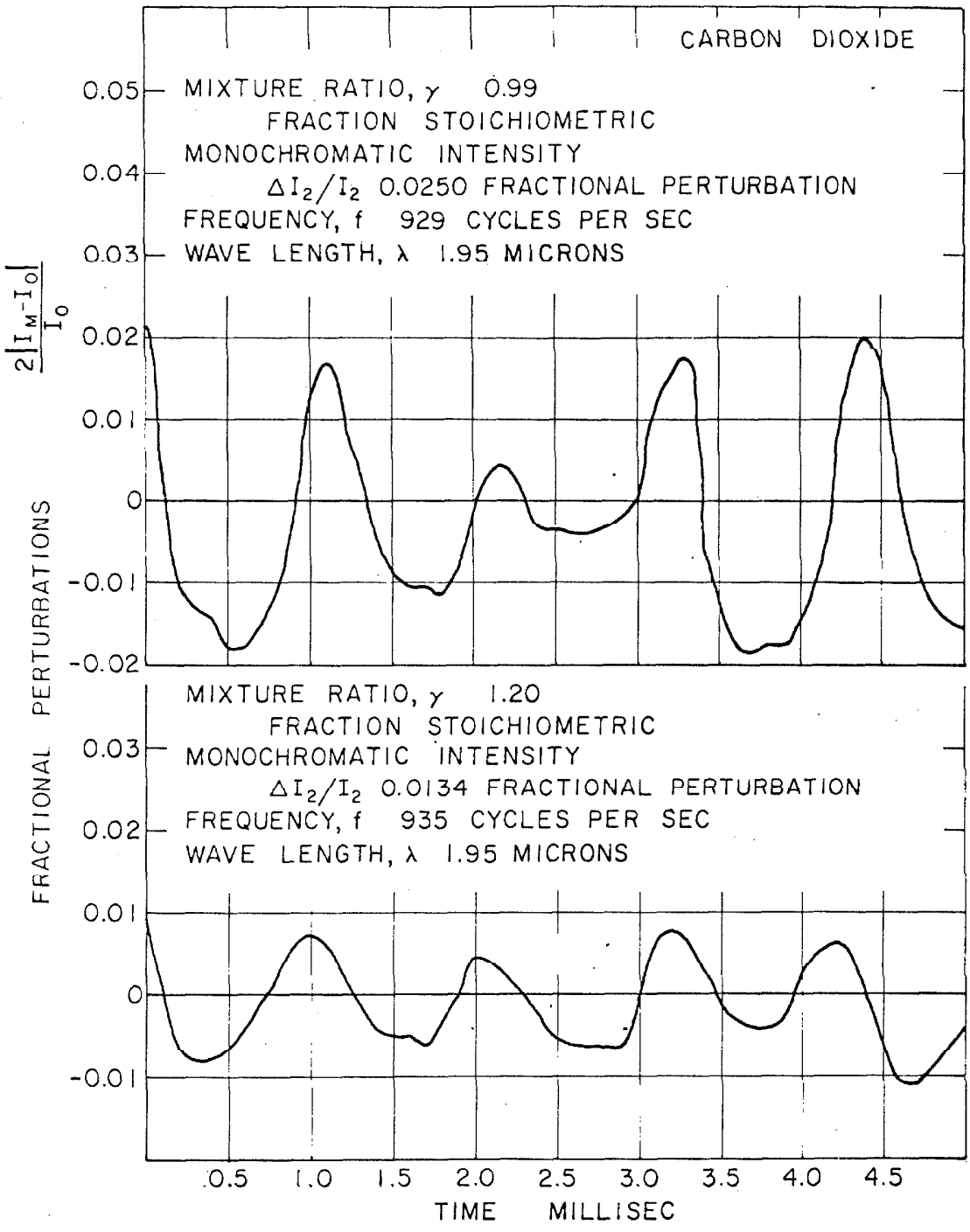

Fig. 16. Perturbations in Monochromatic Intensity Corresponding to a Wave Length of 1.95 Microns.

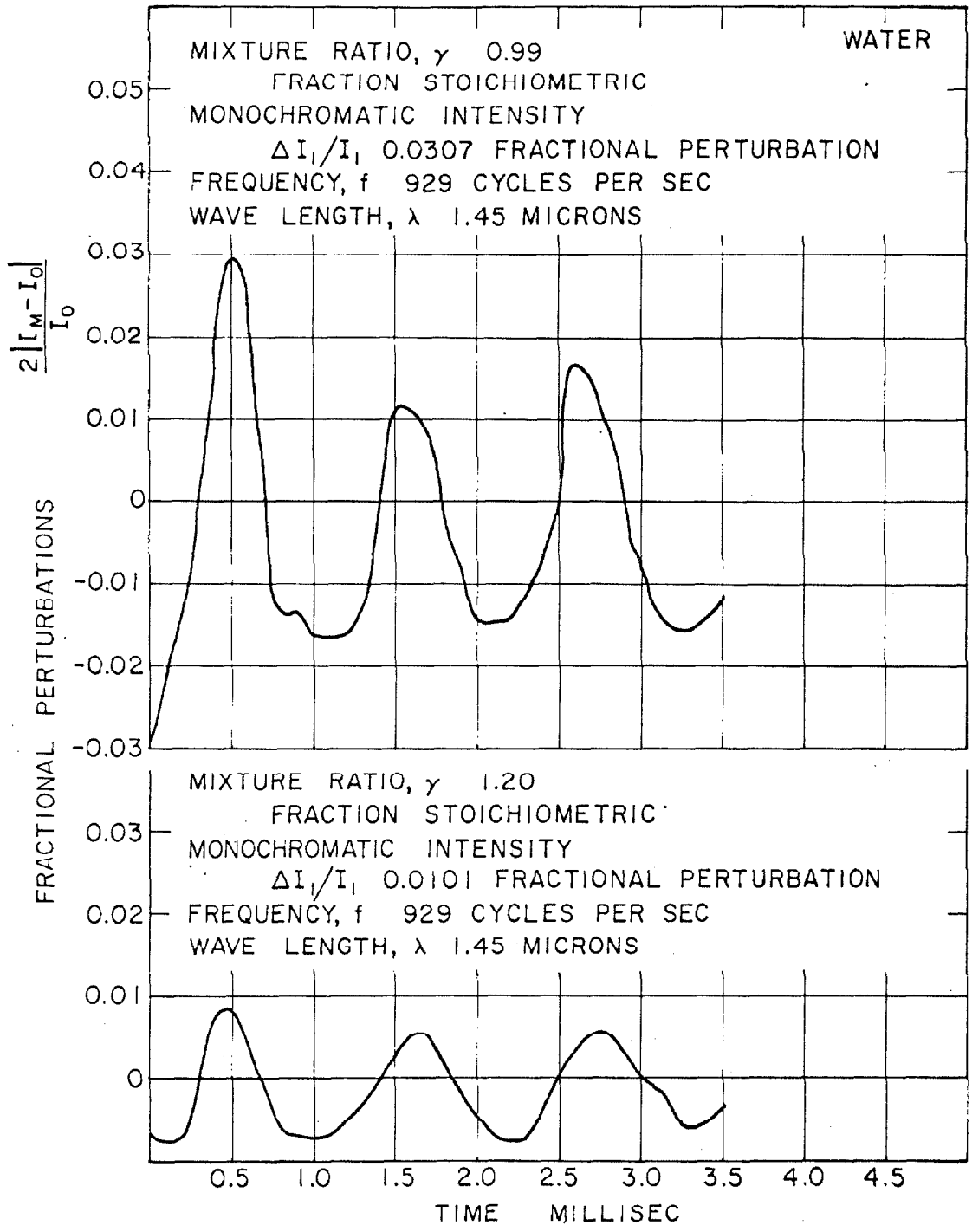

Fig.17. Behavior of the Perturbations in Monochromatic Intensity at a Wave Length of 1.45 Microns.

absolute magnitude of these optical intensities do not appear to have any quantitative significance. However, the relative fluctuation in total optical intensity which has been defined as

$$2\left|I_M - \frac{1}{\theta_2 - \theta_1}\int_{\theta_1}^{\theta_2} I\,d\theta\right| \Big/ \left(\frac{1}{\theta_2 - \theta_1}\int_{\theta_1}^{\theta_2} I\,d\theta\right)$$

$$= \frac{2\left|I_M - I_o\right|}{I_o} = \frac{\Delta I}{I_o} \qquad (6)$$

appears to be useful in the evaluation of the behavior of the system. In addition, the frequency of the perturbations in monochromatic and total optical intensities appears to be in fairly good agreement with that of the perturbations in pressure. The variations of frequency of the perturbations in monochromatic and total optical intensities with the effective length of the combustor followed the same pattern as that shown in Figure 13. Hence it should be recognized that these measurements are at least of semi-quantitative value, although they are subject to more uncertainty of interpretation. The measurements of the perturbations in monochromatic intensities corresponding to the wavelengths of carbon dioxide and water permit the relative quantities of carbon dioxide and water to be estimated. A detailed record of experimental

analysis of the perturbations in monochromatic and total optical intensities is available[54].

The effect of mixture ratio upon the frequency and the amplitude of the combustion oscillations has also been explored. Figure 18 presents the effect of mixture ratio upon frequency with limited information at a fixed length of the combustor of 168 in. It appears that the frequencies remained substantially constant at approximately 770 cycles per sec. until mixture ratios near stoichiometric were encountered. The frequency then increased discontinuously to about 930 cycles per sec. and remained virtually fixed at this value for the higher mixture ratios. In the upper part of Figure 18 are shown the frequencies of the perturbations in total optical and monochromatic intensities as a function of mixture ratio. Within the experimental uncertainty of the measurements, these perturbations have the same frequencies as the perturbations in pressure. The hysteresis pattern shown near the center of the figure was established from earlier studies[11,12].

Figure 19 shows, again for the full-length open combustor of 168 in., the magnitude of the relative perturbations in pressure and in monochromatic intensities, corresponding to the emissivity of water and carbon dioxide

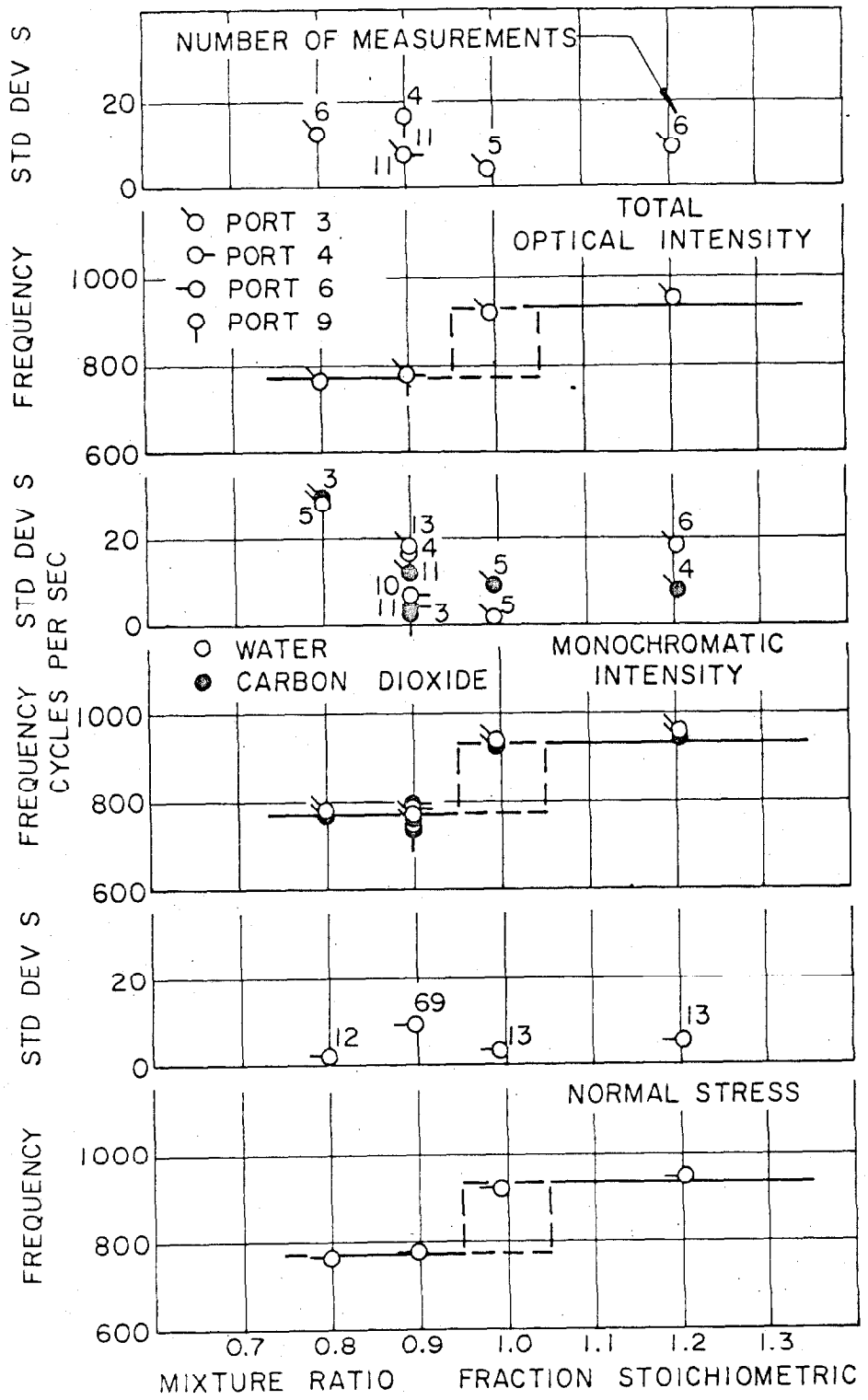

Fig. 18. Effect of Mixture Ratio upon Frequency.

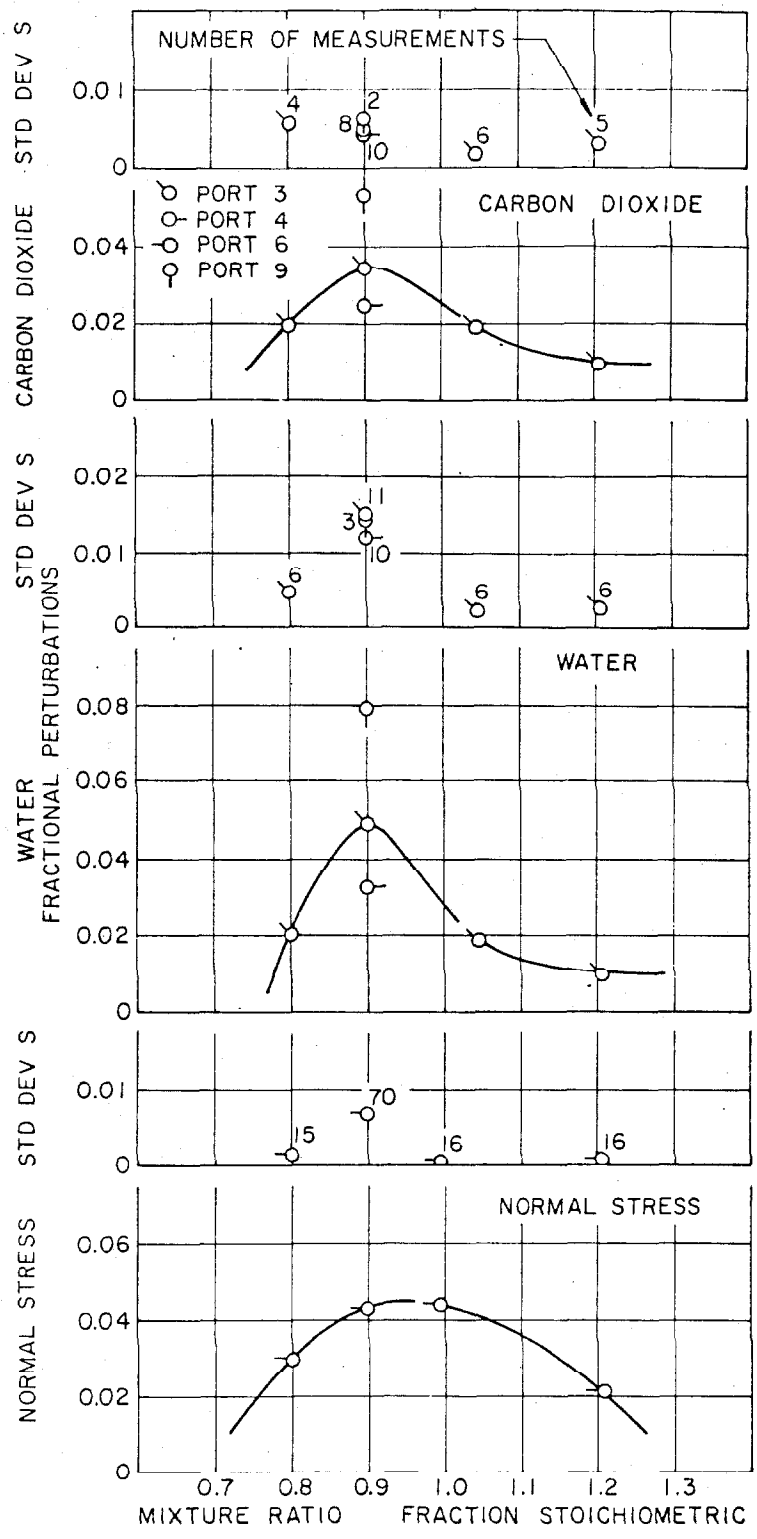

Fig. 19. Effect of Mixture Ratio upon Magnitude of Perturbations.

as a function of mixture ratio. These perturbations reach a maximum in the vicinity of stoichiometric, or perhaps slightly below it, and fall off rapidly in the case of either leaner or richer mixture ratios. The relative perturbations in pressure and in monochromatic intensities seem to be comparable. All of the measurements of the perturbations in pressure presented in Figure 19 were taken at port 6, while most of the measurements of monochromatic intensities were taken at port 3, with a few others taken at port 4 and port 9 for the purpose of comparison. The standard deviations of these measurements are also indicated in the figure.

VI. ANALYSIS AND DISCUSSION OF RESULTS

A. PRELIMINARY CONSIDERATIONS OF SOUND WAVES

In this investigation, the only oscillations considered are those that have frequencies corresponding to the "organ-pipe" frequencies of the system. The organ pipe is usually considered as a tube for which the length is much larger than the diameter. It can be open either at one end or at both ends. Basic considerations[27,55] indicate that, for small amplitudes of oscillations, the pressure and the gas velocity vary in a sinusoidal manner with time at each interior point of the tube. Furthermore, the pressure, as well as the gas velocity, is a sinusoidal function of distance along the tube. Thus the amplitude of the oscillations can be expressed by

$$y_1 = y_M \sin(\kappa x - \omega t) \qquad (7)$$

where ω is the angular frequency and κ is an abbreviation for ω/c. Equation (7) represents a wave traveling along the tube from the flameholder toward the reflecting disk. Similarly, the equation

$$y_2 = y_M \sin(\kappa x + \omega t) \qquad (8)$$

represents a wave traveling down the tube toward the flame

holder having the same amplitude, frequency, and wavelength. In the present combustion system, Equation (8) is also considered as the reflected wave train reflecting at the disk and traveling back to the flameholder, provided that the reflection is perfect at the reflecting disk. The resultant magnitude of these two waves, at any point and at any instant, is the algebraic sum of y_1 and y_2:

$$y = y_1 + y_2 = 2 y_M \sin \kappa x \cos \omega t \qquad (9)$$

Equation (9) represents a standing wave that no longer travels along the tube. The displacement is always zero at points where

$$\kappa x = \ldots -2\pi , -\pi , 0 , \pi , 2\pi , \ldots \quad .$$

These points are known as the nodes of the oscillation. On the other hand, the maximum displacement occurs at points where

$$\kappa x = \ldots -3\pi/2, -\pi/2, \pi/2, 3\pi/2, \ldots \quad .$$

These points are known as the antinodes of the oscillation.

In practice, a compressional wave usually shows some decay in strength as it travels, particularly when it is reflected[24]. Hence the reflected wave can not be exactly represented by Equation (8) because the amplitude may become smaller. Consequently, some traveling waves

will exist along with the standing waves.

Putnam[1] has pointed out that there are probably no pure standing waves in any combustion system, because the inputs and losses of oscillating energy do not match exactly on a point-by-point basis throughout the system. Therefore, it seems to be necessary to have some unbalanced traveling-wave components to distribute the energy input to the points of high loss.

In this study, all discussions will be based on the modes of oscillation of standing waves alone. Such assumed behavior is considered to be of value in understanding the characteristics of the waves that exist in the combustor. Furthermore, the Rayleigh's driving criterion presupposes the presence of pure standing waves[27]. Owing to the principle of superposition, such assumption should not result in any significant influence upon the basic analysis in this investigation when in the presence of a small amount of traveling waves. The principle of superposition[56] states in general terms that partial effects may be added together to obtain resultant effects, and the action of each individual effect will in no way be changed upon addition to or subtraction from it another effect in equilibrium. It applies to waves or wave pulses of any type, provided the differential equation of the wave is

linear[57].

It should be recognized that the energy for a compressional wave involves not only the internal energy, but also the kinetic energy and the elastic potential energy associated with the compression and rarefaction of the wave motion[25]. The transfer of heat to the gas flow from a heat source is in fact the addition of thermal and mechanical energy to the system, which are then stored up as internal energy[39].

In the present work, the combustion tube is open to the atmosphere at the upper end and is closed at the lower end. The closed end always corresponds to a pressure antinode, while the open end normally corresponds to a pressure node. The latter situation seems reasonable, since if the end is open to the atmosphere, it would be expected that the pressure at this end remains constant and equals to atmospheric pressure.

The general equation for the frequencies of such a system may be written as

$$f_n = (2n + 1)\frac{c}{4L} \quad , \qquad n = 0, 1, 2, \ldots \quad (10)$$

The mode of oscillation when $n = 0$ is known as the fundamental mode or first harmonic. The mode of oscillation when

n = 1 is called the first overtone or the second harmonic, and so forth. Simple acoustic theory[27] shows that the node is not precisely at the end of the tube, but that the effective tube length exceeds the actual length by about 0.6 of the radius. Therefore, Equation (10) should be corrected for the effect of the open-end reflection and should be rewritten in the following form:

$$f_n = (2n+1)\frac{c}{4(L+L_r)}, \quad n = 0, 1, 2,..(10)$$

where L_r is 0.6 of the radius of the combustion tube.

For compressional waves in a fluid confined in a tube, it can be shown that the velocity of wave propagation is[57]

$$c = \sqrt{B/\rho_o} \tag{11}$$

where B is the bulk modulus and ρ_o is the density of the fluid under quiescent condition. Here the bulk modulus is defined as[25]

$$B = -\frac{\text{change in pressure}}{\text{fractional change in volume}} = -\frac{\Delta P}{\Delta V/V} \tag{12}$$

It should be recognized that the compressions and rarefactions in a sound wave are much more nearly adiabatic than isothermal[57]. Hence it is the adiabatic rather than

the isothermal bulk modulus that must be used in computing the speed of such a compressional wave.

As shown in Appendix I, the adiabatic bulk modulus B_{ad} of a perfect gas is

$$B_{ad} = \gamma P \tag{14}$$

where γ is the ratio of isobaric to isochoric specific heats, c_p / c_v. The velocity of sound waves in a perfect gas is therefore

$$c = \sqrt{\gamma g b T} = \sqrt{\frac{\gamma g R T}{M}} \tag{15}$$

For air in the range of temperatures under consideration, γ has a value of approximately 1.39, and its variation with either the temperature or the composition of the gas mixture is small. Hence the value of γ is assumed to remain at this constant value throughout the range of conditions covered by this investigation.

B. THE DISTRIBUTION OF LOCAL AVERAGE GAS TEMPERATURE

As was pointed out earlier, the local gas temperature can not be established with certainty by the use of thermocouples at temperatures higher than approximately

1500°F. Therefore, these temperatures have to be estimated by means of certain theoretical considerations, especially at positions near the combustion zone where the temperature was above 2000°F. The experimental measurements of temperature merely serve to check whether the temperature distribution obtained from theoretical means is sufficiently accurate for the purpose of this study.

The best assumption to be made for the theoretical prediction of temperature distribution is the behavior of local physicochemical equilibrium for a perfect gas at constant pressure. A computer program for the calculation of flame temperature and equilibrium compositions was developed for such conditions. The calculation procedure involves a balance of moles of the major reactive components and the equilibrium relations for four of the eleven reactions suggested by Wimpress[58]. For any assumed input of reactants, the resulting compositions were computed according to this routine procedure. The flame temperature was then obtained from the energy balance. The details of this calculation scheme are presented in Appendix II. Undoubtedly, such a simple approach leaves something to be desired, but nevertheless permits an approximation of the temperature distribution to be expected.

From the calculations based upon the assumption of

local physicochemical equilibrium, the thermal losses turned out to vary nearly linearly with gas temperature. Figure 20 presents the thermal losses as a function of equilibrium flame temperature and several values of mixture ratio. For convenience, the thermal loss was assumed to be a linear function of gas temperature in the present analysis, as represented by the following equation:

$$\mathring{q} = -a T + a' \tag{16}$$

where a and a' are constants. It was also assumed that the local heat transfer was directly proportional to the temperature differences between the gas stream and the wall of the combustor. This implies that an average heat transfer coefficient h_i is assumed to be applicable for the range of temperature covered in this analysis. Such condition may be expressed by the following equation:

$$\mathring{q} = \int_0^A h_i (T - T_w) \, dA = a \int_0^x (T - T_w) \, dx \tag{17}$$

where a is an abbreviation for $2\pi r h_i$ and T_w is the wall temperature. A combination of Equations (16) and (17) yields:

$$-a T + a' = a \int_0^x (T - T_w) \, dx \tag{18}$$

If Equation (18) is differentiated with respect to x, there

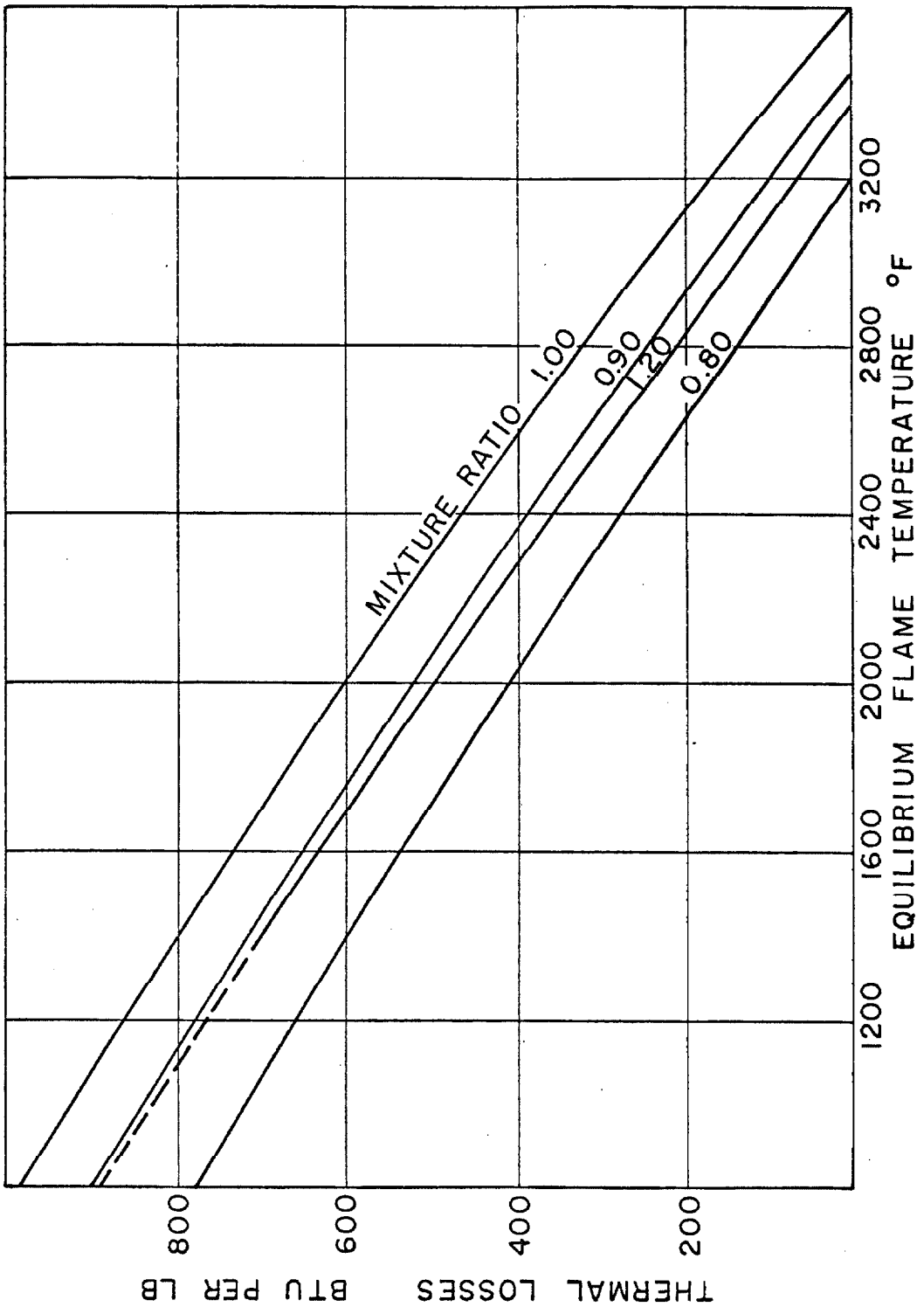

Figure 20. Thermal Losses as a Function of Equilibrium Temperature.

results:

$$-a \frac{dt}{dx} = \alpha (T - T_w) \qquad (19)$$

Upon integrating Equation (19), the following result was obtained:

$$T - T_w = C_2 e^{-C_1 x} \qquad (20)$$

In Equation (20), C_1 is an abbreviation for α/a, and C_2 is an integration constant.

Let T_{ad} be the adiabatic flame temperature and T_e the equilibrium exit temperature. The constants in Equation (20) may be determined from the following boundary conditions:

$$T = T_{ad} \qquad \text{at} \qquad x = 0$$

$$T = T_e \qquad \text{at} \qquad x = L$$

It follows that

$$C_1 = \frac{1}{L} \ln \frac{T_{ad} - T_w}{T_e - T_w} \qquad (21)$$

and

$$C_2 = T_{ad} - T_w \quad . \qquad (22)$$

Both the values of T_{ad} and T_e were determined from equilibrium calculations, while the value of T_w was established

by experimental measurements.

Figure 21 depicts the variation in space-average temperature at a section with position along the length of the combustor at a mixture ratio of approximately 0.90 stoichiometric. These temperatures were calculated from Equation (20) upon the assumption of local physicochemical equilibrium. The calculated temperature distribution is in good agreement with the limited experimental data, as shown in Figure 21. A number of measurements of the average apparent gas temperature as a function of radial position at ports 10 and 11 and at the mixture ratio of approximately 0.90 stoichiometric are reported in Table 4. The curve shown in Figure 21 is dotted in the region near the flameholder because the thermal loss would be large and the assumed behavior of local physicochemical equilibrium may not be attained in this region. The decrease in temperature results entirely from the thermal losses to the walls of the water-cooled combustor.

C. THE CALCULATION OF THE FREQUENCIES OF COMBUSTOR

According to Equation (10), the frequency is proportional to the wave propagation velocity c and is inversely proportional to the effective length of the combustor.

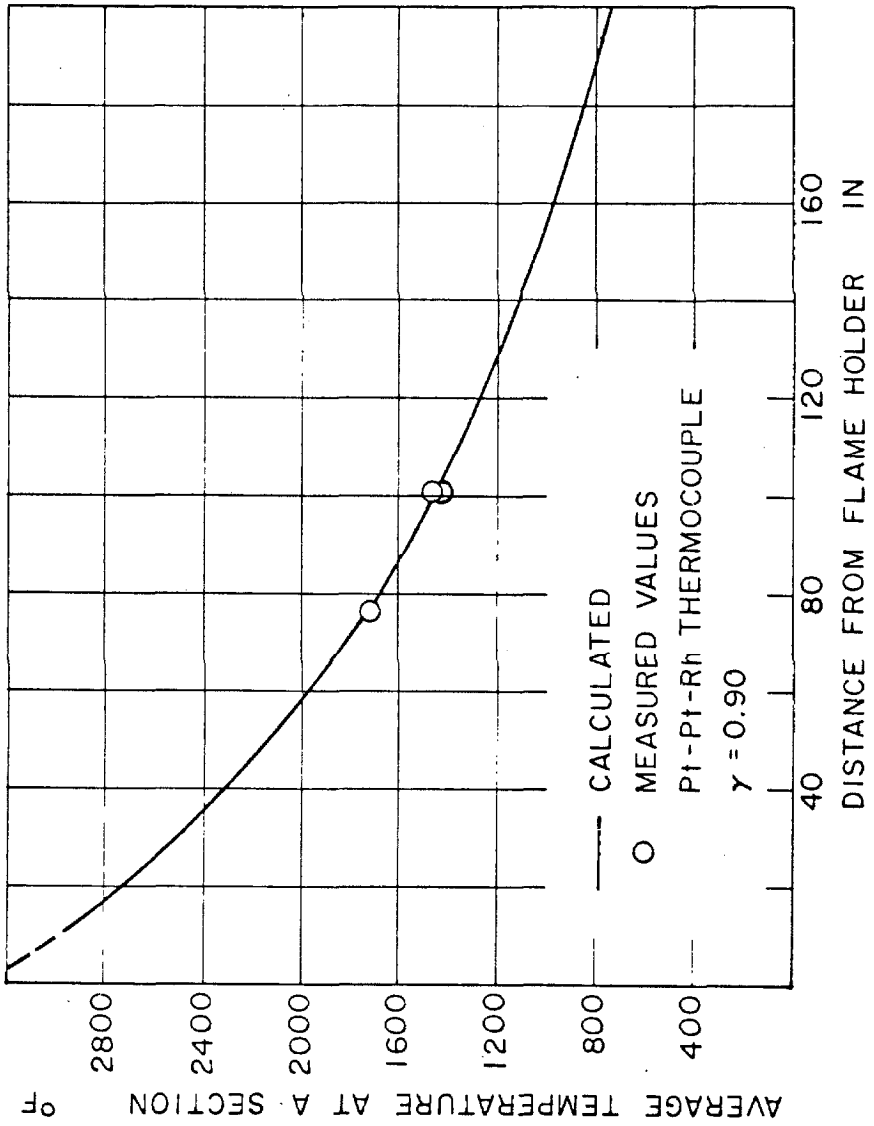

Fig. 21. Temperature as a Function of Distance from Flameholder.

However, it is not easy to use this equation directly to evaluate the frequency, since an appropriate value of the wave velocity c to be employed in Equation (10) is not known. The wave velocity is a function of gas temperature and is hence an implicit function of position along the combustor. Let L' be the effective length of the combustor that has been corrected for the effect of the open-end reflection, as represented by the following expression:

$$L' = L + L_r \tag{23}$$

Then the time taken for a wave particle to travel to the downstream end of the combustion tube and back, which is half the period of the fundamental mode, can be calculated by the following equation:

$$\Theta = \int_0^{L'} \frac{1}{c+u}\,dx + \int_0^{L'} \frac{1}{c-u}\,dx \tag{24}$$

Equation (24) has taken into consideration the effect due to bulk flow of the combustion gases from the flameholder to the exit of the combustor. In Equation (24), the average momentum velocity for a perfect gas may be evaluated from

$$u = \frac{b\,T\,\mathring{\underline{m}}}{P\,A} = \frac{R\,T\,\mathring{\underline{m}}}{P\,M\,A} \tag{25}$$

From Equations (10) and (24), the following expression is proposed as a means of estimating the organ-pipe frequencies of the combustion oscillations:

$$f_n = \frac{2n+1}{2} \frac{1}{\int_0^{L'} \frac{1}{c+u}\,dx + \int_0^{L'} \frac{1}{c-u}\,dx} \quad , \qquad (26)$$

$$n = 0, 1, 2, 3, \ldots$$

A more convenient form of Equation (26) is obtained by combining the two integrals in the denominator:

$$f_n = \frac{2n+1}{4} \frac{1}{\int_0^{L'} \frac{c}{c^2 - u^2}\,dx} \quad , \quad n = 0, 1, 2, \ldots \qquad (27)$$

Equation (27) can be further simplified since c^2 is at least 10^4 times larger than u^2, there results from neglect of the momentum velocity the following:

$$f_n = \frac{2n+1}{4} \frac{1}{\int_0^{L'} \frac{1}{c}\,dx} \quad , \quad n = 0, 1, 2, \ldots \qquad (28)$$

From the calculated temperature distribution and by using Equations (15) and (28), the fundamental frequencies of the combustion tube were computed as a function of the effective length of combustor by means of numerical methods. The variation in frequency with the length of

combustor was then plotted in Figure 22. Figure 22 is the first of a series of diagrams found to be useful in the prediction of the permissible regions of oscillation.

It should be pointed out that a limitation of the higher modes of organ-pipe oscillation exists in any combustion tube when the quarter wavelength of oscillation is nearly equal to or becomes shorter than the diameter of the tube[42]. Otherwise, the organ-pipe oscillation vanishes and oscillation of radial and tangential modes prevails. For a tube open at one end and closed at the other, the wavelength corresponding to the nth-mode of oscillation may be expressed by the following equation:

$$\lambda_n = \frac{4L}{2n+1} \quad , \quad n = 0, 1, 2, \ldots \qquad (29)$$

From Equation (29), the quarter wavelength of the ninth mode of oscillation for the present apparatus is about 4.0 in., whereas the diameter of the tube is 3.826 in. Thus, the maximum longitudinal frequency should not exceed that corresponding to the ninth mode of oscillation, and only those modes of oscillation lower than the ninth need be considered.

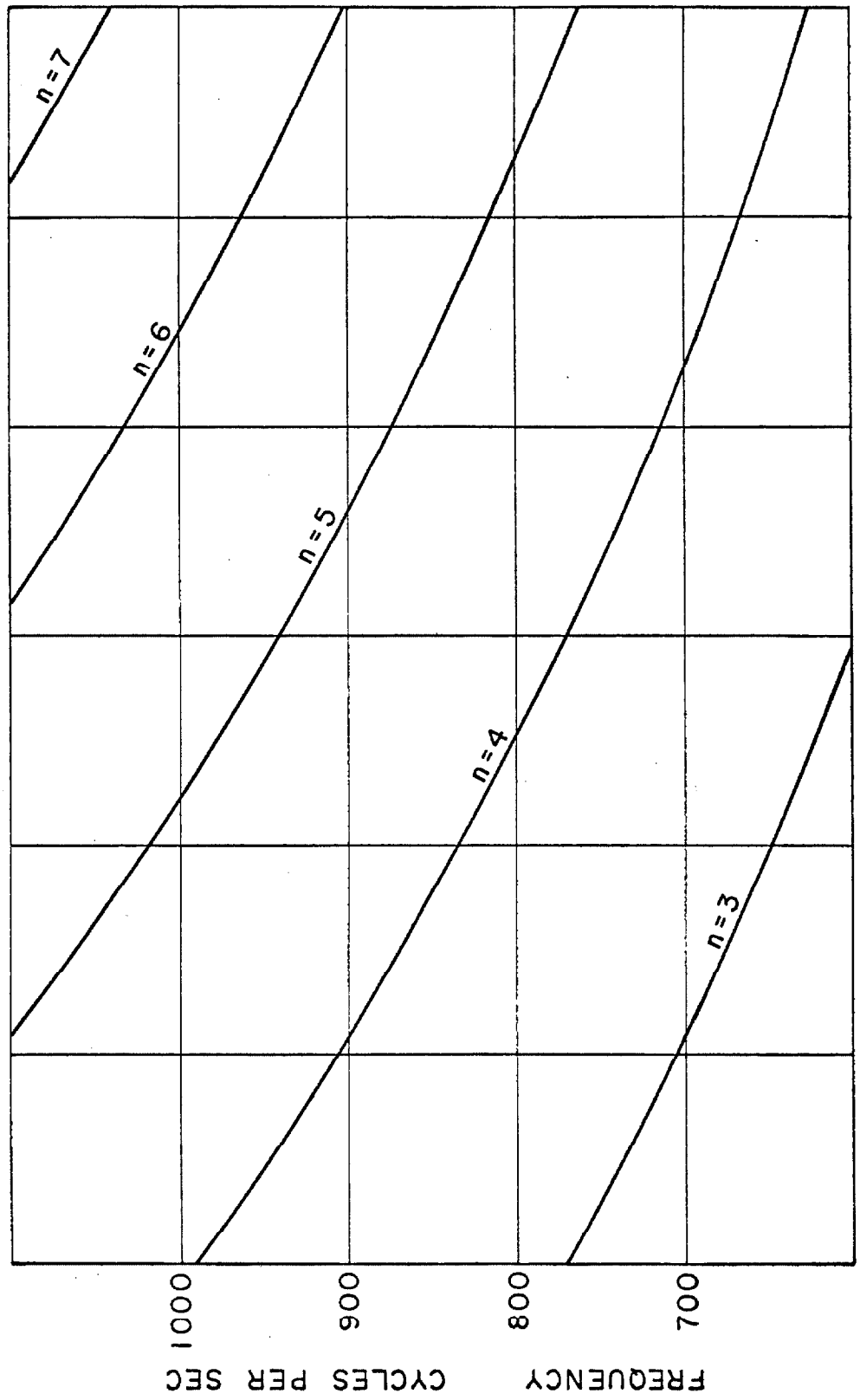

Figure 22. Calculated Frequencies as a Function of Effective Length of Combustor.

D. AN ANALYSIS OF OSCILLATION MECHANISM

The driving mechanism for the observed oscillations is postulated in the following manner primarily based upon Rayleigh's criterion[27]. Figure 23 shows a schematic diagram of the combustion chamber along with the plenum chamber where the driving of oscillations originating in the combustion chamber takes place. Referring to Figure 23, a slight pressure fluctuation caused by some pressure perturbations in the combustion tube is transferred across the flameholder to the plenum chamber. This pressure pulse travels the length of the plenum chamber, is reflected at the lower end, and returns to the flameholder. The pulse causes a local increase in flow rate, which means that the gaseous mixture passes through the flameholder at a higher local flow rate and is burned at some later time. If the time of burning of this extra quantity of gas is in phase or nearly in phase with some subsequent pressure perturbation in the combustion chamber, the oscillation originating in the combustion chamber will be reinforced. The amplified pulse is then again transferred across the flameholder into the plenum chamber, and the process continues with increasing intensity until the driving forces are balanced by the damping losses.

In view of the above described driving mechanism,

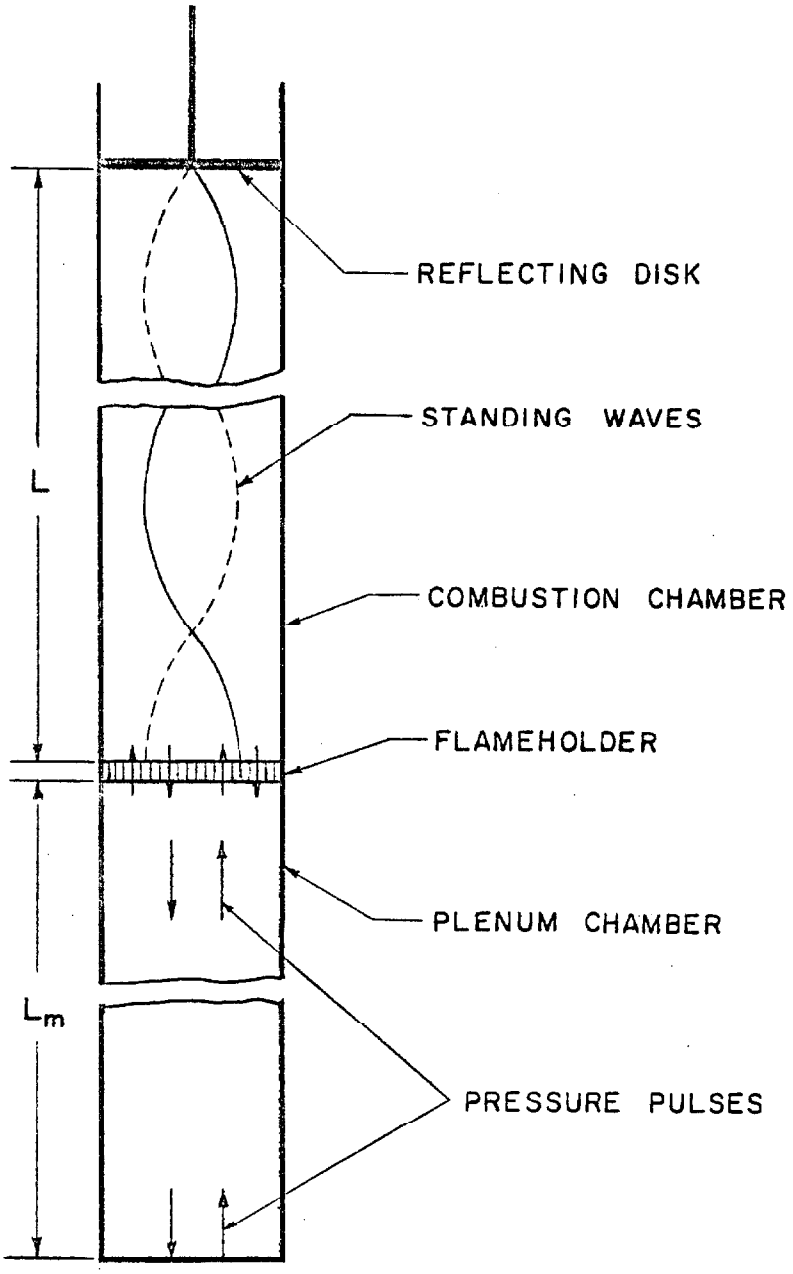

Figure 23. A Schematic Diagram of the Combustion Chamber along with the Plenum Chamber.

the oscillations in the combustion tube will not reach a high intensity unless energy is added periodically to the gases in the combustion tube in such a way as to meet two requirements. First, the periodic transfer of energy must be in phase or nearly in phase with the fluctuations of pressure in the combustion tube. This is known as the time condition for resonance[42]. The second requirement is that energy must be transferred to the gas near a point of maximum pressure. This represents the space condition for resonance. However, in the present combustion system, the flame, and consequently the primary location of the energy release, is at the closed end of the combustion tube where a pressure antinode of any standing oscillation is found. Therefore, the requirement of space condition for resonance is always satisfied in this combustion system and only the time condition need be considered.

Figure 24 shows the graphical presentation of Rayleigh's criterion proposed by Wood[40], where the increment of energy was considered as being proportional to a corresponding increment of pressure. According to the time condition for resonance as stated above, the period of the pulse in the mixing chamber must be close to some multiple of the natural period of the combustion tube. Referring to Figure 24, such a situation implies that the

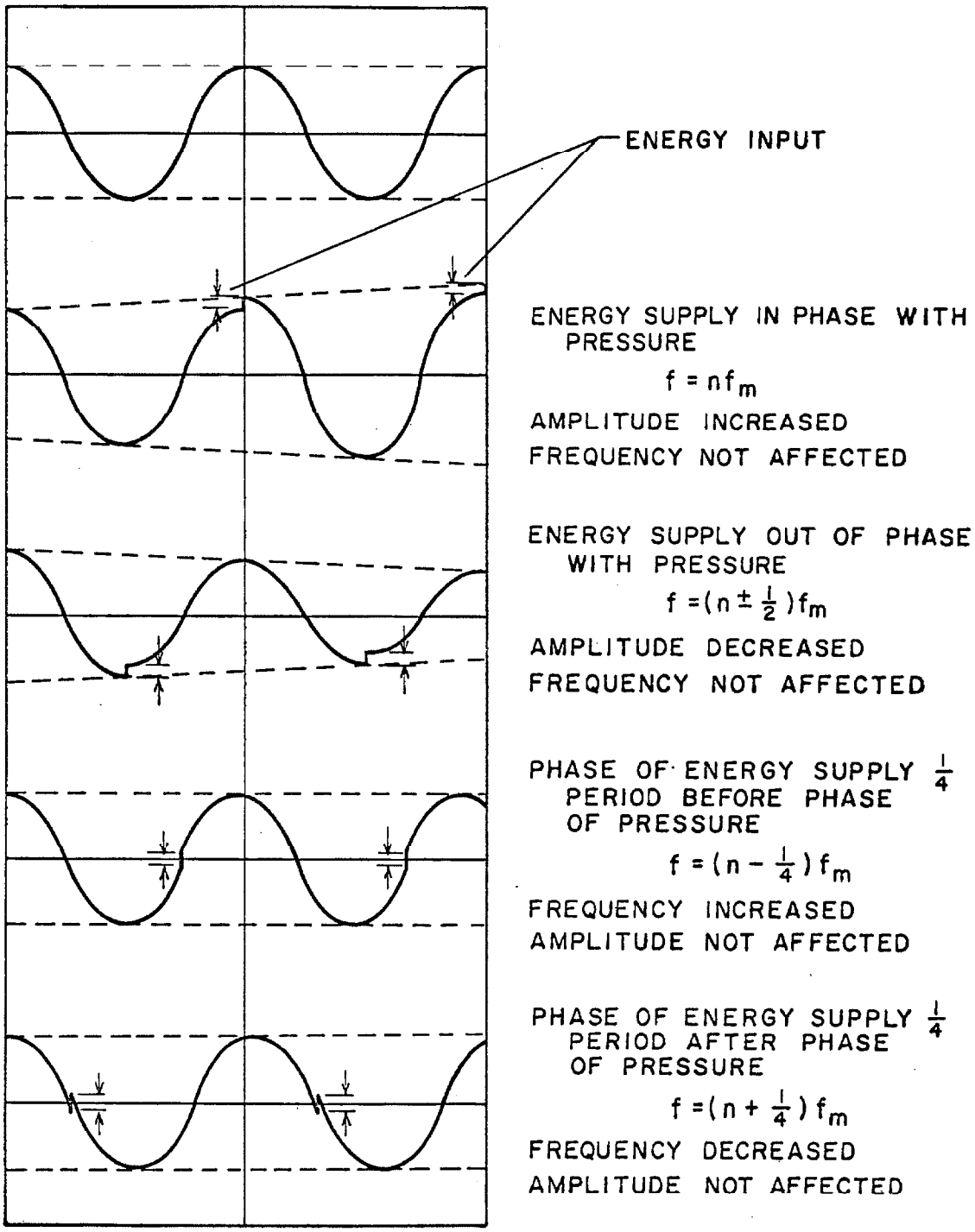

Figure 24. Graphical Presentation of Rayleigh's Criterion of Driving.

period of the mixing unit τ_m must not differ from some multiple of the natural period of the combustion unit $n\tau$ by a factor greater than $\tau/4$. Otherwise, the addition of energy would occur near the time of minimum pressure, thus damping the oscillation. The condition for resonance can therefore be formulated as

$$|\tau_m - n\tau| \leq \tau/4 \quad , \quad n = 1, 2, 3, \ldots \qquad (30)$$

It follows that

$$(n - \tfrac{1}{4})\tau \leq \tau_m \leq (n + \tfrac{1}{4})\tau \quad , \quad n = 1, 2, 3, \ldots \qquad (31)$$

A more convenient form of these inequalities is obtained by substituting the frequencies for the periods since one is the reciprocal of the other. Then there is obtained

$$(n - \tfrac{1}{4}) f_m \leq f \leq (n + \tfrac{1}{4}) f_m \quad , \quad n = 1, 2, 3, \ldots \qquad (32)$$

Equations (31) and (32) represent the instability criterion for which oscillations originating in the combustion tube can be amplified.

The period of the cycle for a pressure pulse to travel the length of the plenum chamber L_m, to be reflected at its lower end, and then to travel back at the sonic velocity c can be expressed by

$$\tau_m = \frac{2 L_m}{c} + \Omega \qquad (33)$$

Here Ω is the time required for the excess quantity of gas to pass through the flameholder and be burned. The value of Ω has been shown[42] to be normally of the order of 10^{-4} sec., while the value of $2 L_m / c$ is of the order of 10^{-2} sec. with the present apparatus. Hence Ω can be neglected in Equation (33) and r_m, as well as f_m, becomes a constant as long as the temperature of the incoming air and natural gas remains constant.

The temperature of the gas mixture was usually maintained at 80°F. Using Equation (15), the velocity of sound at this temperature is approximately equal to 1160 ft./sec. The effective length of the plenum chamber L_m was found to be 117 in. From Equation (33), such a length corresponds to a frequency of 59.5 cycles per sec. in the mixing chamber.

Equation (32) represents a set a horizontal straight lines when the frequency f is plotted against the effective length of the combustion chamber L, as shown in Figure 25. Oscillations only occur in the alternative horizontal narrow regions centered at $f = n f_m$, whereas the shaded area represents the quiet regions where virtually no oscillations occur. The frequencies of the oscillations in the combustion unit are also shown in Figure 25.

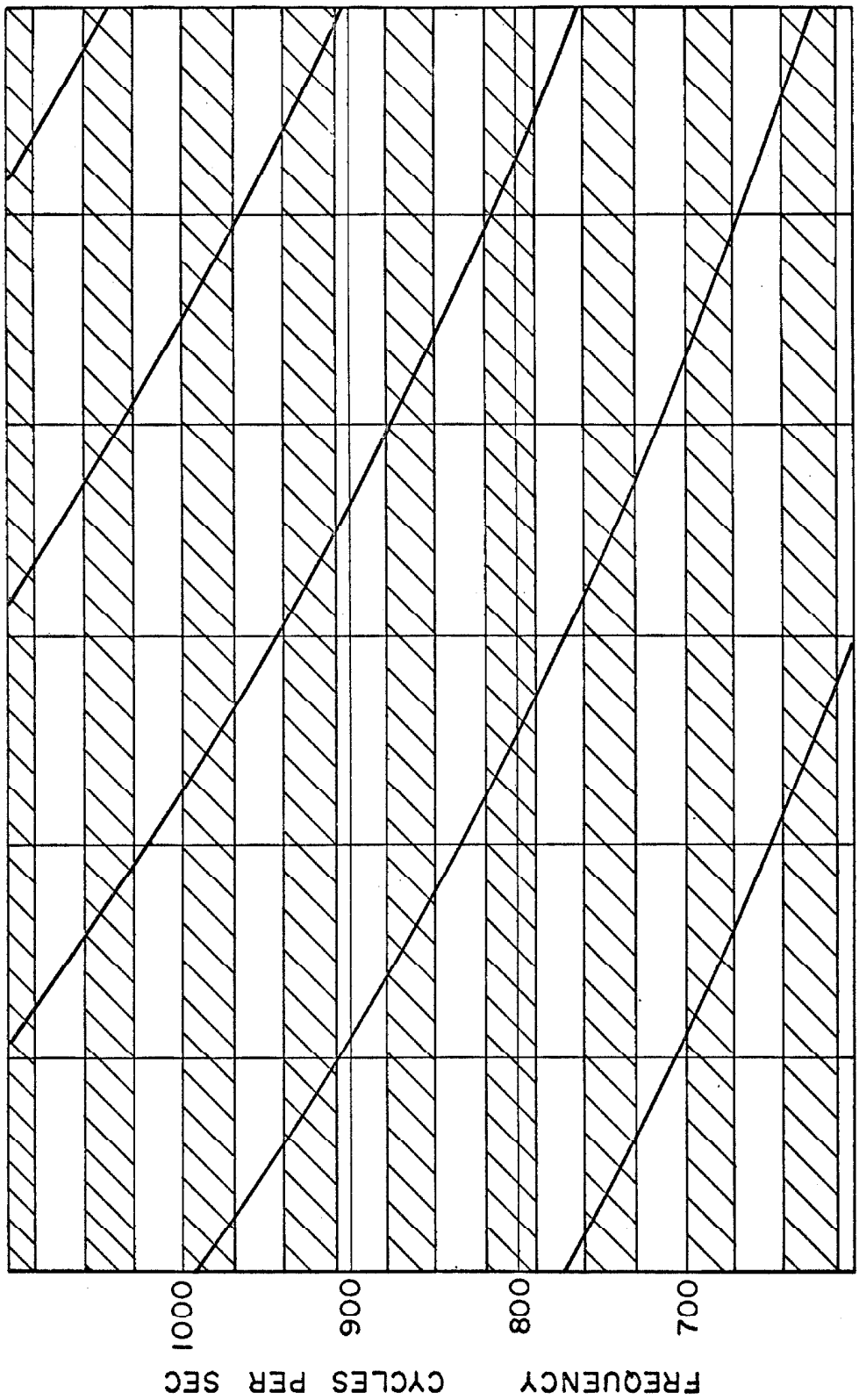

Figure 25. Superposition of the Calculated Frequencies upon the Shaded "Quiet Regions".

E. COMPARISON OF PREDICTED RESULTS WITH EXPERIMENTAL DATA AND DISCUSSION OF RESULTS

In Figure 25, the frequency for the five modes of oscillation in the combustion chamber is plotted against the effective length of the combustor. The oscillation is eliminated in the cross-hatched regions according to the instability criterion represented by Equation (32), which predicts that there should be no oscillation in these regions. The calculated frequency curves in these quiet regions are therefore not significant. Figure 26 shows the predicted intervals of frequency that also satisfy the instability criterion as a function of the effective length of the combustor. This figure is virtually the same as Figure 25 except that the shaded regions have been eliminated, since the calculated frequencies in these regions do not really exist. In Figure 26, the vertical stripes of quiet region are obtained at the length of the combustor where none of the five modes of oscillation show up.

The experimental data that have already been shown in Figure 13 are superimposed upon the predicted information of Figure 26, as shown in Figure 27. The predicted results appear to be in good agreement with the experimental data. The standard deviation for the fourth and fifth

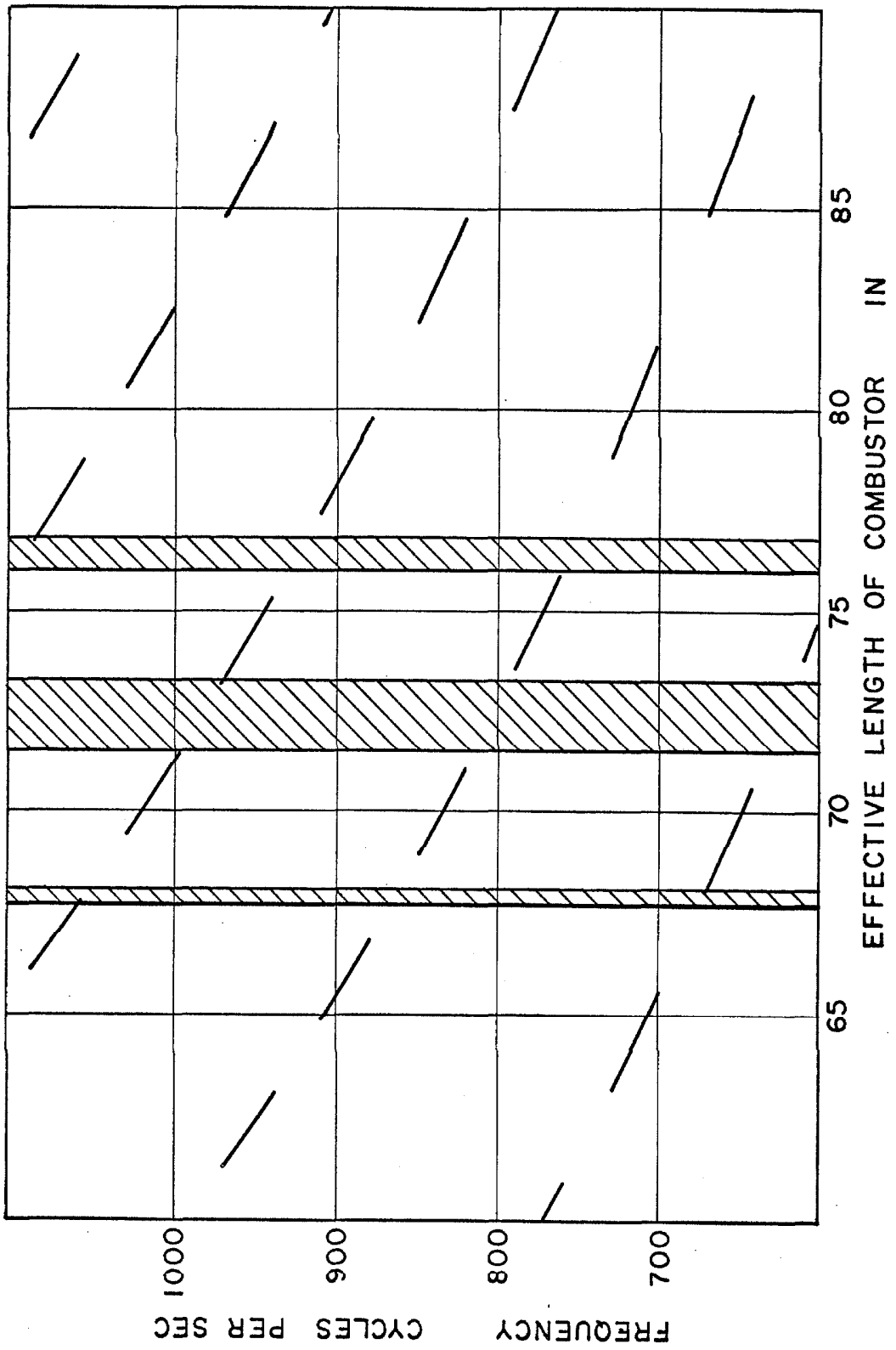

Figure 26. Predicted Intervals of Frequency as a Function of the Length of Combustor.

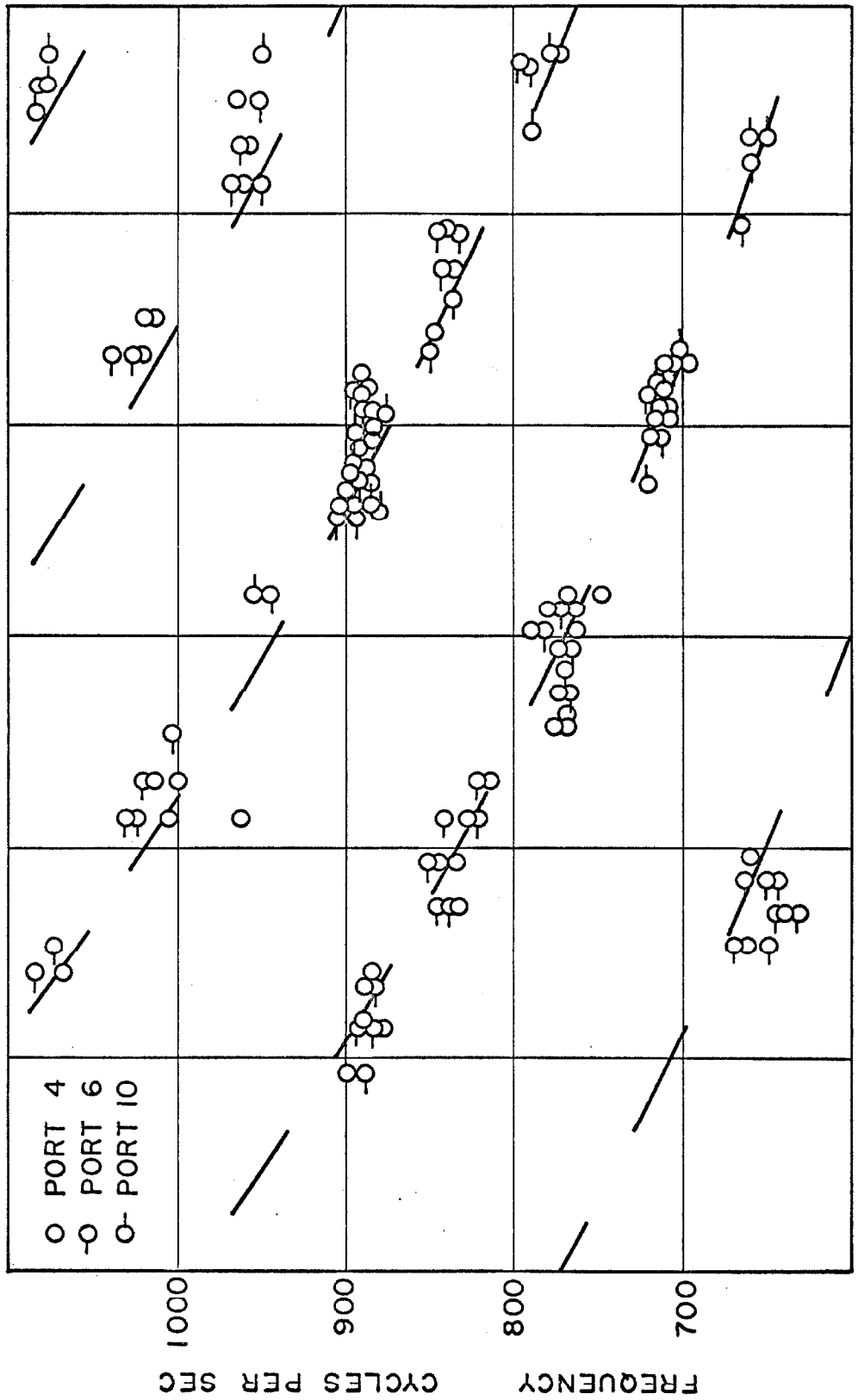

Figure 27. Comparison of Predicted Values of Frequency with Experimental Data.

modes of oscillation was found to be approximately 3.2 cycles per sec., while that for the other three modes of oscillation amounts to about 10 cycles per sec. Following the theoretical analysis described above, the curious behavior that the frequency of the oscillations shifts abruptly as the effective length of the combustor is changed has been explained.

The fact that the observed values of frequency are nearly constant in each interval while the predicted values are not can also be justified by means of Rayleigh's criterion[27]. From the information presented in Figure 24, it is evident that frequency is increased when the phase of energy supply is equal to or less than a quarter period before the phase of maximum pressure, the converse is also true. Consequently, the predicted values of frequency shown in Figures 26 and 27 are subject to the following correction: The frequency at the right half of each interval should be increased slightly and that at the left half be decreased slightly, while the value at the center of each interval remains unchanged. This correction permits the predicted values of frequency in each interval to be nearly constant. However, the amount of this correction can not be determined by Rayleigh's criterion.

Referring again to Figure 24, the amplitude of the

oscillations should reach a maximum at the center and vanish at both ends of each interval. The distribution of the amplitude of the oscillations should be symmetrical in each interval according to the simplified theoretical analysis. However, the observed amplitudes are by no means symmetrical in each interval. As shown in Figure 14, the amplitude of the oscillation grows gradually, followed by a rapid decrease, as the effective length of the combustor is increased. Such behavior may be explained in the following manner: As the length of the combustor is increased, the period for the oscillations of any particular mode also increases. Consequently, a larger amount of combustible gas mixture is injected into the combustion chamber in this period, and more energy is available for driving an oscillation. Therefore, the amplitude of the combustion oscillation increases with the effective length of the combustor. The observed amplitude is considered as the combination of the contribution due to this effect and the symmetrical profile resulted from Rayleigh's criterion. Once the periodical energy supply becomes out of phase with pressure, the oscillation is damped out, no matter how much extra amount of energy is added. This effect permits the sudden decrease of amplitude to be explained.

Some experimental data do not agree well with the theoretical prediction. This is attributed to the effect of the flame pattern and the presence of some intensity of traveling waves. The behavior of local physicochemical equilibrium is also not expected to be fulfilled everywhere. Furthermore, the amplitude and frequency of the perturbations can be affected as a result of change in length of the combustion zone as the effective length of the combustor is changed.

VII. CONCLUSIONS

In this study, the effect of varying the effective length of the combustion tube upon the frequency and the amplitude of the organ-pipe oscillations has been investigated in a long, cylindrical combustor. The experimental results indicate some discontinuous variations in frequency, along with the presence of some quiet regions, as the effective length of the combustor is systematically changed. On the other hand, the amplitude of the oscillation grows gradually in each interval of continuous variation in frequency, followed by a more rapid decrease in amplitude, as the effective length of the combustor is gradually increased.

The observed results were analyzed primarily based upon Rayleigh's criterion. It was found that the oscillations in the combustion tube were predominantly standing waves. The upper end of the combustion tube always corresponds to a pressure node, whereas the lower end always corresponds to a pressure antinode. A slight pressure fluctuation caused by any small disturbance in flow in the combustion tube is transferred across the flameholder to the plenum chamber. This means that the pressure fluctuation originating in the combustion tube induces a

pressure pulse traveling back and forth in the mixing chamber. If the period of this pressure pulse is close to some multiple of the natural period of the oscillation in the combustion tube, the oscillation originating in the combustion tube will be amplified.

The calculated values of frequency based upon this proposed driving mechanism turned out to be in good agreement with the experimental data. However, the amplitude of the oscillations can not be determined quantitatively by means of Rayleigh's criterion. While a formal analytical solution of the differential equations governing the combustion processes is not possible at this time, it appears that the application of Rayleigh's criterion is the most effective method available for analyzing problems concerning organ-pipe combustion oscillations.

The natural frequencies of the combustion tube were calculated based upon the local gas temperature estimated under the assumption of local physicochemical equilibrium. This estimated temperature profile seems to agree quite well with the limited temperature data available, thus confirming the validity of the assumptions.

From knowledge obtained in this study, oscillations may be eliminated by changing the length of either

the combustion tube or the mixing chamber. In addition, the amplitude of oscillation can be reduced if the flame is moved away from the closed end of the combustion tube. Increase in diameter of the combustion tube may also lead to the elimination of some higher modes of organ-pipe oscillation. However, radial and tangential modes of oscillation may prevail under such circumstances.

VIII. REFERENCES

1. Markstein, G. H., Ed., "Non-steady Flame Propagation", Macmillan, N. Y., 183-314 (1964).

2. Blacet, F. E., Ind. Eng. Chem., 44, 1339 (1952).

3. Haagen-Smit, A. J., ibid., 44, 1342 (1952).

4. Haagen-Smit, A. J., C. E. Bradley, and M. M. Fox, ibid., 45, 2086 (1953).

5. Johnston, H. S., ibid., 49, 1488 (1956).

6. Stephens, E. R., P. L. Hanst, R. C. Doerr, and W. E. Scott, Ind. Eng. Chem., 48, 1498 (1956).

7. Olin, J. B., and B. H. Sage, J. Chem. Eng. Data, 5, 16 (1960).

8. Richter, G. N., H. C. Wiese, and B. H. Sage, Combustion and Flame, 6, 1 (1962).

9. Richter, G. N., H. C. Wiese, and B. H. Sage, J. Chem. Eng. Data, 6, 377 (1961).

10. Richter, G. N., H. H. Reamer, and B. H. Sage, Chem. Eng. Sci., 17, 813 (1962).

11. Seagrave, R. C.,and B. H. Sage, Combustion and Flame, 10, 101 (1966).

12. Seagrave, R. C., H. H. Reamer, and B. H. Sage, Combustion and Flame. 8. 11 (1964).

13. Putnam, A. A., and W. R. Dennis, J. Acoust. Soc. Am. 28, 246 (1956).

14. Richardson, E. G., Proc. Phys. Soc. (London), 35, 47 (1922).

15. Jones, A. T., J. Acoust. Soc. Am., 16, 254 (1945).

16. Rijke, P. L., Phil. Mag., 17, 419 (1859).

17. Lehmann, K. O., Ann. Phys., 5th Series, 29, 527 (1937).

18. Kaskan, W. E., and A. E. Noreen, Trans. ASME, 77, 885 (1955).

19. Blackshear, P. L., W. D. Rayle, and L. K. Tower, NACA TN 3567 (1955).

20. Rogers, D. E., and F. E. Marble, Jet Propulsion, 26, 456 (1956).

21. Moore, F. K., and S. H. Maslen, NACA TN 3152 (1954).

22. Crocco, L., and S.-I. Cheng, "Theory of Combustion Instability in Liquid-propellant Rocket Motors". AGARDograph 8, Butterworths Scientific Publications, London (1956).

23. Zucrow, M. J., and J. R. Osborn, Jet Propulsion, 28, 654 (1958).

24. Ellis, H., I. Odgers, A. J. Stosick, N. Van de Verg, and R. S. Wick, "Fourth Symposium on Combustion", 880, Williams and Wilkins, Baltimore (1953).

25. Sears, F. W., "Mechanics, Heat and Sound." Addison-Wesley Press, Cambridge, Mass. (1952).

26. Bertin, L., and B. Salmon, "Combustion Researches and Reviews", Butterworths Scientific Publications, London (1957).

27. Rayleigh, L., "The Theory of Sound", Vol. 2, Dover, N. Y. (1945).

28. Bird, R. B., W. E. Stewart, and E. N. Lightfoot, "Transport Phenomena", John Wiley & Sons, N. Y. (1960).

29. Merk, H. J., Appl. Sci. Res., A6, 317 (1956-57).

30. Merk, H. J., "Sixth Symposium on Combustion", p. 500, Reinhold, N. Y. (1957).

31. Merk, H. J., Appl. Sci. Res., A7, 175 (1957-58).

32. Merk, H. J., ibid., A7, 192 (1957-58).

33. Merk, H. J., ibid., A8, 1 (1958-59).

34. Blackshear, P. L., Jr., "Fourth Symposium on Combustion", p. 553, William and Wilkins, Baltimore (1953).

35. Bailey, J. J., J. Appl. Mech., Trans. ASME 79, Part 2, 333 (1957).

36. Cheng, S. -I., J. Am. Rocket Soc., 23, 89 (1953).

37. Roginskii, O. G., Soviet Physics, 7, No. 2, 107 (1961).

38. Higgins, B., J. Nat. Phil. Chem. and the Arts, 1, 129 (1802).

39. Lacey, W. N., and B. H. Sage, "Thermodynamics of One-Component Systems", Academic Press, N. Y. (1957).

40. Wood, A., "Acoustics", p. 93 , Interscience (1941).

41. Putnam, A. A., and W. R. Dennis, J. Acoust. Soc. Am., 26, 716 (1954).

42. Putnam, A. A., and W. R. Dennis, Trans. ASME 75, 15 (1953).

43. Putnam, A. A., and W. R. Dennis, J. Acoust. Soc. Am., 28, 260 (1956).

44. Raushenbakh, B. V., Appl. Mech. Rev., 8, 159 (1955).

45. Chu, B.-T., NACA RM 56 D 27 (1956).

46. Chu, B.-T., "Fourth Symposium on Combustion", p. 603, Williams and Wilkins, Baltimore (1953).

47. Berry, V. J., Mason, D. M., and B. H. Sage, Ind. Eng. Chem., 45, 1596 (1953).

48. Reamer, H. H., and B. H. Sage, Rev. Instrum., 24, 362 (1953).

49. Benedict, W. A., and E. K. Plyler, "Energy Transfer in Hot Gases", Circ. U.S. Nat. Bur. Stand. No. 523, p. 57 (1954).

50. Shenker, H., J. I. Lauritzen, Jr., R. J. Corruccini, and S. T. Lonberger, Circ. U.S. Nat. Bur. Stand. No. 561, p. 27 (1955).

51. "Second Symposium on Combustion, Flame, and Explosion Phenomena", Chem. Revs., 21, 209 (1937).

52. Beatty, R. L., L. B. Berger, and H. H. Schrenk, "Determination of the Oxides of Nitrogen by the Phenol-disulphonic Acid Method", Bureau of Mines, R. I. 3687 (1943).

53. Miller, D. C., "Sound Waves: Their Shape and Speed", Macmillan, N. Y. (1937).

54. Chia, W. S., J. Jacobs, and B. H. Sage, Technical Report on Studies of Formation of Oxides of Nitrogen during Combustion at Atmospheric Pressure. Report No. 4236, (1968).

55. Morse, P. M., "Vibration and Sound", p. 248, McGraw-Hill, N. Y. (1948).

56. Timoshenko, S., and D. H. Young, "Engineering Mechanics", Fourth Edition, McGraw-Hill, N. Y. (1956).

57. Sears, F. W., "Mechanics, Wave Motion, and Heat", Addison-Wesley (1958).

58. Wimpress, R. N., "Internal Ballistics of Solid-Fuel Rockets", McGraw-Hill, N. Y. (1950).

59. JANAF Thermochemical Tables, Dow Chemical Co., Midland, Mich. (1966).

60. Am. Petro. Inst. Research Project 44, "Selected Values of Properties of Hydrocarbons and Related Compounds." Chemical Thermodynamic Properties Center, Texas A & M University.

61. Kelley, K. K., "Contributions to the Data on Theoretical Metallurgy XIII. High-Temperature Heat-Content, Heat Capacity, and Entropy Data for the Elements and Inorganic Compounds," U.S. Bureau of Mines Bulletin 584 (1960).

IX. NOMENCLATURE

A. Roman Type Symbols

a, a'	Constants.
A	Cross-sectional area of combustor, sq.ft.
b	Specific gas constants, B.t.u./(lb.mass)(^{o}R).
B	Bulk modulus, psi.
c	Velocity of sound, ft./sec.
c_1,c_2	Constants.
c_p	Isobaric specific heat, B.t.u./lb. ^{o}F.
c_v	Isochoric specific heat, B.t.u./lb. ^{o}F.
f	Frequency of oscillations in the combustion tube, cycle/sec.
f_m	Frequency of oscillations in the plenum chamber, cycle/sec.
g	Acceleration due to gravity, ft./sq.sec.
h_i	Local average heat transfer coefficient, B.t.u./(sq.ft.)(^{o}F.)(sec.).
H	Rate of heat release, B.t.u./sec.
I	Instantaneous optical intensity.
k	Thermal conductivity, B.t.u./(ft.)(^{o}F.)(sec.).
L	Effective length of combustor, in.
L_r	Length for the correction of open-end reflection, in.
L'	Length of combustor corrected for the effect of open-end reflection, in.
L_m	Effective length of the plenum chamber, in.

M	Molecular weight.
$\mathring{m}$	Weight rate of flow, lb./sec.
n	Positive integers.
P	Pressure. psi.
P'	Oscillating component of pressure, psi.
$\mathring{q}$	Heat flux, B.t.u./(sq.ft.)(sec.).
r	Radius of the combustion tube, in.
R	Gas constant, B.t.u./(lb.mole)(^{o}R).
t	Time, sec.
T	Temperature, ^{o}F. or ^{o}R.
u	Average momentum velocity, ft./sec.
V	Volume, cu.ft.
$\vec{v}$	Velocity vector, ft./sec.
x	Cartesian coordinate, in.
y	Amplitude of oscillations, in.

Greek Type Symbols

α	An abbreviation for $2\pi h_1 r$, a constant.
β	A complex parameter.
γ	Ratio of isobaric to isochoric specific heats.
θ	Time, millisec.
Θ	Time taken for a wave particle to travel to the downstream end of combustion tube and back, sec.
κ	An abbreviation for ω/c.
λ	Wavelength, in.

μ	Absolute viscosity, lb./ft. sec.
ρ	Density, lb./cu.ft.
ρ_o	Density under quiescent condition, lb./cu.ft.
Ω	Time taken for gas to pass through the flame holder and be burned, sec.
τ	Period of oscillations in the combustion tube, sec.
τ_m	Period of oscillations in the plenum chamber, sec.
ω	Angular frequency, $sec.^{-1}$

Mathematical Symbols

d	Ordinary differential operator.
D	Substantial differential operator.
∂	Partial differential operator.
$\int$	Integration operator.
$\nabla\phi$	Gradient of a scalar ϕ.
$\nabla\cdot F$	Divergence of a vector F.
$\nabla^2\psi$	Laplacian of a scalar ψ.
e,exp	Exponential.
ln	Natural logarithm.
Δ	Difference in, increment in.

Subscripts

ad	Adiabatic.
e	Exit.
is	Isothermal.

m	Mixing chamber.
M	Maximum or minimum.
n	Any positive integer, referring to nth mode of oscillation.
w	Wall.
1	Initial state.
2	Final state.

TABLE I

TYPICAL NATURAL GAS ANALYSES

Component		Mole fraction	
		Sample 1	Sample 2
Methane	CH_4	0.8904	0.8897
Ethane	C_2H_6	0.0725	0.0729
Propane	C_3H_8	0.0163	0.0157
n-Butane	C_4H_{10}	0.0016	0.0022
i-Pentane	C_5H_{12}	0.0006	0.0006
Nitrogen	N_2	0.0104	0.0107
Carbon dioxide	CO_2	0.0080	0.0082
Oxygen	O_2	0.0002	0.0001
Molecular Weight		17.9697	17.9897
Specific Weight ($60^\circ F$ and 30 in. Hg)			
	Dry	0.04735	0.04736
	Saturated	0.04740	0.04741

TABLE II. SUMMARY OF EXPERIMENTAL CONDITIONS

Test No.	Time (sec.)	AIR Entrance Velocity (ft/sec)	AIR Wt. Rate of Flow (lb/sec)	AIR Weight Fraction Water	NATURAL GAS Entrance Velocity (ft/sec)	NATURAL GAS Wt. Rate of Flow (lb/sec)	Mixture* Ratio	Average Pressure (psia)
546	3950	8.56	0.04906	0.0094	0.7646	0.002652	0.89	14.520
	8600	8.38	0.04804				0.91	14.537
	12030	8.59	0.04924				0.89	14.533
547	3140	8.63	0.04912	0.0059	0.7669	0.002657	0.89	14.443
	4420	8.58	0.04882				0.90	14.450
	8040	8.72	0.04963				0.88	14.460
550	1960	8.59	0.04901	0.0067	0.7688	0.002670	0.90	14.475
	9110	8.51	0.04858				0.91	14.481
551	2540	8.27	0.04724	0.0071	0.7657	0.002647	0.93	14.492
	3070	8.50	0.04850		0.7515	0.002598	0.88	14.492
	3640	8.54	0.04876		0.7637	0.002640	0.89	14.503
	5080	8.35	0.04765		0.7640	0.002641	0.92	14.502
	8490	8.44	0.04817		0.7637	0.002640	0.90	14.489
	10000	8.28	0.04729		0.7637	0.002640	0.92	14.509
555	1990	8.52	0.04874	0.0095	0.7538	0.002607	0.88	14.479
	4630	8.24	0.04722				0.91	14.477
557	2570	8.59	0.04894	0.0084	0.7544	0.002667	0.90	14.475
	4200	8.17	0.04660				0.95	14.455

TABLE II. (Continued)

Test No.	Time (sec)	AIR Entrance Velocity (ft/sec)	AIR Wt. Rate of Flow (lb/sec)	AIR Weight Fraction Water	NATURAL GAS Entrance Velocity (ft/sec)	NATURAL GAS Wt. Rate of Flow (lb/sec)	Mixture* Ratio	Average Pressure (psia)
559	1570	8.62	0.04905	0.0076	0.7671	0.002627	0.88	14.473
	3550	8.38	0.04771				0.91	14.488
	5820	8.69	0.04945				0.88	14.473
561	3040	8.44	0.04842	0.0113	0.7630	0.002599	0.89	14.475
	4980	8.27	0.04747				0.90	14.461
563	1870	8.44	0.04828	0.0120	0.7557	0.002630	0.90	14.425
	2740	8.46	0.04844				0.90	14.432
	3080	8.39	0.04803				0.90	14.425
565	3110	8.39	0.04773	0.0125	0.7659	0.002594	0.90	14.376
	7960	8.24	0.04695				0.91	14.358

* Mixture ratio expressed as fraction combustibles relative to stoichiometric quantity required.

TABLE III. ANALYSES OF PERTURBATIONS

Test No.	Time (sec)	Length of Chamber* (in.)	Longitu'l Position** (in.)	Transient Pressure ΔP (psi)	Transient Pressure Frequency (cycle/sec)	Longitu'l Position** (in.)	Transient Pressure ΔP (psi)	Transient Pressure Frequency (cycle/sec)
546	4070	76.72	22.7 (6)	0	0			
	4180			0	0			
	4690	78.52		0.326	889			
	4740			0.309	904			
	7240	79.85		0.714	886			
	7270			0.721	896			
	7550			0.793	714			
	7590	80.57		0.741	720			
	8640	81.67		0.943	699			
	8650			0.029	1047			
	8890			0.936	704			
	9005			0.092	1029			
	9650			0.341	833			
	9780	82.96		0.427	836			
	10210	84.65		0.446	846			
	10350			0.448	833			
	10990			0.468	656			
	11060	86.22		0.410	658			
	11490	86.84		0.589	660			
	11510			0.624	649			
	12060			0.474	787			
	12124	88.82		0.361	780			
	12870	76.72		0	0			
	13030			0	0			

TABLE III. (Continued)

Test No.	Time (sec)	Length of Chamber* (in.)	Longitu'l Position** (in.)	Transient Pressure ΔP (psi)	Transient Pressure Frequency (cycle/sec)	Longitu'l Position** (in.)	Transient Pressure ΔP (psi)	Transient Pressure Frequency (cycle/sec)
547	2840	76.72	22.7 (6)	0	0			
	2880			0	0			
	4580	78.89		0.606	949			
	4620			0.598	945			
	5720	101.03		0	0			
	7160	106.32		0	0			
	9020	137.27		1.218	845			
	9120			1.005	848			
550	1970	77.90	22.7 (6)	0.341	889	76.7 (10)	0.615	889
	2110			0.240	898		0.369	898
	3255	78.17		0.365	889		0.685	893
	3290			0.370	890		0.692	888
	4140	78.40		0.448	886		0.800	886
	4350			0.443	895		0.739	893
	4790	78.67		0.458	893		0.735	893
	4820			0.439	889		0.739	891
	5240	78.92		0.536	890		1.015	889
	5370			0.482	889		0.895	892
	5700	79.15		0.546	883		0.797	886
	5730			0.595	889		1.046	887
	6400	79.42		0.595	887		0.962	892
	6530			0.585	885		0.954	885
	7020	79.64		0.663	883		1.077	883

TABLE III. (Continued)

Test No.	Time (sec)	Length of Chamber* (in.)	Longitu'l Position** (in.)	Transient Pressure ΔP (psi)	Transient Pressure Frequency (cycle/sec)	Longitu'l Position** (in.)	Transient Pressure ΔP (psi)	Transient Pressure Frequency (cycle/sec)
550	7050	79.64	22.7 (6)	0.628	887	76.7 (10)	1.039	889
	7440	79.91		0.721	889		1.115	885
	7810			0.745	883		1.192	883
	8140	80.17		0.793	883		1.169	883
	8170			0.784	870		1.100	883
	8500	80.42		0.676	889		0.977	885
	8550			0.628	885		0.957	885
	8850	80.67		0.630	885		0.926	885
	8890			0.614	889		0.912	889
	9150	80.90		0.585	893		0.915	891
	9230			0.620	883		0.889	886
	9500	81.14		0.604	887		0.877	887
	9550			0.653	889		0.885	889
	10285	81.41		0.994	709		0.915	714
				0.193	925		0.287	897
	10407			1.156	702		0.889	702
	11670	77.90		0.253	906		0.569	886
	11800			0.312	905		0.523	889
	12800	76.10		0.653	769		0.677	769
				0.059	963		0.146	963
	12900			0.721	774		0.715	774
	13220			0.575	769		0.531	769
	13254			0.313	770		0.410	862

TABLE III. (Continued)

Test No.	Time (sec)	Length of Chamber* (in.)	Longitu'l Position** (in.)	Transient Pressure ΔP (psi)	Transient Pressure Frequency (cycle/sec)	Longitu'l Position** (in.)	Transient Pressure ΔP (psi)	Transient Pressure Frequency (cycle/sec)
551	2020	77.90	22.7 (6)	0.318	894	12.7 (4)	0.305	894
	2120			0.361	892		0.345	892
	3090	78.41		0.468	892		0.462	892
	3170			0.402	893		0.435	893
	3670	78.92		0.472	894		0.554	894
	3720			0.507	892		0.529	892
	4150	79.41		0.643	883		0.574	884
	4260			0.610	889		0.646	886
	4700	79.91		0.702	891		0.585	884
	4750			0.651	887		0.551	882
	5147	80.40		0.634	882		0.559	883
	5270			0.649	883		0.554	885
	5570	80.92		0.600	887		0.523	883
	5620			0.577	889		0.415	697
	6280	81.41		1.023	704		0.277	898
				0.273	898		0.431	695
	6420			1.088	695		0.282	887
				0.141	887		-	-
	7880	80.40		0.891	710		0.354	710
	8017			0.864	712		0.308	712
	8240			0.838	714		0.280	714
	8590	77.91		0.351	889		0.314	889
	8610			0.351	894		0.394	894
	9570	76.72		0	0		0	0
	9620			0	0		0	0

TABLE III. (Continued)

Test No.	Time (sec)	Length of Chamber* (in.)	Longitu'l Position** (in.)	Transient Pressure ΔP (psi)	Transient Pressure Frequency (cycle/sec)	Longitu'l Position** (in.)	Transient Pressure ΔP (psi)	Transient Pressure Frequency (cycle/sec)
551	10320	76.10	22.7 (6)	0.604	952	12.7 (4)	0.746	952
				0.595	941		0.739	941
	10420			0.542	947		0.712	947
	10520			0.552	769		0.195	769
	11080			0.468	750		0.220	750
555	1650	76.72	22.7 (6)	0	0	12.7 (4)	0	0
	1790			0	0		0	0
	3380	76.12		0.376	771		0.137	771
	3440			0.182	948		0.410	952
	3614			0.553	769		0.230	769
	3650			0.156	965		0.304	954
	3920	75.72		0.589	765		0.198	765
	3980			0.593	771		0.219	771
	4260	74.72		0.672	771		0.257	765
	4454			0.712	765		0.311	770
	4630	73.72		0.629	765		0.261	772
	4680			0.617	769		0.269	769
	4912	72.74		0.241	777		0.093	777
	4960			0.273	770		0.113	769
	5138	71.72		0.217	1019		0.466	1011
	5140			0.212	1020		0.507	1021
	5440	70.74		0.351	827		0.367	963
	5690			0.405	826		0.226	826

TABLE III. (Continued)

Test No.	Time (sec)	Length of Chamber* (in.)	Longitu'l Position** (in.)	Transient Pressure ΔP (psi)	Transient Pressure Frequency (cycle/sec)	Longitu'l Position** (in.)	Transient Pressure ΔP (psi)	Transient Pressure Frequency (cycle/sec)
557	1974	76.89	22.7 (6)	0	0	12.7 (4)	0	0
	2020			0	0		0	0
	3510	70.72		0.449	826		0.273	829
	3670			0.190	1026		0.433	1021
	3920			0.758	843		0.507	904
	3986			0.401	1032		0.610	1006
	4570	71.74		0.431	1000		0.802	1000
	4600			0.848	811		0.442	809
	4680			0.858	816		0.465	816
	4810			0.561	1019		0.853	1019
	6000	72.74		0.200	994		0.481	994
	6060			0.393	769		0.220	769
	6520			0.190	1006		0.385	1006
	6690			0.180	774		0.055	774
	7305	73.74		0.551	774		0.195	762
	7440			0.571	765		0 211	765
559	1930	75.74	22.7 (6)	0	0	12.7 (4)	0	0
	2030			0	0		0	0
	2610	73.24		0.561	768		0.164	768
	2730			0.382	765		0.104	765
	3010	73.75		0.627	766		0.220	766
	3070			0.588	766		0.195	766
	3320	74.74		0.706	765		0.262	765
	3370			0.667	776		0.237	776

TABLE III. (Continued)

Test No.	Time (sec)	Length of Chamber* (in.)	Longitu'l Position** (in.)	Transient Pressure ΔP (psi)	Transient Pressure Frequency (cycle/sec)	Longitu'l Position** (in.)	Transient Pressure ΔP (psi)	Transient Pressure Frequency (cycle/sec)
559	3830	75.24	22.7 (6)	0.739	762	12.7 (4)	0.258	762
	3910			0.869	762		0.411	762
	4120	75.75		0.745	769		0.279	769
	4150			0.720	763		0.252	763
	4840	76.12		0.289	976		0.320	976
	4954			0.637	995		0.582	995
	5200			0.306	952		0.529	952
	5520			0.598	771		0.205	771
561	2290	76.74	22.7 (6)	0	0	12.7 (4)	0	0
	2440			0	0		0	0
	3710	80.74		0.665	712		0.171	710
	3770			0.619	714		0.159	714
	4070	80.24		0.769	713		0.255	717
	4150			0.706	712		0.201	712
	4370	79.72		0.658	712		0.177	711
	4410			0.704	714		0.214	718
	4690	79.24		0.424	889		0.375	889
	4730			0.432	885		0.394	885
	5010	78.74		0.350	893		0.329	890
	5040			0.364	889		0.354	889
	5260	78.24		0.311	889		0.283	889
	5300			0.315	880		0.300	881
	5670	77.74		0.224	897		0.213	897
	5720			0.224	892		0.222	907

TABLE III. (Continued)

Test No.	Time (sec)	Length of Chamber* (in.)	Longitu'l Position** (in.)	Transient Pressure ΔP (psi)	Transient Pressure Frequency (cycle/sec)	Longitu'l Position** (in.)	Transient Pressure ΔP (psi)	Transient Pressure Frequency (cycle/sec)
563	1270	76.74	22.7 (6)	0	0	12.7 (4)	0	0
	1580			0	0		0	0
	2450	81.74		0.071	1026		0.252	1026
	2500			0.077	1030		0.312	1022
	2780	82.73		0.140	1026		0.355	1022
	2850			0.193	1022		0.427	1026
	3100	83.74		0.400	839		0.219	834
	3140			0.410	839		0.233	842
	3420	84.74		0.433	848		0.216	852
	3460			0.496	851		0.254	854
	3560			-	-		-	-
	3810			-	-		-	-
	3840			-	-		-	-
	4200	85.74		0.079	963		0.191	963
	4260			0.095	949		0.212	960
	4510	86.74		0.186	963		0.432	958
	4560			0.168	954		0.415	958
	4790	87.73		0.273	952		0.505	956
	4910			0.251	952		0.463	967
	5150	88.73		0.100	798		0.034	798
	5280			0.141	792		0.042	769
	5692	85.24		0.219	1143		0.260	1136
	5820			0.192	1133		0.211	1135
	6020			-	-		-	-

TABLE III. (Continued)

Test No.	Time (sec)	Length of Chamber* (in.)	Longitu'l Position** (in.)	Transient Pressure ΔP (psi)	Transient Pressure Frequency (cycle/sec)	Longitu'l Position** (in.)	Transient Pressure ΔP (psi)	Transient Pressure Frequency (cycle/sec)
565	2180	76.77	22.7 (6)	0	0	12.7 (4)	0	0
	2290			0	0		0	0
	3530	69.74		0.482	845		0.238	845
	3590			0.381	844		0.209	842
	3850			-	-		-	-
	4030			-	-		-	-
	4320	68.73		0.306	839		0.170	839
	4360			0.286	847		0.157	842
	4880	67.74		0.039	649		0	0
	5020			0.146	1074		0.148	1081
	5120			0.159	653		0.025	670
	5330			0.080	654		0.052	1081
	5730	66.74		0.225	886		0.177	889
	7190	67.12		0.078	1087		0.173	1087
	7280			0.125	1075		0.237	1074
	7650	65.74		0.396	883		0.335	883
	7700			0.340	889		0.282	889
	8020	64.74		0.305	892		0.278	896
	8080			0.275	889		0.265	887

* Length of chamber as determined from distance between reflecting disk and flameholder.

** Refers to ports shown in Figure 4. Position refers to distance from flameholder in inches.

TABLE IV. APPARENT TEMPERATURE OF THE GAS

Test No.	Mixture Ratio	Port No.	Longitudinal Position (in.)	Radial * Position (in.)	Apparent Temperature (°F.)	Avg. Appt. Temp. in a Section °F.	Estimated Space-avg. Temp. °F.
448	0.90	10	76.7	1.50	1539.7		
				1.00	1706.8		
				0.50	1781.4		
				0.00	1815.9		
				-1.00	1691.9		
				-1.75	1349.0	1690	1708
449	0.89	11	100.7	1.50	1303.3		
				1.00	1401.5		
				0.50	1486.8		
				0.00	1519.5		
				-0.50	1496.3		
				-1.00	1432.0		
				-1.50	1279.6		
				-1.75	1238.6		
				-1.00	1433.4		
				1.00	1439.6	1440	1464
450	0.90	11	100.7	1.50	1305.7		
				0.50	1540.7		
				0.00	1548.7		
				-0.50	1529.6		
				-1.50	1304.7		
				-1.75	1230.7	1475	1464

* Minus sign refers to the radial positions closer to the measuring ports.

APPENDIX I

ADIABATIC AND ISOTHERMAL BULK MODULUS OF A PERFECT GAS

The bulk modulus of a substance is defined as[25]

$$B = -\frac{\Delta P}{\Delta V / V} \quad . \tag{1}$$

In the limiting case of small changes,

$$B = -V\frac{dP}{dV} \quad . \tag{2}$$

For a perfect gas in an adiabatic process,

$$PV^{\gamma} = \text{constant.} \tag{3}$$

Whence

$$P\gamma V^{\gamma-1}\,dV + V^{\gamma}\,dP = 0, \tag{4}$$

and

$$\frac{dP}{dV} = -\frac{P\gamma}{V} \quad . \tag{5}$$

The adiabatic bulk modulus is therefore

$$B_{ad} = -V\left(-\frac{P\gamma}{V}\right) = \gamma P \quad . \tag{6}$$

In an isothermal process, for a perfect gas,

$$PV = \text{constant} \quad . \tag{7}$$

Thus

$$P\,dV + V\,dP = 0 \quad , \tag{8}$$

and

$$\frac{dP}{dV} = -\frac{P}{V} \quad . \tag{9}$$

The isothermal bulk modulus is then

$$B_{is} = -V\left(-\frac{P}{V}\right) = P \quad . \tag{10}$$

It follows that

$$B_{ad} = \gamma B_{is} \quad . \tag{11}$$

Hence for a perfect gas, γ, the ratio of isobaric to isochoric specific heats, is also equal to the ratio of the adiabatic bulk modulus to the isothermal bulk modulus.

APPENDIX II

COMPUTATION OF EQUILIBRIUM FLAME TEMPERATURE AND COMPOSITIONS

The flame temperature and compositions of the gas mixture were calculated under the assumption of local physicochemical equilibrium for perfect gases at a constant pressure. The feed was assumed to contain only CH_4, C_2H_6, C_3H_8, C_4H_{10}, and air and all the other minor components were neglected. Their combustion reactions are then:

1. $CH_4 + 2\,O_2 \rightleftharpoons CO_2 + 2\,H_2O$
2. $C_2H_6 + 3\tfrac{1}{2}\,O_2 \rightleftharpoons 2\,CO_2 + 3\,H_2O$
3. $C_3H_8 + 5\,O_2 \rightleftharpoons 3\,CO_2 + 4\,H_2O$
4. $C_4H_{10} + 6\tfrac{1}{2}\,O_2 \rightleftharpoons 4\,CO_2 + 5\,H_2O$.

In addition to these four reactions the eleven reactions suggested by Wimpress[58] may also take place. However, only Nos. 1, 7, 8, 9, and 11 of those are considered to be important up to a temperature of 3000°F. Since of these five reactions, Nos. 1, 7, and 9 are related and only two of these three are independent and need be considered, an arbitrary choice was made to consider Nos. 7 and 9. The eight equations involved are then:

1. $CH_4 + 2O_2 \rightleftharpoons CO_2 + 2H_2O + \Delta H_1$ (cal/mole CH_4)

2. $C_2H_6 + 3\frac{1}{2}O_2 \rightleftharpoons 2CO_2 + 3H_2O + \Delta H_2$ (cal/mole C_2H_6)

3. $C_3H_8 + 5O_2 \rightleftharpoons 3CO_2 + 4H_2O + \Delta H_3$ (cal/mole C_3H_8)

4. $C_4H_{10} + 6\frac{1}{2}O_2 \rightleftharpoons 4CO_2 + 5H_2O + \Delta H_4$ (cal/mole C_4H_{10})

7. ΔH_7 (cal/mole CO) + $CO + \frac{1}{2}O_2 \rightleftharpoons CO_2$

8. ΔH_8 (cal/mole OH) + $OH + \frac{1}{2}H_2 \rightleftharpoons H_2O$

9. ΔH_9 (cal/mole H_2) + $H_2 + \frac{1}{2}O_2 \rightleftharpoons H_2O$

11. $\frac{1}{2}N_2 + O_2 \rightleftharpoons NO + \Delta H_{11}$ (cal/mole N_2)

A computer program for the calculation of flame temperature and equilibrium compositions was developed. The computer subroutines required were written in Fortran IV and the computer-produced binary decks are available.

The major reactive components of the final products are N_2, O_2, NO, OH, CO, CO_2, H_2O, and H_2. There are eight unknown number of moles. Therefore, eight equations are needed to solve for the aforementioned number of moles. Four of the eight equations involve the balance of moles of carbon, oxygen, hydrogen, and nitrogen atoms, and the four other equations represents the equilibrium relations for reactions 7, 8, 9, and 11. The method of using the

values of equilibrium constants K is according to that reported in Wimpress[58].

The following scheme was employed in evaluating the equilibrium flame temperature. To obtain the initial estimate of final temperature, it was assumed that only reactions 1 through 4 occurred for stoichiometric and rich mixtures and that only reactions 1 through 4, 7, and 9 occurred for lean mixtures. It was further assumed that each of these reactions went to completion. For an assumed input of moles of feed, the final compositions were computed. The flame temperature was then obtained from the energy balance by means of a double iterative procedure. A check was made at the final flame temperature utilizing the equilibrium constants for the reactions not considered to ensure that the number of moles of O_3, NO_3, CH_4, and the number of moles of oxygen, hydrogen, and nitrogen atoms are negligible.

Since table-look-up subroutines are time consuming, it was decided to employ analytical expressions for calculation of the required values of isobaric heat capacity, equilibrium constant, and enthalpy. In some cases it was necessary to evaluate the coefficients over two ranges of temperature to obtain the desired accuracy. The coefficients of the analytical expression for most of the compo-

nents were obtained from JANAF Tables[59]. Those for hydrocarbons other than methane were reported in API[60], while those for argon were contributed by Kelley[61].

PROPOSITION I

The effect of suspensions of solid particles upon the longitudinal dispersion of a soluble matter flowing in a pipe has been studied experimentally. It was found that the presence of the solid particles increased the rate of radial diffusion in both laminar and turbulent flow, while the rate of longitudinal dispersion was reduced appreciably. The appropriate viscosity for use in correlation was found to be the effective viscosity of suspensions.

A. Introduction

The longitudinal dispersion process in a pipe flow has long been considered[1-4] to be characterized by a diffusion-type model governed by the diffusion equation

$$\frac{\partial C}{\partial t} = K \frac{\partial^2 C}{\partial x_1^2} \quad , \tag{1}$$

where $x_1 = x - U t$ is the distance between a fixed point and a plane moving at the mean velocity. In this equation K, which has the units of a molecular diffusion coefficient and is called the longitudinal dispersion coefficient[5], uniquely characterizes the dispersion process. This longitudinal dispersion coefficient also

represents the combined action of molecular diffusion and variation of velocity over the cross-section of the tube. When a pulse of soluble matter is introduced into a stream of flowing fluid, it spreads out under the combined action of convective transfer and molecular diffusion. It is apparent that the effect of convective transfer is to increase the distance over which the soluble substance is dispersed. The effect of radial diffusion tends to eliminate the radial concentration gradients created by the convective effect and to keep the pulse together. Consequently, the dispersion or spread of the pulse is reduced.

A dimensional analysis[5] on the variables affecting the dispersion during steady flow in a smooth straight pipe indicates that the dimensionless group K/dU, which is similar to the reciprocal of the Peclet number, may be expressed as a function of the Reynolds number and Schmidt number

$$\frac{K}{dU} = F(Re, Sc) = F\left\{\left(\frac{dU\rho}{\mu}\right), \left(\frac{\mu}{\rho D}\right)\right\} , \quad (2)$$

where D is the molecular diffusivity of the substance under consideration. In turbulent flow, however, molecular diffusion is much less important than eddy diffusion,

so that the effect of the Schmidt number upon the dispersion coefficient should be very small.

A solution of Equation (1) when the material is initially concentrated at $x = 0$ is[6]

$$C = A t^{-\frac{1}{2}} \exp\left\{\frac{-(x - Ut)^2}{4Kt}\right\}, \qquad (3)$$

where A is a constant depending on the total amount of diffusing material. It should be noted that the concentration-time curve given by Equation (3) is not perfectly symmetrical when measurements are made at a fixed position x. Taylor[4] has suggested, however, that the lack of symmetry is small when measurements are made at positions farther than about 100 pipe diameters downstream in turbulent flow. Under such conditions, the solution given by Equation (3) may be used to calculate the longitudinal dispersion coefficient K from the approximation:

$$\frac{x_{\frac{1}{2}}^2}{4Kt} = \ln 2 , \qquad (4)$$

where $x_{\frac{1}{2}}$, according to Taylor's definition[4], is half the mean length of pipe containing fluid of concentration greater than half the maximum. The length $x_{\frac{1}{2}}$ is in turn equal to

$$x_{\frac{1}{2}} = U t_{\frac{1}{2}} , \qquad (5)$$

where $t_{\frac{1}{2}}$ is the time interval between successive occurrences of the half-maximum concentration. Since $t_{\frac{1}{2}}$ can easily be measured from a concentration-time curve, Equation (4) thus provides a principal basis for calculating the longitudinal dispersion coefficient corresponding to the flowrates at which the asymmetry of the concentration-time curve is small.

The problem of the dispersion of soluble matter in circular pipes has been studied by many investigators[1-4, 7,8]. However, none of them have studied the longitudinal dispersion process in a two-phase flow. The latter problem is considered to be very important as to industrial applications, particularly in catalytic reactor design. Therefore, the purpose of the present work is to investigate the effect of adding solid particles upon the dispersion of a soluble pulse in a flowing stream. The suspensions of spherical solid particles were employed for which the effective viscosity had been measured as a function of solid concentration[9].

B. Equipment and Experimental Methods

The apparatus consisted of a conical-bottomed supply tank, connected to a small rotary pump, which in turn discharged to a 3/4 in. brass pipe. The discharge

line was gradually bushed down to the 3/8 in. test line where measurements of dispersion were made. The test line consisted of a 38 ft. straight length of 3/8 in. i.d. brass pipe. The discharge passed into the supply tank, thus constituting a closed circuit. A flexible buna-N rubber vane was used in the rotary pump when handling suspensions of solid particles in water. A stirrer was employed in the supply tank to provide uniform dispersion and thorough mixing of the suspensions.

The pressure drops along the test line were measured by means of four piezometer bars, which were used in conjunction with mercury- and Meriam Fluid- in-glass manometers. Potassium chloride solutions were introduced into the flowing stream through an injection device which was located at the upstream of the test line. The nozzle in contact with the pipeline was flattened into a slit so that the salt solution being injected could be uniformly distributed across the pipeline.

The passage of the salt pulse was detected by means of five electrodes situated along the test line. The electrodes were immersed to occupy the central part of the cross-section of the pipe, thus were expected to measure the mean concentration of the pulse over the cross-section.

The position of the electrodes immersed in the pipe was varied during a few test runs and the conductivity was not affected. A filament transformer was used to maintain a potential difference of 12.6 volts a.c. across the electrodes to produce a current through the electrode pair. The current set up a potential drop in a 120 Ω resistor connected in series with the electrodes. The potential difference, which is proportional to the conductivity of the pulse, was then applied to a Beckman Dynograph recorder and a cathode-ray oscilloscope.

To prepare for the measurements, the tank was first filled with water and the pump was allowed to run for about ten minutes to remove air from the test line. The stirrer was then turned on and a measured volume of solid particles was added into the tank to make up the desired suspensions. The solids concentration was determined by allowing the solid particles in the sample to settle and observing their total apparent volume. As it was found difficult to maintain the concentration constant with varying flowrates, the readings were repeated each time the velocity was changed.

The accuracy of the experimental measurements has also been investigated. It was found that the error of

the mean velocity measurements was less than 1%. The error introduced by the temperature measurements was less than 0.5°F. In the experimental measurements with the two-phase flow, the error resulted from the measurements of solid concentration was found to be less than 3%, which corresponds to an error of about 2% in viscosity. Therefore, the maximum error of the effective Reynolds number measurements is approximately 3.5%.

C. Experimental Results

In order to make sure that the apparatus operated satisfactorily, the dispersion process was first studied in a stream of clear water for calibration purposes. The injections of salt solution into the pipe were carried out at various flow rates and the responses to each pulse at each electrode were obtained from the recorder. The curves thus obtained represent the time variation of conductivity as the pulse passes each electrode. Since the dispersion coefficient can only be assessed from a concentration-time curve, it becomes necessary to investigate the relationship between the conductivity and the concentration of the salt pulse. Then the concentration-time curves can be plotted.

Most of the measurements were made at the electrode

30 ft. downstream of the injection device and at the Reynolds numbers between 12,000 and 800. As the Reynolds number is reduced, the thickness of the laminar sublayer increases. Salt can only escape from the laminar sublayer by means of molecular diffusion. It follows that the effect of radial molecular diffusion can no longer balance the effect of the variation of velocity over the cross-section of the flow. Consequently, the pulse can not be centered around the plane moving at the mean velocity and the asymmetry of the concentration-time curves increases. At the Reynolds numbers less than about 1,600, the concentration-time curves become noticeably steeper at the front than the rear with a long tail in the rear. However, the lack of symmetry of the concentration-time curves was considered to be small at the Reynolds numbers greater than approximately 2,000. Thus, the longitudinal dispersion coefficients based upon Equation (4) were only calculated at the Reynolds numbers higher than 1,600.

Figure 1 shows the dimensionless group K/dU as a function of Reynolds number for the dispersion of salt pulse in pure water. The current data appeared to be in good agreement with the data reported by Fowler and Brown[7]. The agreement between these two sets of data reflects that no serious error should exist in the pulse-

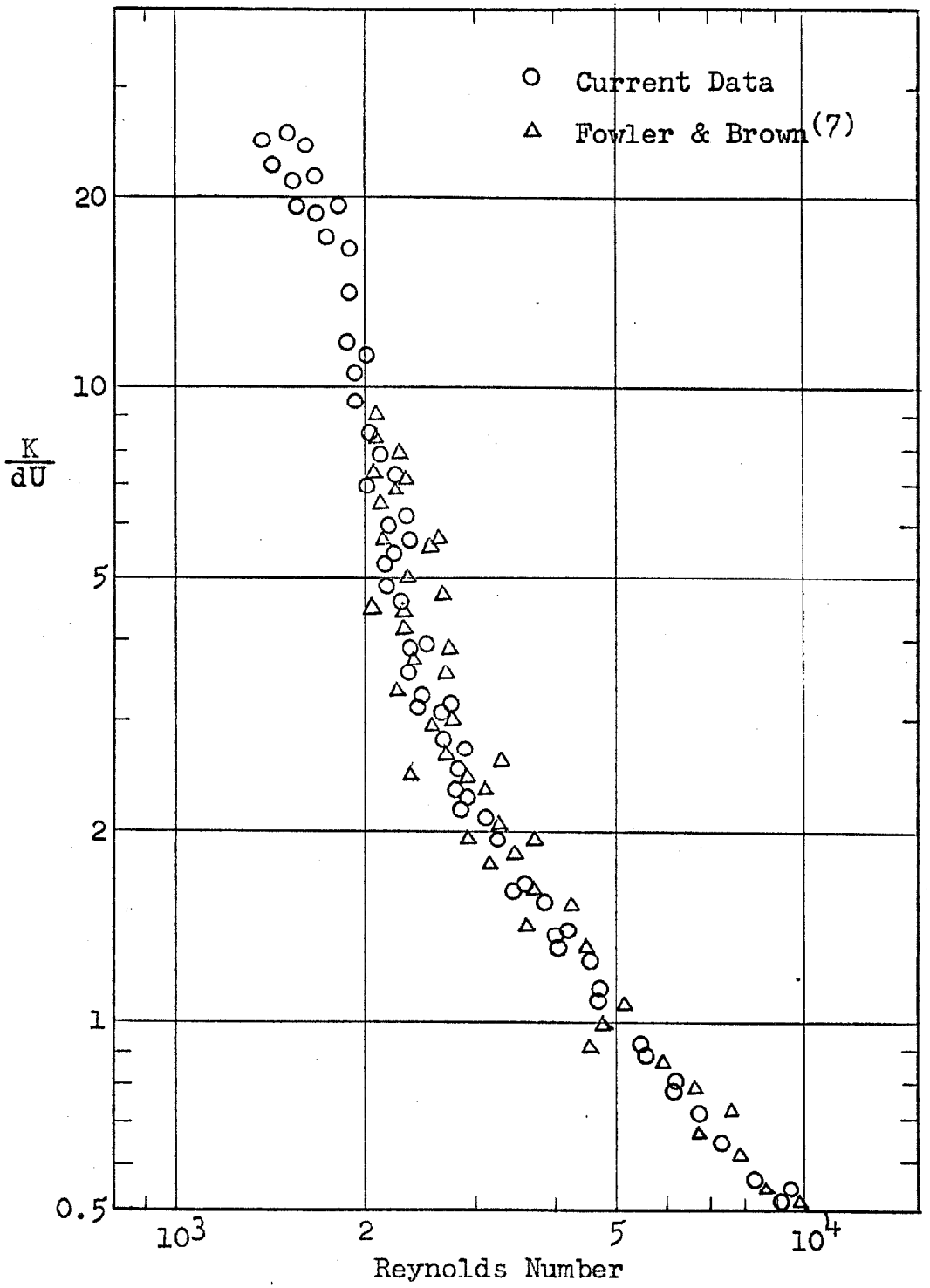

Figure 1. K / d U as a Function of Reynolds Number for Dispersion in Pure Water.

detecting measurements.

In the two-phase flow experiments the solid particles employed were 40/60 mesh polystyrene divinyl benzene copolymer spheres with a density of about 1.08 gr./cm^3. The maximum volume concentration obtained with steady flow was about 35%. Experimental results showed that the terminal falling velocity of a single particle was about 0.6 cm./sec. The porosity of settled beds was investigated by means of the volume displacement method and was found to be 37%.

It is known that the viscosity of suspensions is considerably greater than that of pure water at the same temperature. An effective viscosity of a suspension has thus been proposed under the assumption that the flow of a suspension can be treated with the analytical technique developed for single-phase flow[10]. Consequently, an effective Reynolds number based upon the average density of the mixture and the effective viscosity of suspensions has been defined. The effective viscosity of a suspension has been found to be a function only of the volume concentration of solids[11]. For the polystyrene spheres employed, the experimental work of Mather[9] provided a direct relationship between the effective viscosity of

suspensions and the volume concentration. The data were reported in the tabular form and are plotted in Figure 2.

The effect of suspensions of solid particles upon the dispersion process was then investigated. It was found that the degree of symmetry of the concentration-time curves in laminar flow progressively increased with the concentration of the suspensions. For suspensions with concentration higher than 20%, the concentration-time curves appeared to be symmetrical at the Reynolds numbers as low as 800. It is suggested that, therefore, the presence of solid particles in the stream of water may have produced a considerably higher rate of radial diffusion which tends to keep the pulse together and results in a more symmetrical dispersion of the pulse.

Figure 3 shows the dimensionless group K/dU as a function of the effective Reynolds number for the flow of suspensions of styrene spheres in water. The experimental data obtained at quite different solid concentrations do fall on a single curve; this implies that the hypothesis of single-phase flow is applicable in this study and that the appropriate viscosity for use in correlation is indeed the effective viscosity of suspensions. The magnitude of K/dU for the flow of suspensions is com-

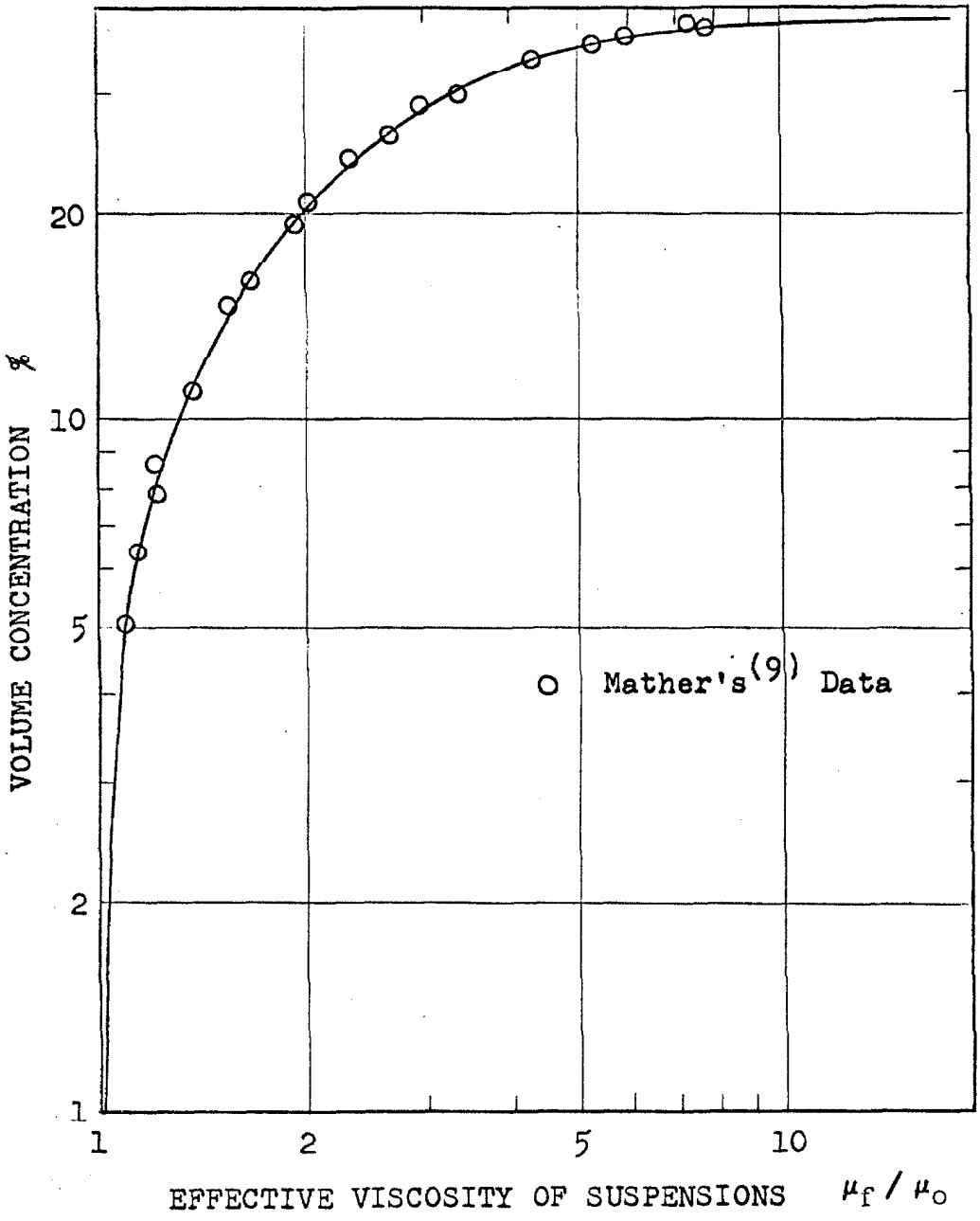

Figure 2. The Effective Viscosity of Suspensions as a Function of Volume Concentration of Solids, as Represented by the Ratio of the Effective Viscosity to the Viscosity of Pure Water.

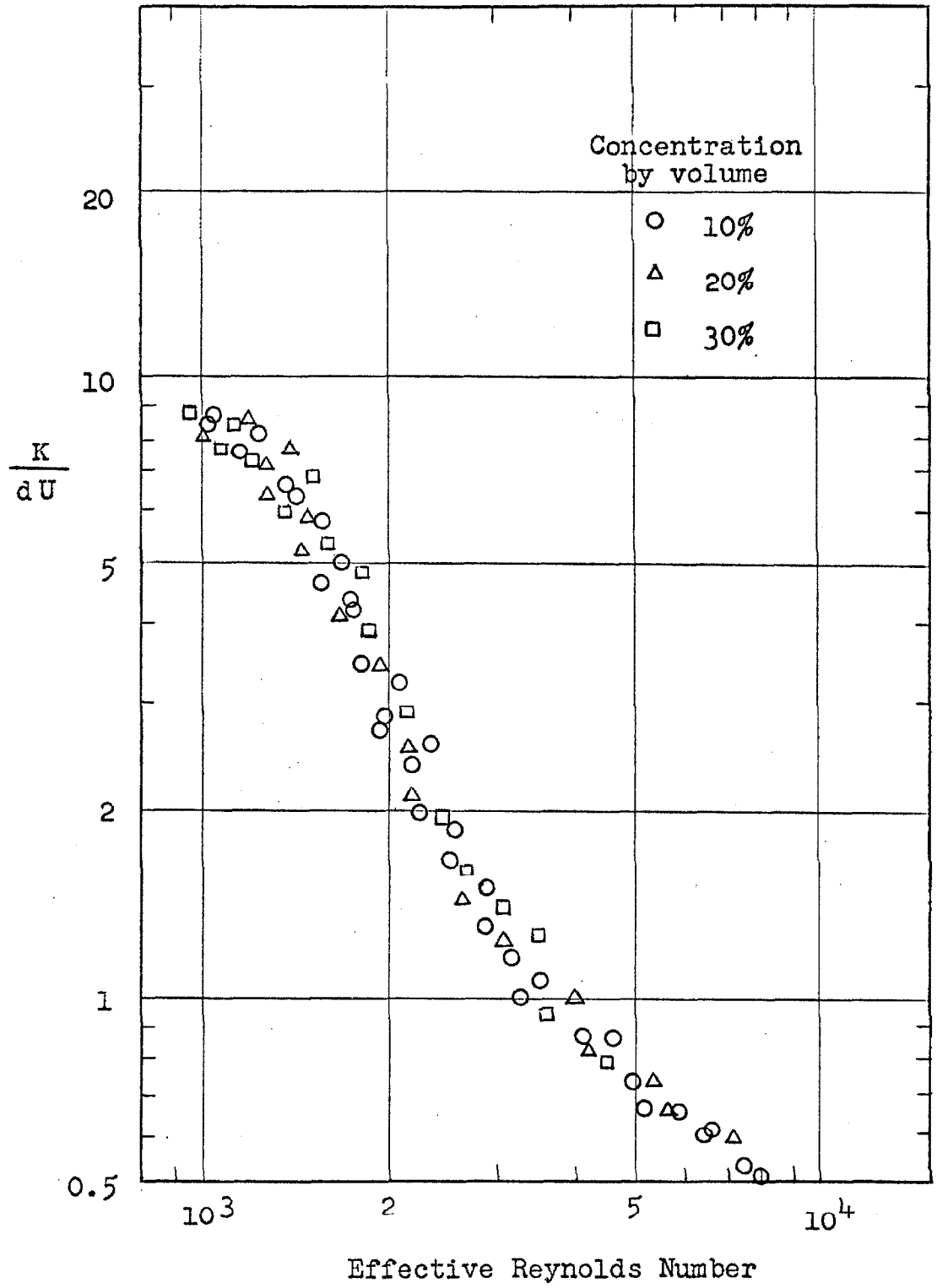

Figure 3. K / dU as a Function of Effective Reynolds Number for the Flow of Suspensions.

pared with that for pure water shown in Figure 1. It appears that the longitudinal dispersion coefficients for the flow of suspensions are much lower than those for pure water. These results reaffirm the conclusion that the presence of solid particles increases the rate of radial diffusion so that the longitudinal spread of the pulse is reduced. The difference between the two sets of data results from differences in the rate of radial diffusion and differences in the convective effect produced by differences in the velocity distribution. In turbulent flow the effect of the altered velocity distribution is probably minor and the lower values of $K/d\,U$ observed when particles were present bear out the hypothesis of increased radial diffusion. In laminar flow, the effect of the altered velocity distribution can be quite significant. However, the fact that the values of $K/d\,U$ are considerably lower than those for pure water lends support to the hypothesis of increased radial diffusion.

D. Literature Cited

1. Danckwerts, P. V., Chem. Eng. Sci., 2, 1 (1953).
2. Lapidus, L, Amundson, N. R., J. Phys. Chem., 56, 984 (1952).
3. Taylor, G. I., Proc. Roy. Soc., 219 A, 186 (1953).
4. Taylor, G. I., Ibid., 223 A, 446 (1954).

5. Levenspiel, O., Ind. Eng. Chem., 50, 343 (1958).

6. Crank, J., "The Mathematics of Diffusion", Oxford University Press (1956).

7. Fowler, F. C., and Brown, G. G., Trans. Am. Inst. Chem. Engrs., 39, 491 (1943).

8. Hull, D. E., and Kent, J. W., Ind. Eng. Chem., 44, 2745 (1952).

9. Mather, A. E., "The Rheology of Suspensions of Spheres - Effect of Size Distribution", Ph.D. Thesis, Univ. of Alberta (1962).

10. Baron, T., Sterling, C. S., and Schueler, A. P., Proc. of Third Mid-western Conference on Fluid Mechanics, Univ. of Michigan (1953).

11. Bagnold. R. A., Proc. Royal Soc.. 225 A. 49 (1954).

PROPOSITION II

Some expressions associated with the properties of local turbulence were found to be wrong in a paper by G. Astarita published in I & EC Fundamentals, Vol. 4, No. 3 (1965). These quantities are discussed and corrected in this proposition.

A. Discussions

In a recent paper by G. Astarita[1], analysis of the mechanism of energy dissipation in turbulent flow is made based upon the consideration of the frequencies of the non-inviscid eddies. This analysis offers the possibility of interpreting the drag reduction phenomenon observed in the turbulent flow of viscoelastic liquids. The interpretation tries to show that the turbulence in viscoelastic liquids is less dissipative. A brief review of this paper is abstracted as follows.

The author asserts that the largest eddies which are present in a circular pipe have a scale of motion equal to the pipe diameter d, and a velocity equal to the average velocity of the fluid u. The Reynolds number for these eddies is equal to the Reynolds number of the flow:

$$Re_{\lambda_{max}} = \frac{d u \rho}{\mu} \gg 1 \quad . \qquad (1)$$

For smaller eddies,

$$Re_\lambda = \frac{\rho u_\lambda \lambda}{\mu} < Re_{\lambda_{max}} \quad , \tag{2}$$

where λ is the scale of motion of eddies and u_λ the turbulent velocity corresponding to this scale of motion. As long as Re_λ is larger than unity, the eddies may be considered to be substantially conservative, i.e., their motion is inviscid. These eddies receive energy from the larger ones and give it up to the smaller ones, but their own motion is nondissipating. The limiting scale of motion λ_o for which the motion remains to be inviscid is defined by:

$$\frac{\rho u_{\lambda_o} \lambda_o}{\mu} = 1 \quad . \tag{3}$$

In a purely viscous liquid, those eddies whose scale of motion is smaller than λ_o are essentially dissipative and the viscous forces are important. For these inviscid eddies, Levich[2] shows that

$$u_\lambda \sim u(\lambda/d)^{1/3} \quad . \tag{4}$$

From Equations (3) and (4), the scale of motion of the largest non-inviscid eddies can be obtained by simple substitutions.

$$u_{\lambda_o} \sim u\,Re^{-1/4} \qquad (5)$$

$$\lambda_o \sim d\,Re^{-3/4} \quad . \qquad (6)$$

Thus the lowest frequency of the non-inviscid eddies is:

$$\omega_{\lambda_o} = \frac{u_{\lambda_o}}{\lambda_o} = \frac{u}{d} Re^{1/2} \quad . \qquad (7)$$

An order-of-magnitude analysis of Equation (7) indicates that the frequency of non-inviscid eddies in the liquids which are usually considered viscoelastic is larger than the inverse of the stress-relaxation time in turbulent flow. Consequently, the non-inviscid eddies are nondissipative or at least less dissipative than in purely viscous liquids.

Some mistakes were found in the foregoing discussions. The following discussions and corrections are primarily based upon the discussions presented in the book "Fluid Mechanics" by Landau and Lifshitz[3].

To realize the real physical picture, some basic concepts concerning the nature of fluid turbulence are introduced first. In turbulent flow there exist many turbulent eddies of different sizes. By the size of an eddy it means the order of magnitude of the distance over which the velocity varies appreciably. As the Reynolds

number increases, large eddies appear first, later appear the smaller ones. For very large Reynolds numbers, eddies of every size from the largest to the smallest are present. An important part in any turbulent flow is played by the largest eddies, whose size is of the order of the dimensions of the region in which the flow takes place. For turbulent flow in a circular pipe, this dimension should, of course, be the pipe diameter d. The velocity in these large eddies is comparable with the variation of the mean velocity over the distance d. The order of magnitude of this variation is denoted by Δu. It should be emphasized at this point that we are dealing with the order of magnitude, not of the mean velocity u itself, but of its variation Δu over distances of the order of d. The reason for this is because it is this variation Δu which characterizes the velocity of the turbulent flow. The mean velocity itself can have any magnitude, depending upon the frame of reference used.

For large eddies which are the basis of any turbulent flow, the viscosity is small and unimportant. The viscosity of the fluid is important only for the smallest eddies, whose Reynolds number is comparable with unity. The energy passes from the large eddies to smaller ones, practically no dissipation occurring during this process.

This flow of energy is dissipated only in the smallest eddies, where the kinetic energy is transformed into heat. Since the viscosity of the fluid is important only for the smallest eddies, we may say that none of the quantities pertaining to eddies of sizes $\lambda >> \lambda_o$ can depend on the viscosity μ.

The order of magnitude of the energy dissipation in turbulent flow can then be determined according to these arguments. Let ϵ be the mean dissipation of energy per unit mass of fluid per unit time. Although the dissipation is ultimately due to the viscosity, the order of magnitude of ϵ can be determined only by those quantities which characterize the large eddies. They are the fluid density ρ, the dimension d, and the variation of velocity Δu. Employing dimensional analysis, it can be found that

$$\epsilon \sim (\ u\ )^3/d \qquad (8)$$

and this determines the order of magnitude of the energy dissipation in turbulent flow. In a similar manner, the order of magnitude of the turbulent velocity variation u_λ over distances of the order λ can also be determined and is found to be

$$u_\lambda \sim (\epsilon\lambda)^{1/3} \ . \qquad (9)$$

The frequencies corresponding to the eddies are also of particular interest. The frequency is defined as the ratio of the mean velocity u to the dimension λ. Again one should notice that the frequency depends only on the velocity u itself, but not on its variation Δu. This is because the frequency determines the period with which the flow pattern is repeated when observed in some fixed frame of reference[3]. Relative to such a system, however, the whole pattern moves with the fluid at a velocity of the order of u.

In view of the foregoing definitions and discussions, some corrections can then be made on these basis. First of all, the lowest frequency of the non-inviscid eddies as given by Equation (7) appears to be wrong. Since the frequency is defined as the ratio of the mean velocity u to the dimension λ, the correct form of Equation (7) should be

$$\omega_{\lambda_o} = \frac{u}{\lambda_o} \sim \frac{u}{d} Re^{3/4} \quad . \qquad (10)$$

This gives the order of magnitude of the upper end of the frequency spectrum of the turbulence. Evidently, the lower end is at frequencies of the order of u/d. Thus the frequency range increases with $Re^{3/4}$, whereas it is $Re^{1/2}$ in Astarita's paper.

Furthermore, the expressions u_λ and u_{λ_o} given by Equations (4) and (5) also seem to be questionable. Combining Equations (7) and (8) yields:

$$u_\lambda \sim \Delta u \, (\lambda / d)^{1/3} \quad . \tag{11}$$

From Equations (11) and (3), we obtain

$$u_{\lambda_o} \sim \Delta u \, Re^{-1/4} \quad . \tag{12}$$

Equations (11) and (12) are apparently different from Equations (4) and (5), respectively. Instead of using the mean velocity u itself, it is the variation of this mean velocity Δu over the distances of the order of d that should be used here. It is believed that all the mistakes that were made by the author are essentially due to the choice of improper frames of reference when handling these turbulent quantities.

B. Literature Cited

1. Astarita, G., I&EC Fundamentals, Vol. 4, No. 3, 354 (1965).

2. Levich, V. G., "Physico-chemical Hydrodynamics", Prentice-Hall (1962).

3. Landau, L. D., and E. M. Lifshitz, "Fluid Mechanics", Addison-Wesley (1959).

C. Nomenclature

d	Diameter of the pipe, L.
Re	Reynolds number.
Re_λ	Reynolds number for eddies with scale of motion λ.
u	Time-averaged mean velocity of the fluid in turbulent flow, L/T.
Δu	Variation of the mean velocity over the distance d, L/T.
u_λ	Turbulent velocity variation over the distance λ, L/T.
ϵ	Mean dissipation of energy per unit mass of fluid per unit time, L^2/T^3.
λ	Scale of motion of eddies, L.
λ_o	Limiting scale of motion of eddies for which the motion remains to be inviscid, L.
ρ	Density of the fluid, M/L^3.
μ	Absolute viscosity of the fluid, M/LT.
ω_{λ_o}	Lowest frequency of the non-inviscid eddies, T^{-1}.

PROPOSITION III

The problem of steady-state diffusion of a material moving with the fluid in laminar flow through a pipe with a first-order chemical reaction has been solved analytically. The final results were expressed in terms of an orthogonal set of eigenfunctions. An approximate solution under the conditions of small pipe diameter, slow chemical reaction, and large distance downstream was also obtained.

The description of diffusion processes in terms of solutions of various simplified forms of the diffusion equation has often appeared in literature. However, in order to avoid mathematical complexity, very few of these solutions have taken into account the effect of chemical reactions. The problem of diffusion of a soluble matter moving with the fluid in laminar flow through a circular pipe with a chemical reaction, a system of great practical importance, has never been solved before. Therefore, an attempt was made to solve such a problem analytically.

The diffusion process in a binary diffusing system is governed by the following binary diffusion equation:

$$\frac{\partial C_A}{\partial t} + \nabla\cdot(C_A \vec{v}) = \nabla\cdot(C D_{AB} \nabla x_A) + R_A \qquad (1)$$

For diffusion in dilute liquid solutions at constant

temperature and pressure, it can be readily assumed that C and D_{AB} are constant. Equation (1) may then be simplified to the form:

$$\frac{\partial C_A}{\partial t} + \vec{v} \cdot \nabla C_A = D_{AB} \nabla^2 C_A + R_A \qquad (2)$$

All the subscripts will be omitted hereafter for the sake of simplicity. For laminar flow in a circular pipe at steady state, Equation (2) yields

$$U\left(1 - \frac{r^2}{a^2}\right)\frac{\partial C}{\partial x} = D\left(\frac{\partial^2 C}{\partial r^2} + \frac{1}{r}\frac{\partial C}{\partial r} + \frac{1}{r^2}\frac{\partial^2 C}{\partial \theta^2} + \frac{\partial^2 C}{\partial x^2}\right) + R \qquad (3)$$

It is usually the case that the radial component of molecular diffusion is much more important than the axial component. In this case the term $\partial^2 C/\partial x^2$ may be neglected. Furthermore, the first-order homogeneous chemical reaction may be represented by

$$R = -k'C \quad , \qquad (4)$$

where k' is the rate constant. Equation (3) then becomes

$$U\left(1 - \frac{r^2}{a^2}\right)\frac{\partial C}{\partial x} = D\left(\frac{\partial^2 C}{\partial r^2} + \frac{1}{r}\frac{\partial C}{\partial r}\right) - k'C \qquad (5)$$

Equation (5) is subjected to the following boundary conditions:

$$C = C_o \qquad \text{at} \qquad x = 0 \tag{6}$$

$$\frac{\partial C}{\partial r} = 0 \qquad \text{at} \qquad r = a \tag{7}$$

$$C \quad \text{bounded} \qquad \text{as} \qquad x \longrightarrow \infty \tag{8}$$

To solve Equation (5), it would be convenient to introduce the following dimensionless variables:

$$\frac{C}{C_o} = \phi \quad , \qquad \frac{r}{a} = \eta \tag{9}$$

Equation (5) then becomes

$$\frac{\partial^2 \phi}{\partial \eta^2} + \frac{1}{\eta}\frac{\partial \phi}{\partial \eta} - \frac{U a^2}{D}(1 - \eta^2)\frac{\partial \phi}{\partial x} - \frac{k' a^2}{D}\phi = 0. \tag{10}$$

If we further define

$$\frac{D}{U a^2} x = \xi \quad , \qquad \text{and} \qquad \frac{k' a^2}{D} = \alpha \quad , \tag{11}$$

the following equation is obtained:

$$\frac{\partial^2 \phi}{\partial \eta^2} + \frac{1}{\eta}\frac{\partial \phi}{\partial \eta} - (1 - \eta^2)\frac{\partial \phi}{\partial \xi} - \alpha \phi = 0 \tag{12}$$

with the boundary conditions:

$$\phi = 1 \qquad \text{at} \qquad \xi = 0 \tag{13}$$

$$\frac{\partial \phi}{\partial \eta} = 0 \qquad \text{at} \qquad \eta = 1 \tag{14}$$

$$\phi \quad \text{bounded} \quad \text{as} \quad \xi \longrightarrow \infty \tag{15}$$

Equation (12) may be solved by using the method of separation of the variables. Let

$$\phi(\eta, \xi) = X(\xi)\,Y(\eta) \tag{16}$$

Substitution of Equation (16) in Equation (12) yields:

$$X\frac{d^2Y}{d\eta^2} + \frac{X}{\eta}\frac{dY}{d\eta} - (1 - \eta^2)\,Y\frac{dX}{d\xi} - aXY = 0 \tag{17}$$

It should be noted that the partial derivatives have become ordinary derivatives. It follows that

$$\frac{1}{X}\frac{dX}{d\xi} = \frac{Y'' + \frac{1}{\eta}Y' - aY}{(1 - \eta^2)\,Y} = -\lambda\ , \tag{18}$$

where λ is an eigenvalue. Thus

$$X(\xi) = e^{-\lambda\xi} \tag{19}$$

From the boundary condition given by (15), λ must be real and positive.

From Equation (18), we have

$$\frac{d^2Y}{d\eta^2} + \frac{1}{\eta}\frac{dY}{d\eta} + [\lambda(1 - \eta^2) - a]Y = 0 \tag{20}$$

Equation (20) is a homogeneous linear second-order differ-

ential equation. Even so, the mathematical treatment is still very difficult. However, it can be much simplified under the transformation

$$\eta^2 = r \ . \tag{21}$$

Equation (20) then becomes

$$4r\frac{d^2Y}{dr^2} + 4\frac{dY}{dr} + [\lambda(1 - r) - a]Y = 0 \ , \tag{22}$$

where $r = 0$ is a regular singularity.

One of the most general methods for solving linear second-order differential equations is that for obtaining a series solution in either ascending or descending powers of the independent variable. A series solution of Equation (22) can be obtained by means of the method of Frobenius. The series assumes the form

$$Y(r) = r^s \sum_{n=0}^{\infty} C_n r^n = \sum_{n=0}^{\infty} C_n r^{n+s} \tag{23}$$

According to the method of Frobenius, the following differential operators are introduced:

$$x^2\frac{d^2f}{dx^2} = \delta(\delta - 1)f \ , \quad x\frac{df}{dx} = \delta f \tag{24}$$

Equation (22) may now be written in terms of δ, using (24).

We have

$$\left\{4\delta(\delta-1)+4\delta+[(\lambda-a)r-\lambda r^2]\right\}Y(r)=0 \quad (25)$$

Substitution of the series (23) gives

$$\sum_{n=0}^{\infty} C_n\left\{4(n+s)^2+(\lambda-a)r-\lambda r^2\right\}r^{n+s}=0 \quad (26)$$

i.e.

$$C_0 s^2 r^s+\left\{C_1(1+s)^2+\frac{\lambda-a}{4}C_0\right\}r^{s+1}$$

$$+\sum_{n=2}^{\infty}\left\{C_n(n+s)^2+\frac{\lambda-a}{4}C_{n-1}-\frac{\lambda}{4}C_{n-2}\right\}r^{n+s}=0 \quad (27)$$

We now equate to zero the coefficient of each power of r. The indicial equation is

$$C_0 s^2 r^s=0 \quad , \quad (28)$$

the roots of which are

$$s_1=s_2=0 \quad , \quad C_0\neq 0 \quad (29)$$

In order to satisfy the boundary condition (13), C_0 must be equal to unity. From the coefficient of r^{s+1} we obtain

$$C_1=-\frac{\lambda-a}{4} \quad (30)$$

The general recurrence relation is

$$n^2 C_n+\frac{\lambda-a}{4}C_{n-1}-\frac{\lambda}{4}C_{n-2}=0 \quad , \quad n\geq 2 \quad , \quad (31)$$

which determines successively the coefficients $C_2, C_3, \ldots$ in terms of C_o. From Equation (31) we have

$$C_2 = \frac{1}{4}\left\{\left(\frac{\lambda - a}{4}\right)^2 + \frac{\lambda}{4}\right\}$$

$$C_3 = -\frac{1}{36}\left\{\left(\frac{\lambda - a}{4}\right)^3 + \frac{5}{4}\lambda\left(\frac{\lambda - a}{4}\right)\right\} \quad , \text{ etc.}$$

The solution of Equation (22) may then be written as:

$$Y(r) = \sum_0^\infty C_n r^n = 1 - \frac{\lambda - a}{4}\eta^2 + \frac{1}{4}\left\{\left(\frac{\lambda - a}{4}\right)^2 + \frac{\lambda}{4}\right\}\eta^4 + \ldots \tag{32}$$

Since the indicial equation (28) has double roots, a second solution of Equation (22) may be obtained from $(\partial Y / \partial s)_{s=0}$ according to the method of Frobenius. The boundary condition given by Equation (14) provides the eigenvalue equation:

$$\sum_1^\infty n C_n = 0 \tag{33}$$

From this relation a set of eigenvalues $\lambda_1, \lambda_2, \ldots$ can be derived. The corresponding eigenfunctions $Y_1, Y_2, \ldots$ form a complete set with the following orthogonality relation:

$$\int_0^1 \eta(1 - \eta^2) Y_m Y_n \, d\eta = 0 \quad , \quad m \neq n \tag{34}$$

The solution of Equation (12) may then be written in the following general form:

$$\phi(\eta,\xi) = \sum_{1}^{\infty} b_K e^{-\lambda_K \xi} Y_K(\eta) \quad . \tag{35}$$

The boundary condition (13) yields

$$\sum_{1}^{\infty} b_K Y_K(\eta) = 1 \quad . \tag{36}$$

Equation (36) can be used to determine the coefficients b_K by means of the orthogonality relation (34). We obtain

$$b_K = \frac{\int_0^1 \psi(1-\psi^2) Y_K(\psi)\, d\psi}{\int_0^1 \psi(1-\psi^2) Y_K^2(\psi)\, d\psi} \quad . \tag{37}$$

If x is large, then ξ will be large as well. It follows that the first term of the series expansion in Equation (35) gives a result that should be sufficiently accurate for most purposes. In this case we have the following approximation:

$$\phi(\eta,\xi) \approx b_1 Y_1(\eta)\, e^{-\lambda_1 \xi} \quad . \tag{38}$$

Furthermore, if a is small, i.e., when the pipe diameter and the rate constant are small, the first eigenvalue λ_1 can be readily obtained in terms of a power series in a:

$$\lambda_1 = 2a - \frac{a^2}{48} + O(a^3) \quad . \tag{39}$$

Substitution of Equation (39) in Equation (32) leads to:

$$Y_1(\eta) = 1 - \frac{a}{4}\eta^2 + \frac{a}{8}\eta^4 + O(\eta^6) \quad . \tag{40}$$

Since $\eta \leq 1$ and a is small, the first two terms in Equation (40) should furnish a good approximation for $Y_1(\eta)$:

$$Y_1(\eta) \approx 1 - \frac{a}{4}\eta^2 \quad . \tag{41}$$

The coefficient b_1 can then be evaluated by substituting Equation (41) in Equation (37):

$$b_1 = 1 + \frac{a}{16} + O(a^2) \quad . \tag{42}$$

Therefore, an approximate solution in the case of small pipe diameter, slow chemical reaction, and large distance downstream has been obtained and can be written in the following simple form:

$$\phi(\eta, \xi) \approx \left(1 + \frac{a}{16}\right)\left(1 - \frac{a}{4}\eta^2\right) e^{-2a\xi} \, , \tag{43}$$

and the corresponding concentration distribution is

$$C(r,x) \approx C_o\left(1 + \frac{k'a^2}{16\,D}\right)\left(1 - \frac{k'a^2}{4\,D}\frac{r^2}{a^2}\right) e^{-2k'x/U} \, . \tag{44}$$

If the foregoing assumptions are not satisfied, the general form of solution given by Equation (35) must be used.